Journal of Alloys and Compounds 827 (2020) 153548

Contents lists available at ScienceDirect

Journal of Alloys and Compounds

journal homepage: http://www.elsevier.com/locate/jalcom

Materials for hydrogen-based energy storage – past, recent progress and future outlook

Michael Hirscher [a, **], Volodymyr A. Yartys [b, *], Marcello Baricco [c], Jose Bellosta von Colbe [d], Didier Blanchard [e], Robert C. Bowman Jr. [f], Darren P. Broom [g], Craig E. Buckley [h], Fei Chang [n], Ping Chen [i], Young Whan Cho [j], Jean-Claude Crivello [k], Fermin Cuevas [k], William I.F. David [l, m], Petra E. de Jongh [n], Roman V. Denys [o], Martin Dornheim [d], Michael Felderhoff [p], Yaroslav Filinchuk [q], George E. Froudakis [r], David M. Grant [s], Evan MacA. Gray [z], Bjørn C. Hauback [b], Teng He [t], Terry D. Humphries [h], Torben R. Jensen [u], Sangryun Kim [v], Yoshitsugu Kojima [w], Michel Latroche [k], Hai-Wen Li [x], Mykhaylo V. Lototskyy [y], Joshua W. Makepeace [l], Kasper T. Møller [h], Lubna Naheed [z], Peter Ngene [n], Dag Noréus [aa], Magnus Moe Nygård [b], Shin-ichi Orimo [v], Mark Paskevicius [h], Luca Pasquini [ab], Dorthe B. Ravnsbæk [ac], M. Veronica Sofianos [h], Terrence J. Udovic [ad], Tejs Vegge [e], Gavin S. Walker [s], Colin J. Webb [z], Claudia Weidenthaler [p], Claudia Zlotea [k]

[a] Max-Planck-Institut für Intelligente Systeme, Heisenbergstrasse 3, 70569, Stuttgart, Germany
[b] Institute for Energy Technology (IFE), P.O. Box 40, NO-2027 Kjeller, Norway
[c] Department of Chemistry and NIS, University of Turin, Via P.Giuria, 9, I-10125, Torino, Italy
[d] Department of Nanotechnology, Helmholtz-Zentrum Geesthacht, Max-Plank-Str. 1, 21502, Geesthacht, Germany
[e] DTU Energy, Department of Energy Conversion and Storage, Anker Engelunds Vej, Building 301, 2800 Kgs. Lyngby, Denmark
[f] RCB Hydrides, LLC, 117 Miami Ave., Franklin, OH, 45005-3544, United States
[g] Hiden Isochema, 422 Europa Boulevard, Warrington, WA5 7TS, United Kingdom
[h] Department of Physics and Astronomy, Fuels and Energy Technology Institute, Curtin University, GPO Box U1987, Perth, 6845, WA, Australia
[i] Dalian Institute of Chemical Physics, Chinese Academy of Sciences, Dalian, 116023, PR China
[j] Materials Science and Technology Research Division, Korea Institute of Science and Technology, CheongRyang, Seoul, South Korea
[k] Univ. Paris Est Creteil, CNRS, ICMPE, UMR7182, F-94320, Thiais, France
[l] Inorganic Chemistry Laboratory, University of Oxford, South Parks Road, Oxford, OX1 3QR, United Kingdom
[m] ISIS Neutron and Muon Source, Rutherford Appleton Laboratory, Harwell Campus, Didcot, OX11 0QX, United Kingdom
[n] Inorganic Chemistry and Catalysis, Debye Institute for Nanomaterials Science, Utrecht University, Universiteitsweg 99, 3584CG, the Netherlands
[o] HYSTORSYS AS, P.O. Box 45, NO-2027, Kjeller, Norway
[p] Max-Planck-Institut für Kohlenforschung, Kaiser-Wilhelm-Platz 1, 45470, Mülheim an der Ruhr, Germany
[q] Institute of Condensed Matter and Nanosciences, Université Catholique de Louvain, Place L. Pasteur 1, B-1348, Louvain-la-Neuve, Belgium
[r] Department of Chemistry, University of Crete, P.O. Box 2208, Voutes, 71003, Heraklion, Greece
[s] Department of Mechanical, Materials and Manufacturing Engineering, University Park, University of Nottingham, Nottingham, NG7 2RD, United Kingdom
[t] Dalian Institute of Chemical Physics, Chinese Academy of Sciences, Dalian, 116023, PR China
[u] iNANO and Department of Chemistry, Aarhus University, Langelandsgade 140, Building 1512, 316, 8000 Aarhus C, Denmark
[v] WPI-Advanced Institute for Materials Research (WPI-AIMR), Tohoku University, 980-8577, Sendai, Japan
[w] Natural Science Center for Basic Research and Development (Department of Advanced Materials), Hiroshima University, 3-1 Kagamiyama 1-chome, Higashi, Hiroshima, 739-8530, Japan
[x] Kyushu University, Kyudai Kyusyu University Platform of Inter/Transdisciplinary Energy Research (Q-PIT), Motooka 744, Nishi-ku, Fukuoka, 819-0395, Japan
[y] HySA Systems (Hydrogen South Africa), University of the Western Cape, Bellville, 7535, South Africa
[z] Queensland Micro- and Nanotechnology Centre, Griffith University, Brisbane, Australia
[aa] Department of Materials and Environmental Chemistry, Stockholm University, Svante Arrhenius Väg 16 C, Stockholm, Sweden
[ab] Department of Physics and Astronomy, University of Bologna, Viale Berti Pichat 6/2, Bologna, Italy
[ac] Department of Physics, Chemistry and Pharmacy, University of Southern Denmark, Campusvej 55, 5230 Odense M, Denmark
[ad] NIST Center for Neutron Research, National Institute of Standards and Technology, Gaithersburg, MD, 20899-6102, United States

** Corresponding author.
* Corresponding author.
E-mail addresses: hirscher@is.mpg.de (M. Hirscher), volodymyr.yartys@ife.no (V.A. Yartys).

https://doi.org/10.1016/j.jallcom.2019.153548

ARTICLE INFO

Article history:
Received 3 October 2019
Received in revised form
20 December 2019
Accepted 24 December 2019
Available online 31 December 2019

Keywords:
Hydrogen storage materials
Porous materials
Liquid hydrogen carriers
Complex metal hydrides
Intermetallic hydrides
Magnesium based materials
Low dimensional hydrides
Electrochemical energy storage
Heat storage
Hydrogen energy systems

ABSTRACT

Globally, the accelerating use of renewable energy sources, enabled by increased efficiencies and reduced costs, and driven by the need to mitigate the effects of climate change, has significantly increased research in the areas of renewable energy production, storage, distribution and end-use. Central to this discussion is the use of hydrogen, as a clean, efficient energy vector for energy storage. This review, by experts of Task 32, "Hydrogen-based Energy Storage" of the International Energy Agency, Hydrogen TCP, reports on the development over the last 6 years of hydrogen storage materials, methods and techniques, including electrochemical and thermal storage systems. An overview is given on the background to the various methods, the current state of development and the future prospects. The following areas are covered; porous materials, liquid hydrogen carriers, complex hydrides, intermetallic hydrides, electrochemical storage of energy, thermal energy storage, hydrogen energy systems and an outlook is presented for future prospects and research on hydrogen-based energy storage.

1. Introduction

The European Commission describes hydrogen as an energy carrier with a "great potential for clean, efficient power in stationary, portable and transport applications." Indeed, presently hydrogen is getting unprecedented focus not only in Europe but across the globe, and is on track to achieve its outstanding potential as a clean energy solution.

The growing applications of hydrogen fueled transportation started in the 20th century with high profile technology breakthroughs such as powering Apollo 11 to the moon. The area is maturing through a growing fleet of hydrogen fuel cell vehicles, hydrogen fuel cell trains commercially operating in Germany, France and the UK, and hydrogen driven ferries in Norway. This is in addition to the high capacity metal hydride fast recharging battery systems for trains and trams in France and in Japan. Hydrogen storage remains a key challenge in rolling out infrastructure to support hydrogen fueled transportation.

As the world's leading energy authority covering exploration of all fuels and related technologies, the International Energy Agency (IEA) is ideally placed to lead global policy on hydrogen. The IEA Technology Collaboration Program (TCP) supports advancing the research, development and commercialization of energy technologies. IEA Hydrogen TCP operates research on hydrogen within tasks. IEA Hydrogen Task 32 HYDROGEN-BASED ENERGY STORAGE has coordinated the efforts of the scientific community in various areas of energy storage based on hydrogen.

IEA Hydrogen Task 32 is the largest international collaboration in this field. It involves more than 50 experts coming from 17 countries. The task consists of seven working groups, working on porous materials, intermetallic alloys and magnesium-based hydrides as energy storage materials, complex and liquid hydrides, electrochemical storage of energy, heat storage and hydrogen storage systems for stationary and mobile applications.

This dynamic collaborative research effort has resulted not only in over 600 publications in international journals (including 20 in a topical collection in Applied Physics A in 2016 and seven in a special issue of International Journal of Hydrogen Energy in 2019) and presentations at international conferences and symposia in the field (lately in a special session at the 16th International Symposium on Metal-Hydrogen Systems (MH2018) on November 1, 2018 in Guangzhou, China), but has also led to the discoveries of new functional materials and their technologies, bridging the gap between fundamental science and real world applications. Nanomaterials, materials for novel rechargeable batteries, for thermal storage, and the development of systems for hydrogen storage and compression of hydrogen gas using metal hydrides, together with beautiful chemistry, structure and properties of new materials attracted the interest of many leading researchers. These researchers are sharing the major outcomes of their work in this review paper, which summarizes the research efforts over the last 6 years, 2013−2018. The review is presented in the following sections. The multidisciplinary and collaborative work crosses many of these sections. The review is inevitably confined by size but it does summarize the most important results and contains an extensive list of references by the members of the IEA Hydrogen Task 32, which will allow the reader to find further details of the presented research effort.

2. Porous materials for H_2 storage

For technological applications, rapid kinetics and full reversibility enable short refuelling times and high cycle life, and so exploration into physisorption in materials is an important area. Hydrogen storage by physisorption in porous materials, using classical systems such as activated carbons and zeolites, has a long history. Maximum storage capacities are closely related to the surface area accessible to H_2 molecules. Gravimetric capacities therefore tend to follow Chahine's rule, which states that the hydrogen uptake is approximately 1 wt% H_2 per 500 $m^2 g^{-1}$ of surface area at 77 K and pressures above 20 bar. Super-activated, porous carbons with large surface areas have been developed in the past, but the field came to some stagnation around 20 years ago.

In the late 1990s, there was a certain amount of hype and hope surrounding hydrogen storage using carbon nanotubes and other carbon nanostructures; however, the initial results were later shown to be due to either contamination of the samples or erroneous measurements [1−3]. At the same time, an entirely new class of highly porous, crystalline materials called coordination polymers or Metal-Organic Frameworks (MOFs) was developed. Following promising results for methane in 2001, the first hydrogen storage results on MOF-5, published in 2003, showed a sharp increase in the H_2 uptake at very low pressures and a maximum of 4.5 wt% below 1 bar at 77 K [4]. However, this was corrected a year later by the same group to 1.3 wt% at 1 bar [5]. Soon after, more results on different MOFs were published showing high H_2 uptakes at 77 K and higher pressures, owing to the large pore volumes and high specific surface areas of these novel frameworks [6,7]. An additional

advantage of these materials is the open pore structure that makes the kinetics of hydrogen ad- and desorption very fast, and highly reversible since no structural change occurs in the framework [8].

The validity of Chahine's rule, which was originally proposed for carbons, was shown for MOFs independently by two groups at the same time [9,10]. Despite the different elements in the building blocks of MOFs, this result is reasonable since at pressures above 20 bar all adsorption sites will be occupied. This result then started a race to synthesize new MOFs with higher specific surface areas.

Over the next 15 years, many studies investigated the correlation between H_2 adsorption and the structure and composition of different MOFs. One example is the correlation of the heat of adsorption to pore size, due to overlapping of the van der Waals forces of neighbouring framework atoms [11,12]. Another is the influence of open metal sites, which adsorb strongly, due to polarization of the H_2 molecules [13,14]. High heats of adsorption have been observed for these sites; however, only a fraction of the total adsorption sites could be enhanced so far. A similar strategy is to post-synthetically exchange the linkers in the MOF structure, i.e. use functionalization, in order to change either the pore or aperture size, or enhance the interaction with H_2 [15–17].

The gravimetric H_2 uptakes at higher pressures above 20 bar and at 77 K, for all porous materials, are proportional to surface area, indicating that specific surface area is crucial for achieving high gravimetric storage capacities. The problem is that high-surface-area porous materials tend to have low material densities and therefore only modest volumetric hydrogen storage capacities. For crystalline materials, such as MOFs, the gravimetric H_2 uptake can easily be converted to volumetric uptake using the single crystal density obtained by X-Ray Diffraction (XRD) structure analysis. For experimental results, a phenomenological model for the volumetric absolute uptake as a function of the gravimetric absolute uptake has been developed [18]. For theoretical studies, via computational screening, a similar correlation was obtained using over 5000 MOF structures [19]. Fig. 1 shows the volumetric absolute uptake for a range of porous materials plotted against gravimetric uptake. The solid lines show the phenomenological model developed by Balderas-Xicohténcatl et al. [18].

So far most of the reported hydrogen storage capacities are still given as the maximum uptake at the upper measurement pressure, whereas for methane storage in porous materials the working or useable capacity is often reported. Useable capacity is defined as the difference between the capacity of the full tank at maximum pressure and the capacity remaining in the tank at the minimum pressure required to run the fuel cell. A detailed analysis based on experimental data of several MOFs has been reported by Schlichtenmayer and Hirscher [20]. Depending on the heat of adsorption, an optimum operating temperature was reported, which maximized the useable capacity for a particular material. Recently, Siegel and co-workers [21] screened half a million MOFs in a theoretical study and found an upper value of about 40 g H_2 L^{-1} for the useable volumetric capacity. One strategy to increase the useable capacity has been recently demonstrated for methane storage through the use of flexible frameworks [22]. However, the lower isosteric heat of hydrogen compared to methane makes it more difficult to design and tailor a flexible MOF for which H_2 adsorption will induce a structural phase transition to an open structure with higher gas storage capacity.

As indicated earlier, measurement accuracy and reproducibility has been an issue in porous materials research [3]. H_2 adsorption is commonly measured using the manometric and gravimetric techniques [23], both of which are susceptible to errors associated with volume calibrations [24,25] and buoyancy corrections [26]. Problems, such as the use of insufficient sample sizes, gas purity, and equilibration times, have also affected measurements, and this has

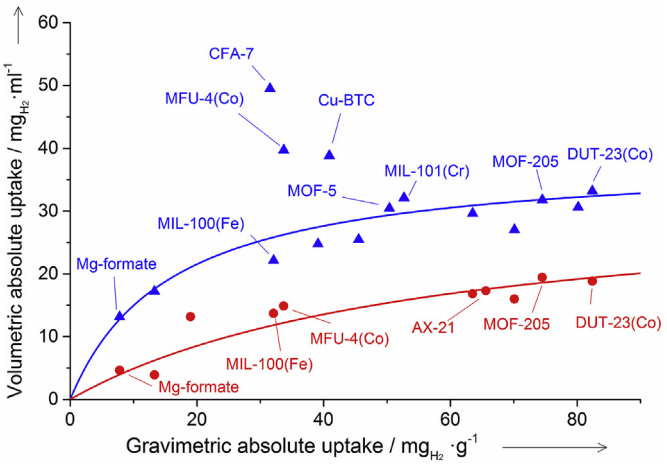

Fig. 1. Volumetric vs. gravimetric absolute hydrogen uptake of porous materials measured at 77 K and 2.0–2.5 MPa. The volumetric uptake was calculated using packing density (red) and single-crystal density (blue). Used with permission from Balderas-Xicohténcatl et al. [18]. (For interpretation of the references to colour in this figure legend, the reader is referred to the Web version of this article.)

been demonstrated by interlaboratory exercises performed on both porous carbon [27] and doped MgH_2 [28]. Better agreement was found in a recent study, which reported high pressure H_2 adsorption measurements on two commercial porous carbons [29]. The use of small sample sizes in manometric instruments, inducing large errors, continues to be a problem in the literature. It has also not yet been demonstrated, via interlaboratory studies, that accurate measurements can be performed reproducibly at both 77 K and high pressures for a wide range of materials, such as MOFs, COFs and polymers [30]; since only porous carbons have been subject to such tests.

High pressure measurements, particularly above standard cylinder pressures of 200 bar, require specialist components, together with a hydrogen compressor [31–34]. As the pressure increases, uncertainties in the measurement increase [24] and problems associated with determining the volume of low density materials also increase [23]. This must be accounted for during instrument design [31]. Such high pressures are of interest due to the possibility of incorporating an adsorbent in the storage tanks of commercial 700 bar compressed gas systems, although this is made difficult by the tendency of adsorptive materials to have the majority of the useable capacity at low pressures. As an example, uptake isotherms for excess and net gravimetric capacity to 2000 bar at ambient temperature are shown in Fig. 2. This demonstrates that the maximum in the advantage of the adsorbing material over an empty tank occurs at only 100 bar, and that over 300 bar, the material constitutes a disadvantage compared to an empty tank.

An alternative approach for characterizing hydrogen adsorption in porous materials, by measuring one adsorption isotherm at 20 K, has been proposed by Streppel and Hirscher [35]. A single low-pressure, high-resolution isotherm of hydrogen at the boiling temperature can be used to analyze the specific surface area by applying the BET theory and to determine the upper physical limit for hydrogen uptake up to the filling of the pores by condensation [36]. Using compacted materials in the form of pellets allows direct measurement of the volumetric uptake based on the packing density.

Porous materials can also be used as substrates for metal nanoparticles. Several reports on noble metal particles finely dispersed inside porous materials claimed an enhanced hydrogen

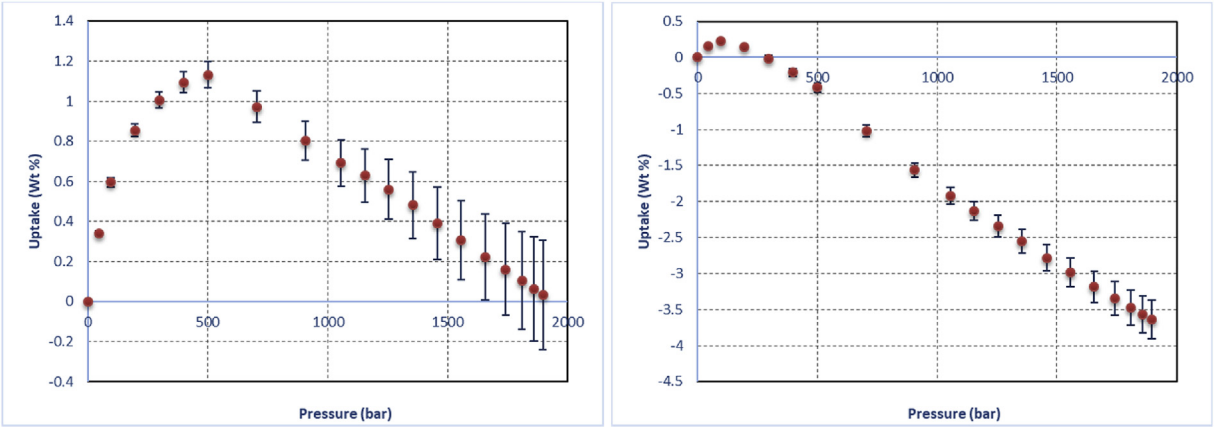

Fig. 2. Experimental excess (a) and net (b) isotherms of porous carbon Filtrasorb 400 at ambient temperature to 2000 bar. Net is defined as the amount of hydrogen due to adsorption over and above what would be in the same volume at the same pressure without the adsorptive material.

storage capacity at ambient temperature and ascribed it to a so-called "spillover effect". None of these reports claiming high storage capacities could be independently reproduced [3]. If the spillover effect occurs at all, it is minor and technologically irrelevant [37–39]. On the other hand, noble metal particles in frameworks often exhibit special catalytic activities. Under hydrogen atmosphere organic gases or liquids can be hydrogenated under mild conditions in these metal-doped frameworks [40,41].

The inverse of this approach is the utilization of frameworks to nano-confine metal hydrides and use their structure as a scaffold [42,43]. While this does not add any adsorption contribution, this novel approach does offer the possibility that nanoconfinement may improve the thermodynamic and the kinetic properties of the hydride. In addition, by employing an oxygen-free porous metal scaffold that partially reacts with the nano-confined hydride, the remaining metal scaffold is expected to substantially improve the thermal conductivity of the hydride bed. Low thermal conductivity is a key constraint of hydrides as illustrated in the following sections. By carefully matching the amount of metal scaffold to the hydride encapsulated within it, enough of the metal scaffold remains upon reaction with the complex hydride to maintain structural integrity of the scaffold [44–49]. This also maintains the kinetic advantages of nanoconfinement by minimising segregation of the desorption products.

Together with the above experimental work, theory has also played a significant role in the development of the field, by helping explain experimental results and by leading experiments [50–58]. There are several methods for investigating gas storage in MOFs. For many years, multiscale modelling of various physical and chemical phenomena such as gas adsorption and diffusion has been developed. Multiscale modelling consists of applying different levels of theory depending on the length scale of the system under investigation and the time evolution of the physical phenomenon. In this way, the accuracy of the lower scale can be combined with the system size of the higher, without requiring prohibitively large computations. This approach has been undertaken in the modelling of H_2 physisorption in nanoporous materials. For example, Froudakis and co-workers developed a multiscale scheme presented in Fig. 3 – left [50–52]. At the lowest level, *ab-initio* techniques allow high accuracy calculation of the molecular H_2 interaction with the different building blocks of a MOF. At the next level, Potential Energy Surfaces (PES) are constructed, for fitting the classical interatomic potentials used in the highest level. These massive computations use either dispersion corrected Density Functional Theory (DFT) or Mixed Quantum Mechanics/Molecular Mechanics (QM/MM) models. At the final level, classical Molecular Dynamics (MD) and Monte Carlo simulations in the Grand Canonical ensemble (GCMC) reveal the adsorption of H_2 in MOFs, taking into account several thousands of atoms. Such multiscale modelling of hydrogen storage in nanoporous materials has proved significant in developing our understanding, and has paved the way for further experimental studies [59,60]. One such study is the directed assembly of a high surface area 2D MOF displaying the augmented "kagomé dual" (kgd-a) layered topology. This showed a high H_2 uptake (209.9 cm^3(STP) g^{-1} at 77 K and 1 bar).

Over the last couple of years, Machine Learning (ML) techniques have also been introduced, for predicting adsorption of different gases in MOFs. In the field of material science, the computational cost of ML methods is several orders of magnitude lower than that of the previously mentioned multiscale approaches. However, their ability to provide accurate predictions strongly depends on determining appropriate parameters (descriptors) to allow the algorithm to efficiently learn from existing data and the quality of the data fed in.

For ML techniques, shown in Fig. 3-right, a large dataset is needed for training and an algorithm is required to perform the training. Appropriate descriptors also have to be identified. While the training part may need computational time, the production runs for obtaining properties of unseen materials require only milliseconds. It has recently been shown that ML techniques are a powerful tool for the large-scale screening of materials [61,62]. An example is the chemically intuited large scale screening of MOFs by machine learning techniques done at the University of Crete in cooperation with the University of Huddersfield.

During IEA Hydrogen Task 32, the field of porous materials for hydrogen storage progressed from fundamental studies on synthesising, characterizing and understanding novel MOFs to improving and optimising technologically relevant parameters, such as volumetric, gravimetric and useable storage capacities. The first larger prototype storage tank systems have been built and operated introducing different heat-exchanger concepts. The achievements within the porous materials working group of IEA Hydrogen Task 32 are summarized in two recent articles [63,64].

3. Liquid hydrogen carriers

The liquid state is considered a practicable option for the large-scale transport and storage of hydrogen, towards an international hydrogen-based energy market [65]. Recent dramatic declines in auction prices for electricity from renewable energy installations

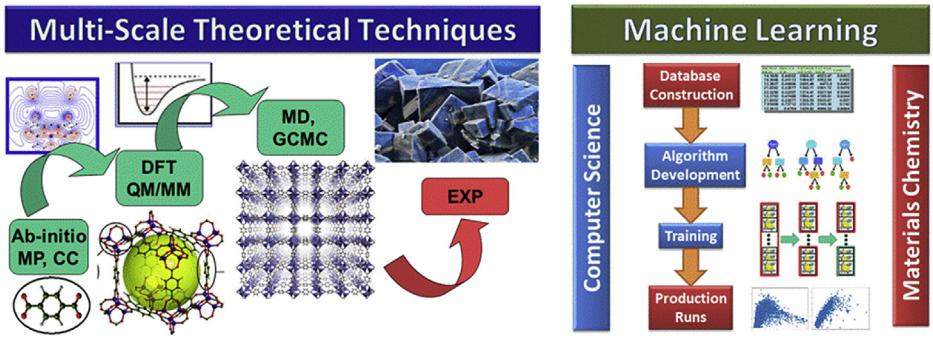

Fig. 3. Multiscale theoretical methodologies (left) vs Machine Learning techniques (right) for modelling hydrogen storage in MOFs.

have occurred in areas with favorable wind and solar conditions [66]. These low prices have highlighted the opportunity for energy supply chains which can transport renewable energy, via a carrier, from renewable rich areas such as Morocco, Saudi Arabia, UAE, Brazil, Chile and Australia (Fig. 4). The conversion of renewable electricity to hydrogen and long distance maritime transport of that hydrogen in a liquid form is seen as an economically attractive method of energy transport [67]. This may also be a viable option for remote areas with high renewable electricity generation potential, with no direct grid connections [68–70].

Liquid hydrogen storage is also an important component of domestic grid-balancing alongside electrochemical energy storage. A high energy density store which can be produced and stored at scale would help manage inter-seasonal imbalances in supply and demand, a task that is problematic for batteries due to self-discharge [71]. An example of this is the winter heating demand in the UK, which is around 200 TWh each year and is currently met by the natural gas grid [72]. Here again, production of hydrogen and storage either in geologic features or as a liquid is seen as the most viable means of achieving long-duration energy storage, giving advantages in volumetric energy density and cost of storage and distribution.

Liquid hydrogen is the most conceptually simple means of hydrogen storage; however, the complexity and cost associated with the extremely low temperature (20 K) required for hydrogen liquefaction [73,74] has prompted the consideration of other liquid carriers with moderate storage conditions. Most attention, including within IEA Task 32, has been given to two carriers in particular: ammonia and liquid organic hydrogen carriers (LOHCs) [75–80]. Both have more moderate storage requirements than liquid hydrogen which results in significantly lower projected transportation and storage costs [67,73,74]. This has led to the active development of hydrogen supply chains based on conversion to these carriers [65,67,81–84]. Most of the planned applications of liquid carriers do not involve dehydrogenation on-board a fuel cell vehicle, but rather models of either centralised dehydrogenation at ports or other facilities for local distribution as hydrogen gas, or decentralised hydrogen release at refuelling stations.

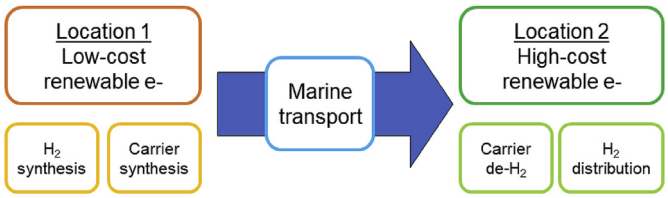

Fig. 4. Schematic of the use of liquid hydrogen carriers to store energy produced in areas with cheap renewable electricity for use in areas with more expensive local electricity.

While the synthesis costs of ammonia and LOHCs compare well with the cost of liquefying hydrogen [74,82,83], use of these liquid carriers introduces an extra step of converting the carrier back to hydrogen. The cost and efficiency losses associated with this reconversion step limit their use. As such, much of the research from Task 32 in this area has focused on improving the chemistry of hydrogen release through catalyst development.

3.1. LOHCs

The first LOHC compounds explored were cyclic alkane compounds, such as cyclohexane, methylcyclohexane and decalin, with dehydrogenation to the related aromatic compounds achieved largely with platinum-based catalysts at 300–350 °C [75,77,85]. These simple materials, which can release up to 6 wt% hydrogen with similar volumetric hydrogen density to 70 MPa hydrogen gas are attractive because they are already produced at commercial scale (e.g. benzene and toluene [86]) and have a high level of technological readiness. However, the high dehydrogenation temperature and the expensive catalysts required hinder their commercial application. As such, research on these carriers has focused on:

- Reducing the temperature of dehydrogenation by modification of the LOHC molecule to reduce the enthalpy of the reaction.
- Searching for more active, stable and earth-abundant catalysts for dehydrogenation.

Attempts to modify the enthalpy of dehydrogenation have largely centred on the introduction of heteroatoms, particularly nitrogen, into the cyclic structures [87–89]. A number of these materials (e.g. N-ethyl carbazole) have been shown to have superior hydrogen storage and release characteristics than unsubstituted systems [90,91].

Recently, a metallation strategy was employed to optimize the hydrogen storage properties of organic compounds through the replacement of their reactive H by alkali or alkaline earth metal to form the metallated counterparts. Crystalline lithiated amines were synthesised by ball milling primary amines with LiH, demonstrating a mild endothermic dehydrogenation and an enhanced selectivity to hydrogen release [92,93]. The sodium phenoxide-cyclohexanolate pair was also developed, which has an enthalpy change of dehydrogenation of 50.4 kJ/mol-H_2, substantially less than that of pristine phenol-cyclohexanol pair (64.5 kJ/mol-H_2). This enthalpy change was found to correlate with the electron delocalization from the oxygen to the benzene ring of phenoxide. Hydrogen uptake and release were achieved below 150 °C [94].

Ruthenium is the most active hydrogenation catalyst for these

N-substituted systems, while supported palladium has been found to be the most active catalyst for dehydrogenation. In some catalyzed dehydrogenations, complete reaction is not observed, producing partially-dehydrogenated products which limit the accessible hydrogen content [95]. Among the catalyst supports, materials have been found to increase the hydrogenation rate, as evidenced by the increased activity of palladium nanoparticles supported on a covalent triazine framework [96]. Homogeneous catalysts have also been investigated, with iridium pincer complexes used to catalyze the dehydrogenation of a number of heterocyclic species, showing appreciable activity at 150–200 °C [97,98].

3.2. Ammonia

Ammonia is also an attractive liquid carrier for hydrogen storage. It is already one of the most consequential synthetic chemicals through its role as a fertiliser feedstock [99] – with production at around 180 Mt per year [100] – so this means existing synthesis and distribution infrastructure are technologically mature. However, there are several active research areas aiming to improve the cost and efficiency of ammonia-related hydrogen storage.

Hydrogen release from ammonia is not a well-established technology, as it does not form a significant part of the existing markets for ammonia. Ammonia decomposition catalysis has been studied in some depth for transition metal systems as a proxy for catalytic activity for ammonia synthesis. Ruthenium is the most active metal [101,102], but high performance is also achieved using more earth-abundant metals such as iron, cobalt and molybdenum [103–105]. In-situ diffraction techniques have proved valuable for understanding the formation of nitride phases in iron and manganese under ammonia decomposition conditions [106,107,107].

Temperature is also a consideration, with even the most active ruthenium-based catalysts requiring relatively high temperatures (>450 °C) to approach 100% conversion to hydrogen. Delivering significantly lower operating temperatures requires new catalysts to be developed. Recently, metal-nitrogen-hydrogen materials (principally light metal amides and imides) have been shown to effectively mediate ammonia decomposition achieving catalytic activities that are comparable to supported ruthenium catalysts [108–110].

For these new catalyst systems, two parallel paths of investigation have been explored: metal amide/imide as individual catalysts [108,110,111] and in composites with transition metals and their nitrides [109,112–116]. The catalytic activity has been rationalized by the cyclic formation and decomposition of ternary lithium nitrides (e.g. Li_7MnN_4 and Li_3FeN_2) in the transition metal composites (Fig. 5a) [109], or a metal/metal-rich species, such as sodium (Fig. 5b) or lithium nitride-hydride (Li_4NH) (Fig. 5c), in isolated metal imides [117]. Lithium imide (Li_2NH) containing species have been the most active catalysts reported to date. In-situ neutron and X-ray powder diffraction experiments have shown that the active state of the lithium imide is a solid solution of lithium amide and lithium imide, the precise stoichiometry of which depends on the reaction conditions [110,118].

$$(1\text{-}x)Li_2NH + xNH_3 \rightarrow Li_{2\text{-}2x}NH_{1+2x}$$

Furthermore, isotope exchange reactions have revealed that both the hydrogen and nitrogen in the imide are exchangeable with ammonia under operating conditions [110,117], indicating a bulk exchange mechanism which is in contrast to transition metal nanoparticle catalysis and more closely related to the Mars van Krevelen mechanisms of metal nitride based ammonia synthesis [119].

Metal amides and imides have also recently been reported as part of novel ammonia synthesis pathways (Fig. 5d). They are hypothesized to be the mediating species in the lithium hydride – transition metal (nitride) composites, which are proposed to be two-site ammonia synthesis catalysts which break the scaling relations between nitrogen activation and the binding strength of intermediate species, achieving very high ammonia synthesis activity [120,121]. Additionally, they have been shown as part of a chemical looping approach to ammonia synthesis, where a combination of barium hydride (BaH_2) and nickel is able to produce ammonia from hydrogen and nitrogen through the formation and subsequent hydrogenation of barium imide (BaNH) at 1 bar and at a temperature as low as 100 °C [122].

These milder approaches to ammonia synthesis may well enable smaller-scale synthesis units which require much less capital investment and are better equipped to couple to variable renewable electricity supplies.

Electrochemical ammonia synthesis is another interesting approach [123], though a good electrocatalyst for nitrogen reduction has so far been elusive. Indeed, there is evidence that many published results are susceptible to ammonia derived from contaminants rather than from true nitrogen reduction, emphasizing the need for isotopically labelled experiments [124,125]. Theoretical approaches based on DFT have identified a range of nitrides as potential catalysts [126,127], if high activity catalysts which suppress the competing hydrogen evolution reaction can be identified [128,129].

Another challenge is preventing the release of ammonia from storage vessels or in hydrogen/exhaust streams to avoid: environmental effects of ammonia through toxicity in waterways and as an atmospheric pollutant [130]; shielding PEM fuel cells from degradation by ammonia [131]; and human exposure to corrosive ammonia gas. Approaches to purifying hydrogen to ensure ammonia levels are below the 0.1 ppm standard for mobile applications include absorption of ammonia by metal halides [132] or zeolites [133], or by filtering H_2 gas streams using membranes [134].

Sorption materials can also be used to store ammonia with a significantly reduced vapour pressure [135–138]. Metal halides ammine complexes can have ammonia densities similar to liquid ammonia. It has been shown that, by tailoring the combination of metal ions in a ternary metal halide system, the conditions for ammonia release can be matched to the desired application. Combinations of genetic algorithms and DFT calculations were used to identify mixed-metal systems which best matched a specific performance metric [139–142]. An example structure of a barium-strontium-calcium chloride ammine was then synthesised and demonstrated impressive agreement with the expected ammonia desorption behaviour [139,143,144]. Metal borohydride ammines can also store significant quantities of ammonia [145,146], up to 6 ammonia groups per molecule in the case of $6Mn(BH_4)_2 \cdot 6(NH_3)$, forming often analogous structures to the metal halide ammine [147–149]. Thermal decomposition of these species can give either pure ammonia or mixtures of ammonia and hydrogen. While the factors governing this are not fully understood, it is hypothesized that the relative stability of the metal borohydride may play a significant role, with the ammines of low-stability borohydrides more likely to release mixed gases [149]. These decomposition pathways could be of interest in tailoring gas release for particular applications like combustion of ammonia, where hydrogen is a useful co-fuel.

4. Complex metal hydrides

Complex metal hydrides are a class of materials containing an

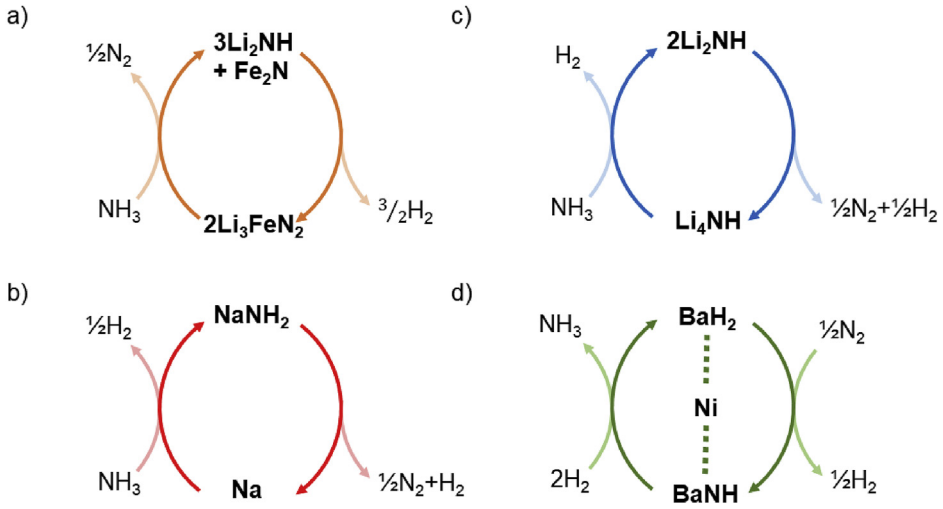

Fig. 5. Examples of proposed reaction cycles involving metal amides and imides in catalytic decomposition of ammonia using a) lithium imide – iron nitride composite b) sodium amide c) lithium imide and d) the catalytic or chemical looping synthesis of ammonia with barium hydride – nickel composite.

anion where hydrogen is covalently bonded to a metal or a non-metal. The late transition metals (TM) form homoleptic hydrido complexes with the general formula $[TH_n]^{m-}$ [150,151]. Theoretical studies have been undertaken to predict the probable existence of transition metal complex hydrides and a number have been synthesised and characterised including $Na_2Mg_2NiH_6$, $Na_2Mg_2FeH_8$, $Na_2Mg_2RuH_8$, $YLiFeH_6$, and Li_4RuH_4 [152–167]. Research efforts in the past two decades have increasingly focused on solids with the light element complexes of boron, aluminium, and nitrogen, i.e. $[BH_4]^-$, $[AlH_4]^-$, $[AlH_6]^{3-}$, $[NH_2]^-$, or $[NH]^{2-}$ coordinated to one or more metals [168–174].

4.1. Synthesis and crystal structures

Originally, mechanochemistry (ball milling) was the dominant synthesis approach for complex metal hydrides, via a metathesis (double substitution) reaction [175,176]. This method has been used to synthesize a number of new rare-earth (RE) based borohydrides. These compounds have a very rich chemistry, structural diversity, and thermal properties. Recently, solvent-based approaches have produced more phase pure products [177,178]. Such methods often rely on the initial synthesis of an ionic or polar covalent hydride, which is then reacted with a borane (BH_3) donating solvent such as dimethylsulfideborane, $(CH_3)_2SBH_3$. The reaction occurs via a nucleophilic attack on the electron deficient boron on the metal hydride. This reaction is only possible for an ionic or polar covalent metal hydride, MH_x. The product is often a metal borohydride solvate ($M(BH_4)_x$·solvent), which can be removed to obtain $M(BH_4)_x$ [177,179]. This approach allows purification by filtration, and to obtain a polymorphic pure product as well as the ability to recycle old samples of metal borohydrides. This was recently illustrated by synthesis of a series of rare earth metal borohydrides [180]. It was observed that only the ionic SmH_3 can react (and not the more metallic dihydride, SmH_2). The product, in this case, is $Sm(BH_4)_3$·$(CH_3)_2S$, which produces $Sm(BH_4)_2$ via reductive desolvation [177,180].

The crystal structures of monometallic borohydrides (Fig. 6) often resemble structures of metal oxides, illustrated by the structures of $Ca(BH_4)_2$-polymorphs, which are isomorphous to TiO_2 polymorphs [172]. This structural analogy is because BH_4^- and O^{2-} are isoelectronic [181]. The most electropositive metals, e.g. Na, K, Rb, and Cs are the most ionic and have high melting points and stabilities. Divalent rare earth (RE) metal borohydrides also form relatively ionic structures, and polymorphs of $Yb(BH_4)_2$ resemble polymorphs of $Ca(BH_4)_2$ [182]; whereas $Sm(BH_4)_2$ and $Eu(BH_4)_2$ are isostructural to different polymorphs of $Sr(BH_4)_2$ [183,184]. In contrast, more electronegative metals, such as Al and Zr, form molecular, covalent, and volatile compounds, e.g. $Al(BH_4)_3$ and $Zr(BH_4)_4$ [185]. Mono-metal borohydrides in between these two extremes have often pronounced directional bonding and some

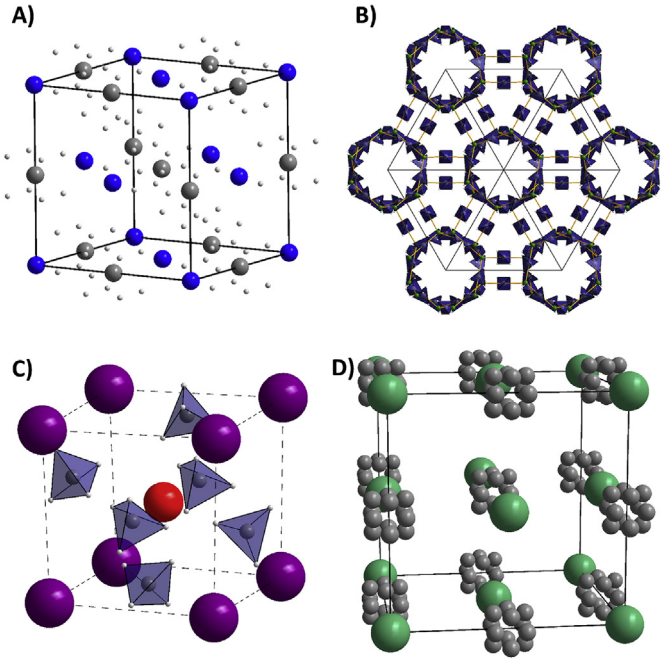

Fig. 6. Crystal structures of selected metal borohydrides highlighting the fascinating structural diversity. (A) The ionic Rock salt structure of $NaBH_4$, with averaged H positions shown (B) The porous and partly covalent framework structure of γ-$Mg(BH_4)_2$ with ~33% open space [189]. (C) The structure of cesium strontium borohydride, $CsSr(BH_4)_3$, is highlighting the resemblance to the perovskite structure [202]. (D) The crystal structure of β-KB_3H_8 [230]. The multiplicity of boron illustrates the dynamics of the B_3H_8- groups in this compound and thus hydrogen has been omitted. Colour code: H: white; B: gray; Mg: light green; Cs: purple; Sr: red; K: dark green. (For interpretation of the references to colour in this figure legend, the reader is referred to the Web version of this article.)

degree of covalency and exist as framework structures; for example, rare earth metal borohydrides, $RE(BH_4)_3$, with framework structures related to that of $Y(BH_4)_3$ [180,186]. This can lead to polymorphism as observed for $M(BH_4)_2$, M = Mg or Mn, which has both a high pressure polymorph, δ−$M(BH_4)_2$, with high hydrogen densities, and a polymorph with an open zeolite-type structure, γ−$M(BH_4)_2$; among a total of seven known polymorphs [187–190].

Transition metal borohydrides with electron configurations d^0, d^5, or d^{10} are often stable at room temperature, e.g. $Zr(BH_4)_4$, $Mn(BH_4)_2$, and $Cd(BH_4)_2$ [191,192]. Other compounds can be stabilised by ammonia or a coordination solvent to form, for example, $[Fe(NH_3)_6](BH_4)_2$ and $[Co(NH_3)_6](BH_4)_2$ [193,194]. Another approach is to stabilise these compounds as bi-metallic borohydrides, e.g. $LiZn_2(BH_4)_5$, which has an interpenetrated framework structure. The structure of $LiZn_2(BH_4)_5$ can also be described as being built from anionic complexes, i.e. $[Zn_2(BH_4)_5]^-$ [195–197].

Structures consisting of discrete anionic complexes often occur for bi-metallic borohydrides (Fig. 6), as a consequence of the electronegativity difference between the two metals. The most electronegative metals form partly covalent bonds to BH_4^- complexes, usually by edge sharing, e.g. $MSc(BH_4)_4$, M = Li, Na, or K, consisting of $[Sc(BH_4)_4]^-$ [198–200]. Known structure types are also adopted by metal borohydrides, e.g. the perovskite structure [201–203]. The structure types formed from the metathesis reaction between $LiBH_4$ and $RECl_3$ include $LiRE(BH_4)_4$ ($CuAuCl_4$-type with RE = Sc, Yb, Lu), α-$RE(BH_4)_3$ (distorted ReO_3-type, RE = Y, Pr, Sm, Gd, Tb, Dy, Ho, Er, Yb), and β-$RE(BH_4)_3$ (ReO_3-type, RE = Y, Ce, Pr, Sm, Ho, Er, Yb). A small number of trimetallic borohydrides are also known, e.g. $Li_3MZn_5(BH_4)_{15}$, M = Mg or Mn [204].

Mixed-cation, mixed-anion borohydrides with ordered structures have also been discovered, such as spinel-type $LiRE(BH_4)_3Cl$ (RE = La, Ce, Pr, Nd, Sm, Gd) [182,205–214]. This structure contains isolated tetranuclear anionic clusters of $[Ce_4Cl_4(BH_4)_{12}]^{4-}$ charge balanced by Li^+ cations occupying two-thirds of the available positions [215–219]. Another example of double-anion hydrides with ordered structures is $KZn(BH_4)Cl$ [220]; otherwise, anion disorder is more common, as observed for $NaY(BH_4)_2Cl_2$ [221].

The anion substitution of metal borohydrides contributes to the structural diversity, reactivity and changes of properties [172]. Fluorine substitution of the hydride atom in the borohydride complex of alkali metal borohydrides was observed, but unfortunately it was accompanied by release of diborane [222,223]. The heavier halides, Cl^-, Br^-, and I^-, often readily substitute the borohydride complex [224], which in many cases leads to disordered structures or solid solutions [225–229].

4.2. Complex metal aluminium hydrides

The properties of $NaAlH_4$ and $LiAlH_4$ continue to be studied to elucidate the process involved in catalytic cycling initiated by titanium and other transition metal containing compounds [231–235]. Advances in instrumentation and sample containment have allowed for *in situ* characterization of these processes using NMR spectroscopy, and X-ray and neutron diffraction. Such studies show that $NaAlH_4$ formation and decomposition progress via the formation of Na_3AlH_6 [232,233], whereas the solvent-mediated synthesis of $LiAlH_4$ occurs directly [233,234]. In addition, the titanium additive tends to form a range of $Al_{1-x}Ti_x$ phases including Al_3Ti [231,232]. Destabilization of $NaAlH_4$ has also been studied by the addition of aluminium sulphide and by nano-confinement [236,237].

One of the first intensively studied complex light metal aluminium hydrides of type $MAlH_4$ was $LiAlH_4$, originally considered as a reducing agent [238]. The most explored metal alanate for solid-state hydrogen storage is $NaAlH_4$, including its crystalline dehydrogenation intermediates. A few mol% of Ti catalysts significantly enhances the kinetics of hydrogenation of alanates [239]. More recently, crystal structures of complex aluminium hydrides with large metal cations, i.e. $Eu(AlH_4)_2$ and $Sr(AlH_4)_2$, as well as that of their intermediate decomposition products $EuAlH_5$ and $SrAlH_5$, were solved [240]. The structure of potassium alanate, $KAlH_4$, is also known, but not three of its intermediates [241]. The hydrogen (deuterium) positions in $SrAlD_5$ could be determined from neutron diffraction data and, based on this, the connectivity of corner-sharing $[AlD_6]^{3-}$ octahedra was established [242]. $CsAlH_4$ and $RbAlH_4$ can be prepared either by ball-milling of salts with $NaAlH_4$ or $LiAlH_4$, or directly by hydrogenation of the metals by ball-milling at elevated hydrogen pressures with small amounts of Ti catalysts [243–245]. Even though the storage capacity of 2.5 wt% H_2 is relatively low, direct synthesis from the metals indicates that both compounds form and decompose reversibly. The decomposition pathway is complex compared to that of the light alkali metal alanates and intermediate structures are difficult to isolate. Transition metal and rare earth aluminium hydrides have been shown to be unstable [246,247]. However, $TaH_2(AlH_4)_2$ and $Y(AlH_4)_3$ possess a remarkably high stability [248]. Recently it has been shown that, upon heating, $Y(AlH_4)_3$ dehydrogenation proceeds via four steps with the first dehydrogenation step being reversible [249]. Only a limited number of unstable complex metal aluminium hydrides have been reported so far and most of their crystal structures still remain unknown. Below Al we find Ga in the periodic table. Ga is more likely to form complex hydrides with the help of electrons from an electropositive counterion. With one electron added, Ga will form a carbon like chemistry, as exemplified by $Rb_8Ga_5H_{15}$ where $Ga[GaH_3]_4^{(5-)}$ forms an entity with a neopentane structure, where carbon has been substituted by gallium [602]. Similar species with hydrocarbon structures are for example $[GaH_2]_n^{(n-)}$ with a polyethylene structure and $Ga_3H_8^{3-}$ with a propane structure [603]. If this property could be transferred to Al, we could expect to make possible a large number of new Al complexes.

4.3. Aluminium based complex hydrides

Aluminium is a cheap and abundant element, having low weight per electron exchanged. The small size and high charge make the Al^{3+} cation highly polarizing and thus complex forming. Three coordinate Al^{3+} in $Al(BH_4)_3$ easily converts to four-coordinate complexes upon a reaction with more ionic borohydrides, yielding $M[Al(BH_4)_4]$ composites with very high hydrogen content, where M is an alkali metal or ammonia cation [250–252].

Nitrogen donor atoms compete successfully for the Al^{3+} coordination sites, producing homoleptic $[Al(en)_3](BH_4)_3$ [253] or heteroleptic $[Al(en)(BH_4)_2][Al(BH_4)_4]$ complexes [254], depending on the ratio of Al^{3+} and ethylenediamine (*en*) in the reaction mixtures. The stoichiometry control enables a series of borohydride complexes with nitrogen-containing ligands, similar to ammoniates of Mn and Y borohydrides [149,255–257], of potential interest for hydrogen storage and ion conductivity. The heteroleptic Al complex with ammonia borane (NH_3BH_3, AB), namely $[Al(BH_4)_3(AB)]$ shows an endothermic dehydrogenation to a single decomposition product, identified as $[Al(BH_4)_3(HBNH)]_n$ [258]. The coordination of the starting and of the dehydrogenated AB to Al^{3+} allows one to consider the latter as an effective template for a reversible dehydrogenation of the hydride complexes with Al^{3+} [258,259]. Recently, this idea was further explored in a series of complexes between various Al salts and AB-derived RNH_2BH_3 ligands [254]. It was shown that two ABs can be coordinated to a single Al atom, opening a way to materials with a higher H-content.

Ball milling of metal alanates with AB results in Al amidoborane complexes, $M[Al(NH_2BH_3)_4]$, where the N-donor ligand becomes

anionic and thus shows high affinity to Al^{3+} [260,261]. For M = Na, a partial hydrogen reversibility was reported for the amorphous decomposition products. Ball milling of $LiAl(NH_2)_4$ and $LiBH_4$ resulted in $Li_2Al(NH_2)_4BH_4$, which was the first reported compound containing both $[Al(NH_2)_4]^-$ and BH_4^- anions [262]. Aluminium amidoborane ammoniate complexes have also been reported to form via the reaction of AlH_3Et_2O with ammonia borane ammoniate forming $[Al(NH_2BH_3)_6^{3-}][Al(NH_3)_6^{3+}]$ [263]. This solution based synthesis prevents possible decomposition of the products by avoiding the high-energy impact associated with ball milling.

Despite pure aluminium hydride (AlH_3, alane) not being classified as a formal complex hydride, complexes of alane have been synthesised with a range of Lewis bases including amines, ethers and phosphines [264–266]. A number of complexes have been recently synthesised and characterised including tetramethylpropylenediamine (TMPDA) alane, trimethylamine alane, and dioxine alane. DFT has been used to predict the stability of other complexes to identify potential for reversible hydrogenation. Many complexes are liquid at or above room temperature and as such may be of interest as liquid hydrogen carriers.

4.4. Thermodynamic predictions

The thermodynamic properties of a complex hydride can be obtained by the CALPHAD approach [267]. The goal is to describe the dependence of the Gibbs Free Energy (GFE) as a function of temperature. The dependence from pressure and composition of their free energy can be neglected because complex hydrides are condensed phases with a fixed stoichiometry. For simple compounds, the temperature dependence of the GFE can be described using the following polynomial expression [268]:

$$G = A + BT + CTlnT + DT^2 + ET^3 + FT^{-1} + \sum_n G_n T^n \quad (1)$$

where parameters A–G_n are optimized on the basis of available experimental data. When thermodynamic data are available at low temperatures, a more complex expression of GFE, based on the Einstein model for the molar heat capacity can be used. In the absence of experimental information, the output of various thermodynamic or quantum mechanical models can be used [269]. An estimation of the energy of formation of a compound can be obtained by ab-initio modelling. If necessary, different sets of parameters can be used to describe GFE in different temperature ranges. A CALPHAD assessment of various complex hydrides has been carried out in recent years. A summary of thermodynamic description of selected complex metal hydrides is reported in Table 1.

4.5. Hydrogen release and uptake

The stability of metal borohydrides based on the observed decomposition temperature, T_{dec}, is correlated to the metal-borohydride coordination via the Pauling electronegativity, see Fig. 7 [172,180,276]. The reaction mechanism for hydrogen release and uptake in complex hydrides has been extensively studied since the discovery of hydrogen desorption and absorption at moderate conditions in Ti-catalyzed $NaAlH_4$, as mentioned above [239]. However, analogous reactions for hydrogen release and uptake for metal borohydrides are complex and poorly understood [199]. Bi- and tri-metallic borohydrides usually decompose via formation of more stable mono- or bimetallic borohydrides. Eutectic melting of metal borohydrides may also be involved in their decomposition reactions, for example, in the systems $LiBH_4$–$CaBH_4$ and $LiBH_4$–$NaAlH_4$ [277–284].

The possible effect of additives in metal borohydrides has been extensively studied recently [237,285–293]. Several studies have shown a decrease in temperature for the first desorption of different polymorphs of $Mg(BH_4)_2$ by using TM based additives. During absorption, the major kinetic effect has been observed for partly decomposed $Mg(BH_4)_2$ at moderate conditions (<12 MPa H_2 and <260 °C).

The reversible hydrogenation of metal borohydrides, such as $NaBH_4$ and $Mg(BH_4)_2$, has been studied with additives [285,286,294]. Additives to $NaBH_4$ reduce the decomposition temperature by at least 85 °C, which allows the event to occur below its melting point, enabling the possibility of rehydrogenation. Following the success of transition metal boride additives on $NaBH_4$, these compounds were also added to $Mg(BH_4)_2$ in order to enhance the reaction kinetics during hydrogen cycling and to inhibit the formation of $[B_nH_n]^{2-}$ ($n = 10, 12$) species. An isotopic exchange study of porous and dense Mg-borohydride with Raman spectroscopy showed that solid state H (D) diffusion is considerably slower than the gas-solid H→D exchange reaction at the surface and is thus a rate-limiting step for hydrogen sorption in $Mg(BH_4)_2$ [295]. These systems have been studied by XRD, X-ray absorption spectroscopy, NMR, and FT-IR [296–300].

Rehydrogenation of the composite KB_3H_8–2 KH ($T = 100$–200 °C, $p(H_2) = 380$ bar and $t = 24$ h) reveal formation of higher borates, e.g. $B_nH_n^{2-}$, $n = 9$, 10 or 12, and about one-third of the boron as KBH_4 [230]. Rehydrogenation of the *closo*-borate composites $M_2B_nH_n$–$(n-2)$MH, ($T = 300$–400 °C, $p(H_2) = 0.5$–1.0 kbar and $t = 24$ h) reveal formation of MBH_4 only for the $M_2B_{10}H_{10}$ precursor at the physical conditions applied [301]. Unidentified intermediate compounds were also observed using *in situ* diffraction experiments [296,297,301].

Nano confinement has been shown to have a significant influence on hydrogen release and uptake, and has received significant interest. Volatile complex hydrides such as $Ti(BH_4)_3$ have been stabilised by nanoconfinement in MOFs for several months. Upon confinement, the density of the $Ti(BH_4)_3$ is twice that of the gaseous material [302]. Nanoconfinement has been used to change the hydrogen release and uptake properties of a range of compounds and composites. The effect is strongest in the first cycle [236,278,279,303–312].

4.6. Reactive hydride composites

While many complex hydrides show very high gravimetric hydrogen storage densities, they suffer from sluggish reaction kinetics and/or unfavourable thermodynamic properties [313]. However a combination of $LiNH_2$ and LiH showed superior kinetic and thermodynamic properties to the pure hydrides by themselves [314]; followed by systems consisting of a metal hydride and a metal amide or borohydride [315]. More recently, a range of other composites have been discovered [316–322] such as:

$$Mg(NH_2)_2 + 2\ LiH \leftrightarrow Li_2Mg(NH)_2 + 2H_2 \quad (2)$$

as well as MgH_2 and $LiBH_4$ [323]. With the addition of suitable additives, the latter shows an extremely high reversible gravimetric storage density of around 10 wt%, according to the reaction:

$$MgH_2 + 2\ LiBH_4 \leftrightarrow MgB_2 + 2\ LiH + 4H_2 \quad (3)$$

During desorption, the components of the different hydrides react to form a stable compound, by which the total reaction enthalpy is lowered and the kinetics improved. However, in spite of improvements in the thermodynamic and kinetic properties of such high capacity hydrides, the working temperatures of such two

Table 1
Assessed Gibbs Free Energy as a function of temperature (T) for selected complex hydrides. R is the gas constant.

Compound	Phase	Reference system	Gibbs Free Energy (J/mol of f.u.)	T range (K)	Ref.
$LiBH_4$	Ortho	Li_{cub}, H_{gas}, B_{rhomb}	−206438.80 + 312.84347*1.5R+3R*T*LN(1-EXP(-312.8434*T^{-1}))-0.0568714*T^2-3.01186·10^{-5}*T^3	300–383	[270]
$LiBH_4$	Hex	Li_{cub}, H_{gas}, B_{rhomb}	−210953.207 + 328.4978*T-56.52963*T*LN(T)-0.05777964*T^2+4.303902·10^{-6}*T^3+766385.13*T^{-1}	383–551	[270]
$LiBH_4$	Liq	Li_{cub}, H_{gas}, B_{rhomb}	−222466.273 + 751.660356*T-124.7*T*LN(T)	551–1000	[270]
$Li_2B_{12}H_{12}$	Cub	Li_{cub}, H_{gas}, B_{rhomb}	−7.833·10^5+702*T	300–1000	[270]
$Li_2B_{10}H_{10}$	Hex	LiH_{cub}, H_{gas}, B_{rhomb}	−3.48·10^5+480*T	300–1000	[270]
$NaBH_4$	Cub	Na_{cub}, H_{gas}, B_{rhomb}	−215396.375 + 362.347799*T-65.62694*T*LN(T)-.039943205*T^2+2.0758·10^{-6}*T^3+82445.5*T^{-1}	300–600	[271]
$NaBH_4$	Cub	Na_{cub}, H_{gas}, B_{rhomb}	−246176.6 + 712.133426*T-116.5235*T*LN(T)-.00822906*T^2-2.133325·10^{-7}*T^3+3283588.5*T^{-1}	600–900	[271]
$NaBH_4$	Cub	Na_{cub}, H_{gas}, B_{rhomb}	−156907.445−242.126185*T+22.42824*T*LN(T)-.1050230*T^2+1.253794·10^{-5}*T^3-7527375*T^{-1}	900–1000	[271]
$NaBH_4$	Liq	$NaBH_{4,cub}$	+16926−21.756*T	300–505	[271]
$NaBH_4$	Liq	Na_{cub}, H_{gas}, B_{rhomb}	−217735 + 693*T-119.233*T*LN(T)	505–1000	[271]
KBH_4	Cub	K_{cub}, H_{gas}, B_{rhomb}	−293231.57 + 1332.6103*T-226.809*T*LN(T)+.19700505*T^2-5.85629833·10^{-5}*T^3+1955620*T^{-1}	300–600	[271]
KBH_4	Cub	K_{cub}, H_{gas}, B_{rhomb}	−488023.684 + 3356.66883*T-514.005*T*LN(T)+.3227912*T^2-5.0464016·10^{-5}*T^3+2333251*T^{-1}	600–800	[271]
KBH_4	Cub	K_{cub}, H_{gas}, B_{rhomb}	−288613.971 + 822.480344*T-134.187*T*LN(T)+.0033015*T^2-3.8573666·10^{-7}*T^3+3833085*T^{-1}	800–1000	[271]
KBH_4	Liq	$KBH_{4,cub}$	+19176−21.841*T	300–1000	[271]
$LiK(BH_4)_2$	Ortho	$LiBH_{4,cub}$, $KBH_{4,cub}$	−1300 + 3.53*T	300–1000	[271]
α-$Mg(BH_4)_2$	Hex	Mg_{hex}, H_{gas}, B_{rhomb}	−222624.9 + 158.46145*T-35.22138*T*LN(T)-0.035975*T^2	300–1000	[272]
β-$Mg(BH_4)_2$	Ortho	$Mg(BH_4)_{2,hex}$	+12954.437−26.4266*T	300–1000	[272]
γ-$Mg(BH_4)_2$	Cubic	$Mg(BH_4)_{2,hex}$	+3900	300–1000	[272]
$Mg(AlH_4)_2$	Tetr	Mg_{hex}, H_{gas}, Al_{cub}	−79000 + 386*T	300–1000	[273]
$NaMgH_3$	Tetr	Na_{cub}, Mg_{hex}, H_{gas}	−156905.827 + 186.831990*T-33.6064520*T*LN(T)-0.0612717213*T^2	300–1000	[274]
$LiNH_2$	Tetr	Li_{cub}, H_{gas}, N_{gas}	−196871.25 + 161.64083*T	300–1000	[275]
$Li_2(BH_4)(NH_2)$	Tetr	$LiBH_{4,\ ortho}$, $LiNH_{2,\ tetr}$	−6600	300–1000	[275]
$Li_4(BH_4)(NH_2)_3$	Cub	$LiBH_{4,\ ortho}$, $LiNH_{2,\ tetr}$	−13900	300–1000	[275]

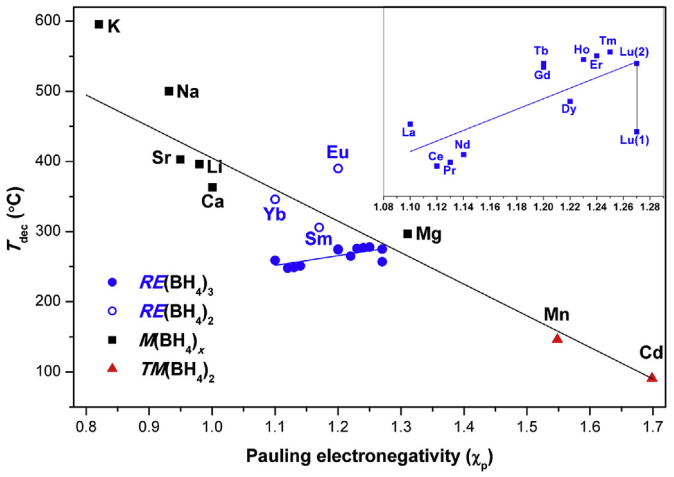

Fig. 7. Comparison of the Pauling electronegativity and the decomposition temperature of complex metal hydrides. Generally, a decreasing decomposition temperature is observed with increasing Pauling electronegativity of the metal. However, the opposite trend is observed for the series of rare-earth metal borohydrides, as further highlighted in the inset [180,276]. Trend lines have been added for clarity.

component reactive hydride systems are significantly above 100 °C. However, recent work showed that by combining the three different hydrides, $LiBH_4$, $Mg(NH_2)_2$, and LiH, high capacity complex hydrides can indeed be used for hydrogen storage at temperatures below 100 °C [324]. The influence of LiH and/or $LiBH_4$ on the hydrogen sorption properties and rehydrogenation has been further investigated for La-, Er- and Pr-based borohydrides [325–327]. For the $3LiBH_4 + Er(BH_4)_3 + 3LiH$ composite, 3.5 wt% H was desorbed after the third cycle from a maximum of 6 wt% [327].

4.7. New properties

Research efforts during the past two decades have led to the discovery of many new series of hydrides, in some cases with unexpected and fascinating properties [172–174]. Optical properties were discovered for perovskite-type metal borohydrides [201,328]. Rare earth metal borohydrides have magnetic properties which deviate somewhat from the Landé formula for calculation of magnetic moments, suggested to be due to strong coupling of orbitals [180]. Among the rare earth metal borohydrides, $RE(BH_4)_3$, praseodymium has the most extensive polymorphic chemistry with five polymorphs, denoted as α–, β–, β'–, β''–, and r–$Pr(BH_4)_3$ [329]. This series of polymorphs appear to be the first example of stepwise negative thermal expansion, which appears to depend on gas atmosphere, e.g. H_2 or Ar.

4.8. Metal closo-borates as solid-state electrolytes

The pursuit of a solid-state electrolyte with high ion conductivity has resulted in the identification of a range of metal *closo*-borates and their derivatives that show great promise [172,330]. Many *closo*-borates exhibit a polymorphic structural transition at elevated temperature, which can exhibit structural dynamics such as reorientational disorder of anions and partial occupancy of cations [331,332]. The most promising ion conductors are metal *closo*-borate derivatives with monovalent anisotropic charge density of the anion, e.g. $[CB_{11}H_{12}]^-$ and $[CB_9H_{10}]^-$. Impressive ion conductivity is also observed in isotropic metal *closo*-borates such as $[B_{12}Cl_{12}]^{2-}$, albeit at elevated temperatures [333]. Particular solvated *closo*-borates have also been shown to melt near 130 °C and display a step-function increase in ion conductivity in the molten state [334]. Thus, complex hydrides have potential applications in electrochemical, as well as hydrogen, storage. Recent progress in electrochemical storage is detailed in Section 9.

5. Intermetallic hydrides. Structure-properties relationship

5.1. Intermetallic hydrides – a short historical overview

Binary metal hydrides are either very stable (LaH_2, YH_2, ZrH_2, TiH_2) releasing hydrogen on heating to several hundred °C (as an example, 800 °C for YH_2) [335], or very unstable requiring application of kbar level of hydrogen pressure to form a hydride in the metal-hydrogen system (NiH, FeH) (as an example, above 5 kBar H_2 for Ni–H system) [336]. Both alternatives are inconvenient for the

practical storage of hydrogen gas. Thus, the discovery of intermetallic hydrides having intermediate stabilities between these two mentioned groups of hydrides opened attractive new possibilities to build practical systems for the storage of hydrogen gas in a form of solid hydride.

Early works on intermetallic hydrides, which appeared in the 1950s, had already shown that intermetallic compounds containing hydride-forming (Zr) and transition (Ni) metals can reversibly absorb large amounts of hydrogen. Even though the very first examples of such hydrides, ZrNiH and $ZrNiH_3$, formed by ZrNi intermetallic still appeared to be rather stable, studies showed that the H content in $ZrNiH_3$ (H/Me = 1.5), was superior to the value reached at the same P-T conditions for the equivalent amounts of two individual metals, Zr and Ni (H/Me = 1.0) [337]. Furthermore, a decrease in the H_2 release temperature by several hundred °C as compared to the binary hydride ZrH_2 was another significant benefit. From a structural viewpoint, the reason for the decreased hydride stability is that the interstitial sites occupied by hydrogen atoms in intermetallic hydrides have mixed chemical surroundings so the hydrogen interacts with both hydride-forming (e.g. Zr) and non-hydride-forming (e.g. Ni) metal atoms in the metal sublattice. Such interactions decrease the stability relative to the pure binary hydride (e.g. ZrH_2). Neutron scattering is recognized as an important tool of choice to directly locate H/D atoms inserted into the metal sublattice, as was demonstrated in 1961 during an investigation of one of the first structures of the ternary hydrides, Th_2AlD_4, which was probed by neutron diffraction and showed that H/D atoms occupy tetrahedral Th_4 sites [338,339].

Nevertheless, these interesting behaviors of ternary hydrides required significant improvements before becoming suitable for practical applications. The discovery of metal hydrides appropriate to conveniently store hydrogen was announced in the late 1960s when intermetallic hydrides of the AB_5 composition with A = Rare Earth metal and B = Ni or Co, including $LaNi_5$, showed excellent performance as chemical reversible stores of hydrogen gas. In fact, the excellent performance of $LaNi_5H_{6.7}$ as a hydrogen storage material [340,341] was discovered by fortune during systematic studies of $SmCo_5$ as a high coercivity permanent magnet material at Philips Research Labs in Eindhoven, Netherlands led by Prof. K. H. Jürgen Buschow [342].

It was observed that the coercivity of the $SmCo_5$ powders significantly decreased when storing the material in open air because of the chemical interaction with water vapour which released hydrogen gas in the following process:

$$2\ SmCo_5 + 3H_2O \rightarrow Sm_2O_3 + 10\ Co + 3H_2$$

while in a subsequent step a formation of intermetallic hydride $SmCo_5H_{2.8}$ [340]

$$SmCo_5 + 1.4H_2 \rightarrow SmCo_5H_{2.8}$$

occurred, causing a decay in coercivity.

A nonmagnetic analogue of $SmCo_5$ was selected for the study of the hydrogenation process to understand the fundamental aspects of the interactions in the metal-hydrogen system by utilizing NMR, and $LaNi_5$ was the choice [343].

This resulted in the discovery of excellent features of H storage in $LaNi_5$ and its analogues as they are able to quickly, in just seconds, form hydrides when the metal alloy is exposed to hydrogen gas and to reversibly release H_2 when lowering the pressure in the system, while reaching high H/Me ratios exceeding 1.0 and high volumetric H capacity surpassing the values for liquid hydrogen. Particularly attractive behaviors were found for $LaNi_5H_{6.7}$ as it was formed at pressures just slightly higher than atmospheric pressure ((PH_2 absorption/PH_2desorption @ 20 °C of 1.83/1.36 atm H_2) and it was able to provide stable hydrogen pressure during hydrogen absorption and desorption at equilibrium conditions [344]. Substitutions on the Ni and La sites to form $(La_{1-x}R_x)Ni_4M$, where M represents Pd, Co, Fe, Cr, Ag or Cu, and for $La_{0.8}R_{0.2}Ni_5$ where R represents Nd, Gd, Y and Er, also Th and Zr, significantly changed the thermodynamics of the metal-hydrogen interactions yielding hydrides with a broad range of stabilities, which were significantly different from the characteristics of $LaNi_5H_{6.7}$.

As the equilibrium pressure of hydrogen for $LaNi_5H_{6.7}$ is close to atmospheric pressure, a natural progression was to use $LaNi_5$ as a negative electrode and to charge it electrochemically with hydrogen when using an aqueous electrolyte. This has been successfully realized and $LaNi_5$ showed an electro-chemical capacity of 330–390 mAh/g corresponding to the composition $LaNi_5H_{5\text{-}6.7}$ [345–347].

Even though $LaNi_5$ was found to be unsuitable for use as an electrode in the Ni-Metal Hydride battery because of its corrosion degradation in KOH solution, changing the composition by doping on both La and Ni sites to form $La_{0.8}Nd_{0.2}Ni_{2.5}Co_{2.4}Si_{0.1}$ resulted in a drastic improvement of the cycling stability, which was related to decreased stresses in the material because the doping reduced the lattice expansion during the hydrogenation and therefore reduced the corrosion, as it was caused by repeated large expansion and contraction of the lattice [346].

The early stages of the development of intermetallic hydrides received an outstanding contribution from the work performed at Philips Research Laboratories with a leading role of Prof. K. H. J. Buschow who, in addition to the discovery of $LaNi_5$ and characterization of the basic features of the metal-hydrogen interactions in the $(La,R)(Ni,TM)_5$ systems and a huge number of novel intermetallic hydrogen absorbing compounds, also developed a fundamental modelling approach allowing explanation and prediction of the formation of the hydrides by using Miedema's rule of reversed stability [348,349]. This was complemented by systematic studies of the interrelations between structure, chemical composition and magnetism of intermetallic hydrides [350].

Studies of magnetism were particularly important as hydrogen appeared as an indispensable medium in the manufacturing of rare earth based permanent magnets, allowing the improvement of magnet performance by obtaining oxygen free powders and/or recycling $SmCo_5$, $Sm_2(Co,FeCu,Zr)_{17}$ and NdFeB-type magnets by using a Hydrogen Decrepitation process [351,352] and by using a Hydrogen-Disproportionation-Desorption-Recombination route [353,354].

Finally, for the intermetallics exhibiting a magnetocaloric effect, the cooling efficiency of the alloys can be improved by hydrogenation; indeed, for $La(Fe,Si)_{13}$ as hydrogen is accommodated in the metal lattice, the critical temperature increases significantly (by 200 K) reaching 450 K for the hydride $La(Fe,Si)_{13}H_1$. This is accompanied by a parallel increase of the average magnetic moment per Fe during a transformation of $La(Fe,Si)_{13}$ into its hydride $La(Fe,Si)_{13}H_1$ as a consequence of a hydrogen-caused volume expansion of 1.5% [352].

5.2. General characteristics of intermetallic hydrides

Metal hydrides are formed via the reversible interaction of a hydride-forming metal/alloy, or intermetallic compound (IMC), with H_2 gas:

$$M(S) + x/2\ H_2(g) \underset{\text{desorption}}{\overset{\text{absorption}}{\rightleftharpoons}} MH_x(S) + Q$$

where M is an individual metal, or a multicomponent alloy or IMC.

Typical M components include individual metals – for example, rare earths such as La, Ce, Nd or Pr, and elements such as Zr, Ti, Mg, Ca and V – and IMCs, which can include AB_5 (e.g. $LaNi_5$, $CaNi_5$), AB_2 (e.g. $ZrMn_2$, ZrV_2, $ZrCr_2$), AB (e.g. TiFe), and A_2B (e.g. Ti_2Ni, Zr_2Fe) compounds. For a binary IMC, A is typically a hydride-forming element, while B is a transition or non-transition metal/element that does not form a stable hydride under normal conditions.

Hydride formation is normally exothermic, with the amount of heat released being closely related to the host element or compound. In contrast, the reverse process of hydride decomposition is usually endothermic, thus requiring a supply of heat to induce hydrogen desorption. Hydrogen is stored in metal hydrides in atomic form (or as screened protons), so this results in a very high volumetric H capacity, up to 150 g_H/L, to be achieved; more than double the H density in liquid H_2 (70.8 g/L).

Many IMCs rapidly react with hydrogen. At ambient conditions, they also have equilibrium H_2 pressures that are convenient for practical use. Metal hydrides can therefore be used to safely store H_2, particularly in stationary [355] and portable applications [356]. Furthermore, heat can be stored using metal hydrides [357], such as hydrogen energy systems integrated with solar energy. Another application is metal hydride-based compression of H_2 gas [356], in which heat can be used to boost pressures to several hundred bar [358] (see Section 11).

The hydrogen storage properties of the most extensively studied groups of H storage alloys have been presented in several reviews, which can be consulted for further detailed data on the main classes of hydride-forming compounds, including AB_5 and AB_2 IMCs, and BCC alloys [349,359,360]. Practically achievable reversible H storage capacities of most intermetallic hydrides do not exceed 2 wt% H – for example, 1.5 wt% for AB_5 hydrides, 1.8 wt% for AB_2, and 2.0 wt% H for BCC alloys. Light metal hydrides, such as MgH_2 and AlH_3, have therefore been investigated widely for H storage applications. Although these materials have high gravimetric capacities – 7.6 wt% H for MgH_2 and 10.1 wt% H for AlH_3 – they have other drawbacks, such as the high working temperature for MgH_2 [361,362] and the difficulty of directly synthesising AlH_3, which requires kbar H_2 pressures and high temperatures [363,364].

Generally speaking, recent efforts have aimed at improving the properties of metal hydride systems for practical applications by:

(a) increasing reversible H storage capacity by modifying the composition of known materials and by studying novel alloys;
(b) improving the kinetics of hydrogen absorption and desorption – as materials and on a system level – while adopting more convenient conditions for the operation of H energy systems;
(c) adapting the properties of metal-hydrogen systems by making them better suited for efficient H storage, for electrochemical applications as metal hydride battery anodes, as materials for heat storage, and for use in the compression of H_2 gas.

One interesting example involving MgH_2 is the use of reactive composites of MgH_2 with $LiBH_4$ catalyzed by additives [320]. This decreases the temperature for reversible H_2 desorption and absorption, while achieving a high rate of hydrogenation and H_2 release. FeF_3 was used as a catalyst, producing 5 wt% H_2 at a working temperature of 275 °C for the composite Mg–10 mol% $LiBH_4$–5 mol% FeF_3 [320].

5.3. Crystal and electronic structures of the intermetallic hydrides

Hydrogen storage properties of IMCs are closely related to their crystal and electronic structures, and their magnetic properties. Thus, we will briefly review fundamental features of metal-hydrogen systems from these three perspectives.

5.3.1. Structural chemistry

During hydrogen absorption by IMCs, H_2 dissociates at the surface and is stored as atomic H in the metal lattice by filling interstitial sites, most commonly tetrahedral and octahedral. As the number of these sites is higher than the number of metal atoms, H/M ratios exceeding 1, and reaching as high as 3.75, can be achieved in stable metal hydrides, if they have the appropriate chemical composition. This provides a high volumetric density of stored H in the solid state [365,366].

IMCs exhibit a close interrelation between their crystal chemistry and hydrogen sorption behaviour (H storage capacity and stability of the hydrides) allowing alteration and optimization of their H storage performance. Hydrogen accommodation by the metal lattice is typically accompanied by a modest (few percent) change of interatomic metal–metal distances. This results in a much more significant, 10–30%, increase in volume; normalizing this to the number of absorbed hydrogen atoms gives 2.5–3.0 $Å^3$/atom H. As an example, $LaNi_5H_6$ has a volume expansion of 18.9% [365] with two times smaller expansion along the axes of the unit cell, resulting in 7–8% expansion of the interatomic Me–Me distances. This leaves the Me-Me coordination number (CN) in the structure unchanged, as shown in Fig. 8. H atoms enter the interstices, which are available in the virgin intermetallic. Thus, such "isotropic" structures of the hydrides, with nearly even expansion along crystallographically inequivalent directions, are dominated by the Me–Me interactions. Hydrogen-metal interactions appear to be non-directional ones often with simultaneous partial occupancy of various types of positions [367,368].

Three important rules describe the formation of the intermetallic hydrides as related to their structural chemistry:

(a) structures should contain a significant number of active hydrogenation sites - sites with a high proportion of rare earth metals, Zr, Ti, Mg - that H atoms show a preference to occupy;
(b) size of a sphere to accommodate H atom in the filled interstices should be at least 0.4 Å;

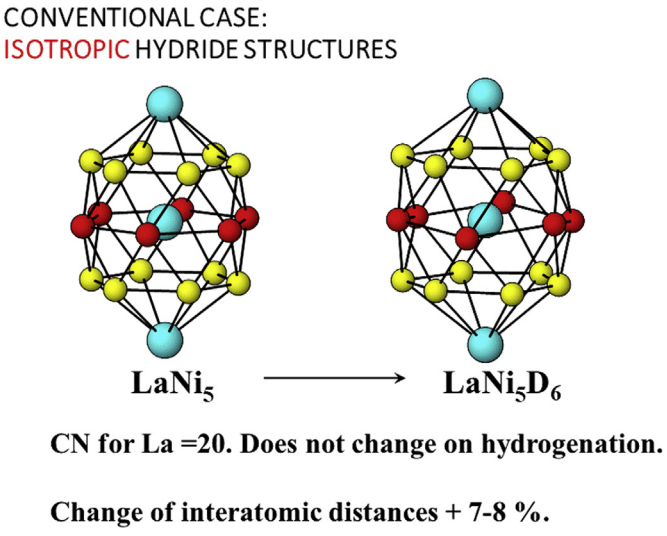

Fig. 8. Changes in a 20-vertex coordination polyhedron of La atom in $LaNi_5$ (hexagonal, ($a = 5.0125$; $c = 3.9873$ Å) during the formation of $LaNi_5H_6$ hydride (hexagonal; $a = 5.426$; $c = 4.269$ Å).

(c) the shortest H—H separations between the filled interstices should be at least 1.8—2.1 Å.

Formation of stable hydrides takes place following these rules, as shown in [367,368].

However, this "typical" case does not cover a large group of interesting yet insufficiently studied compounds, the so-called "anisotropic" hydrides [367].

5.3.2. Electronic structures

The stability of the hydrides is linked to their electronic structures. Formation of the hydrides is, in this regard, influenced by:

(a) chemical interaction between hydrogen and metals resulting in the appearance of new states below the Fermi level of the metal;
(b) changes in the cohesive energy of the host alloy induced by the expansion of the host structure with H insertion [369].

While (a) results in energy release because of the *M*-H bonding, (b) needs energy consumption used to achieve deformation of the metal sublattice during the expansion of the metal framework. Their balance defines the stability of the formed metal hydrides.

Interaction of hydrogen with the atoms of the metal sublattice results in various phenomena including modification of the long-range structural order, changes of the magnetic order and the valence state of the constituting metal atoms (most significantly appearing for the rare earth metals, e.g. Ce).

The chemical effect (a) can be influenced by tailoring the position and density of states at the Fermi level, while (b) is an effective way of influencing the formation energy of hydrides. Therefore, to design relatively less stable hydrides (allowing hydrogen to be easily released) one approach is to vary the cohesive energy of the alloys by performing compositional modifications [369].

For $LaNi_5H_6$ [370], belonging to the AB_5 Haucke phases, one of the first and the most studied group of reversible hydrogen storage alloys, its electronic structure is dominated by the 3*d*-Ni states, which become narrower than in the host structure due to lattice expansion. The structure of $LaNi_5H_6$ is characterised by a nondirectional bonding between the metal sublattice and hydrogen since H atoms show statistical distribution in three types of tetrahedral sites - La_2Ni_2, $LaNi_3$ and Ni_4, with a preference to the La-containing sites. The role of (a) and (b) effects have been illustrated with the investigation of elemental substitutions in the AB_5 phase [371].

More recently, the AB_y stacking structures described by Khan, where $y = (5n + 4)/(n + 2)$ and n is an integer [372], have been a point of interest from both fundamental and application viewpoints [373—375].

Adjusting the y ratio and the *A* and *B* chemical composition, with multiple substitutions, where *A* is usually a RE and *B* is a TM element, can tune both hydrogen-absorption and magnetic properties of the metal sublattice.

For these hydrides with more complexity, a systematic study has been done for AB_3 and A_2B_7 IMCs. Fig. 9 shows the density of states (DOS) for $Y_2Ni_7H_8$, $La_2Ni_7H_8$ and $La_{1.5}Mg_{0.5}Ni_7H_8$ (La_2Ni_7 with an ordered substitution of La by Mg). The DOSs are characterised by a broad low energy structure extending from about −11 eV to -5 eV corresponding to the bands arising from nickel-hydrogen bonding. The *A* element contribution to the electronic structure is much more modest despite the larger affinity of *A* to hydrogen. Interestingly, the La-based hydrides show a continuity of the occupied states in their band structure while $Y_2Ni_7H_8$ shows the presence of well localized electronic states with a band gap around −5 eV [376,377].

This continuity of electronic states is associated with a simultaneous hydrogen insertion into a large number of interstitial sites, as much as 9 in the case of $La_{1.5}Mg_{0.5}Ni_7H_9$, Fig. 10 [378]. Formation of the structure proceeds via an even expansion of the hexagonal unit cell ($\Delta a/a = 7.4\%$; $\Delta c/c = 9.6\%$; $\Delta V/V = 26.3\%$). However, the expansion is more pronounced for the Laves type AB_2 layer, as detailed in Fig. 10, because of the higher content of H in this layer, $LaMgNi_4H_{7.56}$, compared to the AB_5 layers, 4.92 and 5.71 at.H/$LaNi_5$.

For the layered structures composed of AB_5 and AB_2 slabs, AB_3 ($1^*AB_5 + 2^*AB_2$) and A_2B_7 ($1^*AB_5 + 1^*AB_2$), their structural chemistry, electronic structure and metal-hydrogen interactions are described by two principally different mechanisms of interaction. In contrast to the conventional isotropic expansion of the lattice with nondirectional Me—H bonding, a totally different type of hydrogen interaction with metals has been observed, characterised and explained for the layered structured based anisotropic hydrides of AB_3 — $CeNi_3H_{2.8}$, and A_2B_7 — $Ce_2Ni_7H_{4.6}$ [379—381].

The main features of such an interaction are summarized in Table 2 in comparison with isotropic structures. The formation of directional Ni—H bonding takes place on hydrogenation and proceeds because of the transfer of electronic density from Ce to both Ni and H atoms. Thus, further to a partial negative charge on H, 0.5 to 0.6 e^-, Ni is also carrying a negative charge reaching a maximum value of 0.3 e^-. However, a partial positive charge on Ce is rather low (<1.5) and, obviously, far away from Ce^{3+} or Ce^{4+} configurations. Chains of H—Ni—H—Ni with strong covalent bonding can be found in the structure of $CeNi_3H_{2.8}$, Fig. 11, while the strongest Ni—H bonding is observed for H occupying Ni_4 tetrahedra.

Magnetic properties reflect variations in the electronic subsystem and are defined by the electronic structure of the material and will be considered in a separate publication [382].

6. Novel intermetallic hydrides and high entropy alloys

In 2004, a new paradigm of alloying strategy emerged based on the original concept of multi-principal-element alloys (MPEAs), which was initially proposed to develop materials with enhanced mechanical properties [383]. The principle is based on the mixing of elements giving close to equimolar compositions in the systems containing up to five and more elements. This may lead to the formation of simple single-phase solid solutions (body centred cubic-*bcc*, face centred cubic-*fcc* and hexagonal close packed-*hcp*). In each case, there is only one available lattice site to occupy by the

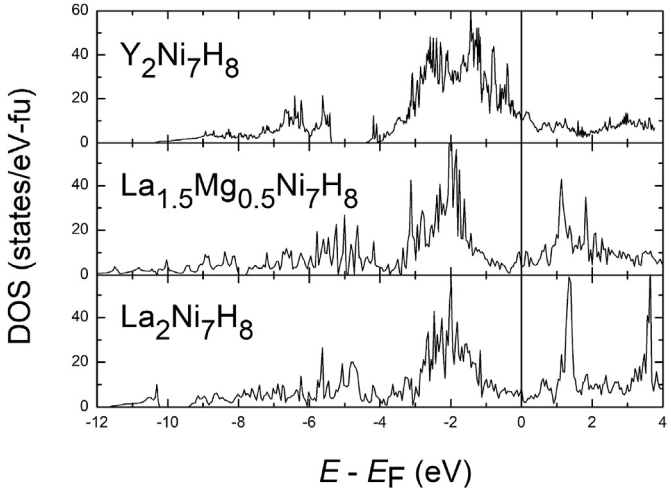

Fig. 9. Density of states for several $A_2B_7H_8$ hydrides [376,377].

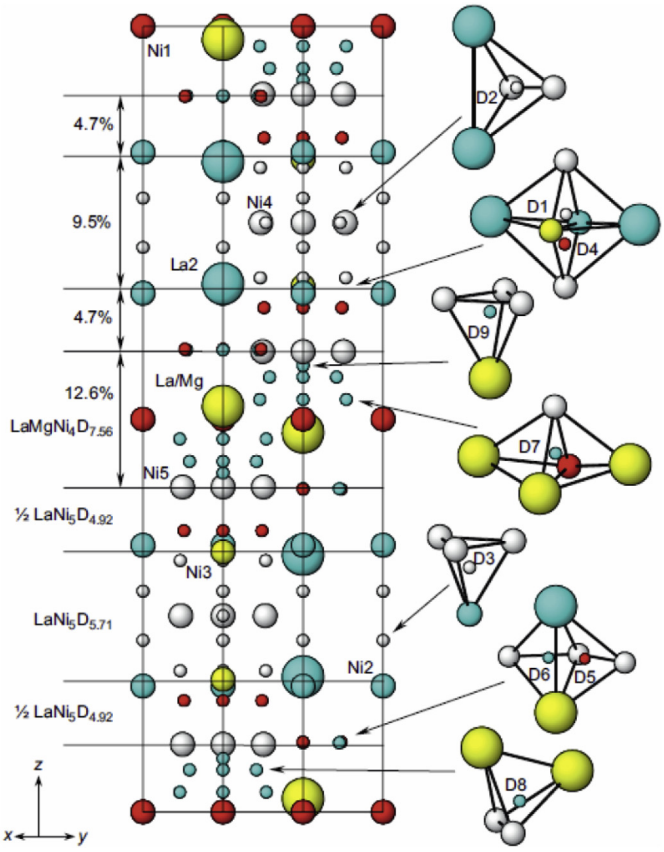

Fig. 10. Hexagonal crystal structure of $La_{1.5}Mg_{0.5}Ni_7H_{9.1}$ with 9 types of occupied by H sites. The H atoms are situated inside the $(La,Mg)_2Ni_2$, $(La,Mg)Ni_3$ and Ni_4 tetrahedra; La_2Ni_3 tetragonal pyramids and $(La,Mg)_3Ni_2$ trigonal bipyramids [378].

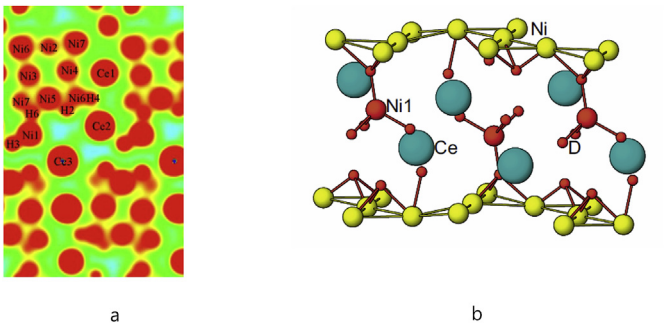

Fig. 11. Crystal and electronic structure of $CeNi_3H_{2.8}$. (a) Calculated charge density distributions in the 101 plane. The H−−Ni bonds are clearly seen. (b). .H−−Ni−−H−−Ni… chains with covalent Ni−H bonding.

different elements over which the elements are randomly distributed. The stability of such phases seems to be based on several chemical and physical characteristics, such as configurational entropy, mixing enthalpy, atomic misfit, valence electron concentration [384]. Among MPEAs, alloys with at least five principal elements with atomic concentrations in the range 5−35% are called high entropy alloys (HEAs) [383,385]. The underlying concept of "high entropy alloys", based on the formation of concentrated solutions, is illustrated in Fig. 12. It has been suggested that the high entropy of mixing is the cause of the stabilization of the single-phase solid solutions. It appears that a larger degree of solubility can be achieved in these alloys than what is suggested by the Hume-Rothery rules. Therefore, this alloying concept enables more flexible tuning of the material's properties.

Due to their multi-principal-element nature, this new class of alloys possesses exciting physical and mechanical properties [384,386]. Among four core effects known for these alloys [384], the development of large lattice strain distortions due to the atomic size mismatch among different component elements is particularly interesting and relevant for hydrogen storage. A quantitative parameter to describe the strained or distorted crystal lattice due to the mixing of many metals with different atomic radii is the lattice distortion, δ [385]. Despite the expected formation of large interstitial sites in MPEAs/HEAs, hydrogen sorption properties are scarcely investigated. Until recently, only a few reports investigated the hydrogen sorption properties of MPEAs/HEAs [387].

Among different classes of MPEAs/HEAs, refractory alloys with *bcc* lattice and related substitutions with lightweight elements have attracted particular interest. ICMPE and Uppsala University proposed the *bcc* alloy TiVZrNbHf as a promising material with improved hydrogen storage performance [388,389]. Hydrogenation of this alloy is a single step reaction (*bcc* ↔ *bct*) with a storage capacity exceeding the value for the conventional dihydride MH_2

Table 2
Distinguished crystal structure features of typical isotropic - $La_{1.5}Mg_{0.5}Ni_7H_9$ − and anisotropic - $CeNi_3H_{2.8}$ − structures.

Type of intermetallic hydride and typical representative References	Expansion mechanism	Interstices filled/H coordination	Metal-H bonding	Electronic structure features
Isotropic $La_{1.5}Mg_{0.5}Ni_7H_9$ [378]	Mostly uniform for AB_5 ($CaCu_5$) and AB_2 (Laves type) layers. Metal sublattice is a moderately expanded initial structure with linear expansion not exceeding 10 %.	Conventional interstices which are present in the initial intermetallics. Most commonly tetrahedra.	Non-directional *M*-H bonding while the most electropositive metals (rare earths, Mg) form ions	Continuity of occupied states in the band structure
Anisotropic $CeNi_3H_{2.8}$ [379]	Huge differences between the AB_5 and AB_2 layers. AB_5 layers do not expand, even though they undergo a deformation. No H atoms in these layers. AB_2 layer accommodates all H atoms and enormously expands, around 50 %, with all expansion exclusively proceeding along the *c*-axis. Metal sublattice is totally rebuilt but returns to the initial intermetallic structure upon hydrogen desorption.	New types of coordination for hydrogen (e.g. $A_3B = Ce_3Ni$) together with conventional interstitial sites (e.g. $A_2B_2 = Ce_2Ni_2$)	Directional Ni−H bonding resulting in covalently bound Ni−H−Ni−H frameworks. Electron density transferred from Ce to both Ni and H.	Distinguished peaks of electron density in the PDOS of H and Ni manifesting a directional Ni−H bonding

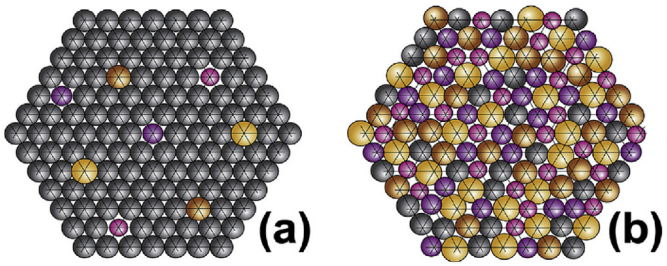

Fig. 12. The effect of atomic size difference on atom position in (a) dilute solution and (b) concentrated solution with no dominant atom species and atom positions deviate from mean lattice position. The variability in atom positions, as illustrated in (b), contributes to an excess configurational entropy [384].

formed by each of the constituting transition metals. Values as high as 2.5 H/*M* (2.7 wt% H) are comparable to rare-earth metal hydrides (H/*M* > 2.3). Such high hydrogen content, as in $TiVZrNbHfH_{2.5}$, has never been observed in hydrides based only on transition metals and this implies that hydrogen occupies not only tetrahedral but also the octahedral interstices in the pseudo-fcc lattice. We note, however, that no direct observation confirming a mixed T + O occupancy of the interstitial sites has been provided so far. Certain systems, such as TiVNbTa, TiVZrNb and TiVZrNbHf, have also been observed to phase-separate during hydrogen absorption/desorption cycling [390,391] at the high temperatures often needed to desorb the hydrogen from the hydrides [392–394].

To provide deeper understanding of this behaviour, V in the equimolar TiVZrNbHf alloy has been completely substituted by an isoelectronic element, Ta, resulting in TiZrNbHfTa [393]. Surprisingly, the single-phased *bcc* TiZrNbHfTa alloy behaves as the conventional *bcc* materials with two distinct phase transitions during hydrogen absorption: *bcc* ↔ *bct* ↔ *fcc*, which are associated with a step-by-step formation of the mono- and di-hydrides.

Recently, the hydrogen absorption properties of the Zr-deficient TiVZrNb alloy with a non-equimolar composition have been studied to optimize the synthetic optimization and cycling behaviour [395]. This alloy crystallizes in a single-phase *bcc* lattice. Hydrogen absorption occurs within a single step, similar to the TiVZrNbHf alloy. The maximum uptake is around 1.75 H/*M* (2.5 wt% H). The best hydrogen cycling performance was observed for the *bct* hydride with a similar capacity (1.8 H/*M*) obtained by reactive ball milling. A stable reversible capacity of around 2.0 wt% H has been observed, which is associated with the absence of disproportionation or irreversible segregation during the hydrogenation.

To explain the different hydrogenation behaviour of different HEAs (either one or two hydrogenation steps) we hypothesize that lattice distortion, δ, plays an important role. It is suggested a larger δ (6.8% for TiVZrNbHf and 6.0% for TiVZrNb) would favour a single-step reaction with hydrogen, whereas a small δ (4.6% for TiZrNbHfTa) would favour a two-step phase transition, as encountered for conventional *bcc* alloys.

Furthermore, many of the hydrogen storage properties of HEAs are intimately connected to the valence-electron concentration (*VEC*) of the HEA [391]. Systematic investigation of the hydrogen storage properties for a series of ten HEAs (bcc solid solutions) that are chemically related to the ternary system TiVNb (*VEC* = 4.7) shows that if the *VEC* ≤ 5.0, the corresponding metal hydrides form CaF_2-type structures (Fm-3m) following a gas-solid-state reaction. The volumetric expansion of the lattice from the alloy to the hydride increases linearly with the *VEC*. At the same time, the onset temperature for hydrogen desorption decreases with the *VEC*. Therefore, it seems that a larger expansion destabilizes the HEA-based metal hydrides and that this effect can be tuned by altering the *VEC*.

It can be concluded that the most promising materials for hydrogen storage are *bcc* MPEAs/HEAs based on refractory metals with *VEC* ≥ 5.0 and with large lattice distortion δ and single-phase transformation during hydrogenation. Importantly, due to the magnitude of the number of variations of chemical compositions, this new class of alloys holds promise for the discovery of fascinating multifunctional materials.

For example, based on these insights, $TiVCrNbH_8$ (*VEC* = 5.0) was identified as a material with suitable thermodynamics for hydrogen storage in the solid state. This HEA-based hydride has a reversible hydrogen storage capacity of 1.96 wt% H at room temperature (*RT*) and moderate H_2 pressures. Moreover, it is not dependent on any elaborate activation procedure to absorb hydrogen. Thus, the insights provided in [391] might serve as a roadmap towards developing novel bcc HEA-based metal hydrides that are cost-efficient and reversible at *RT* with higher gravimetric hydrogen capacities.

As a conclusion, the study of hydrogen absorption/desorption properties of this new class of alloys is only at the beginning and holds promise of interesting findings, at least in terms of fundamental knowledge. Large research efforts are needed in the future to attempt to rationalize the behaviour of these alloys towards hydrogen due to the vast number of elemental combinations (in terms of chemical composition, elemental concentration, VEC and lattice distortion).

7. Improved kinetics of hydrogen absorption and desorption and decreasing working temperatures for Mg-containing systems

Using magnesium as a component of H storage alloys or to store hydrogen has a cost benefit, as the commercial price of magnesium metal is < 3 USD/kg. Here we detail recent work on layered structures and nanocomposites.

7.1. Optimization of the hydrogen sorption properties of layered structure AB_x (A = rare earths; B = transition metal; 2 < x < 5) systems by magnesium substitution

Archetypal intermetallic compounds such as $LaNi_5$ are able to store 6 .7 at. H per formula unit [396]; however, different chemistries offer a wide range of related compositions. Indeed, binary phase diagrams of rare earths (*A*) and transition metals (*B*) contain different phases, AB_x ($2 < x < 5$), consisting of a stack of different blocks, [AB_5] and [AB_2]. These phases can store larger quantities of hydrogen, but they suffer from poor stability and low reversibility. To overcome these drawbacks, investigation of pseudo-binary or ternary systems adding alkali earths like magnesium is of great interest. Magnesium is a light element with strong hydrogen affinity, inducing a molar mass reduction and thus increased weight capacities, and its substitution has been recently systematically investigated. Examples include $La_{3-x}Mg_xNi_9$ and $(La,Pr,Nd)_2MgNi_9$ [397], with an increasing amount of Mg reaching a maximum at $LaMg_2Ni_9$. Replacement of La by Mg and Pr/Nd has a strong influence on the stability of the hydrides. When the Mg content increases from x = 0.7 in $La_{2.3}Mg_{0.7}Ni_9$ to 2 in $LaMg_2Ni_9$, equilibrium pressures of hydrogen desorption change by a factor of more than 1000, from 0.011 bar H_2 to 18 bar H_2 at RT, which was reflected also by correspondingly large changes in the enthalpies of hydride formation, from −24 to −40 $kJ(molH_2)^{-1}$. Together, Pr/Nd and Mg substitution allow the plateau pressure to be tuned for practical applications (Fig. 13).

Similar beneficial effects were also reported by Ferey et al. [398] in the neighbouring system A_5B_{19} ($n = 3$) for La_5Ni_{19}. Replacement

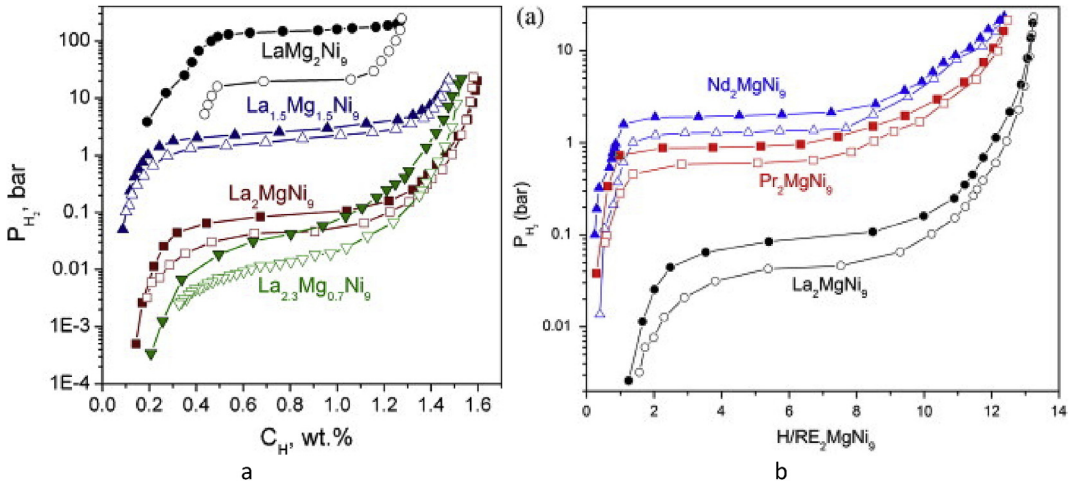

Fig. 13. Evolution of isotherms and equilibrium pressures of H absorption and desorption at room temperature as a function of x for the system $La_{3-x}Mg_xNi_9$ [460] and RE_2MgNi_9 (RE = La,Pr,Nd) [463], showing that the optimal performance is reached at x = 1.

of La by Mg leads to a reduction of the molecular weight and stabilization of the structure by cell volume reduction, agreeing with recent results of improved behaviour in terms of reversible capacity and the working pressure window. This substitution opens a new route to develop more capacitive materials for hydrogen storage applications.

7.2. Improved kinetics and cycling stability of MgH_2 nanocomposites

To make MgH_2 efficient as a reversible hydrogen store, intensive research has been recently undertaken both to lower its decomposition temperature and to accelerate sorption kinetics [168,361,362,399]. A successful strategy to promote fast reaction kinetics is grounded on the immiscible property of Mg-*ETM* binary systems (*ETM* = Early Transition Metal) [362,400–405]. In contrast to Late *TMs* (e.g. *LTM* = Fe, Co and Ni) and Zn [406], *ETM*s such as Ti, V, Zr and Nb do not form any stable intermetallic phases with Mg, nor any ternary Mg-*ETM*-H compound. Thus, nanostructured composite materials formed by intimate mixtures of MgH_2 and $ETMH_x$ phases can be successfully synthesized by advanced techniques, such as mechanochemistry of elemental metal powders under H_2 gas. MgH_2–TiH_2 nanocomposites have attracted much attention due to their improved hydrogenation properties [401,402,407,408]. TiH_2 as an additive promotes fast hydrogen uptake in Mg and release from MgH_2, with reaction rates in the minute range at 300 °C, while ensuring good cycling stability.

From studies on MgH_2–TiH_2 nanocomposites, the role of TiH_2 as promoter of hydrogen kinetics in Mg/MgH_2 as well as stabilizer of cycling properties can be summarized as follows:

a) TiH_2 acts as a nanostructuring agent during mechanochemical synthesis of the nanocomposite [402]. Short diffusion lengths are required to achieve fast kinetics in Mg;
b) TiH_2 acts, at the nanocomposite surface, as a gateway for hydrogen transport to and from the Mg/MgH_2 matrix. It catalyses surface reactions, while hydrogen diffusion in TiH_2 at 300 °C is fast due to fluorite-type structure of TiH_2 [402,409];
c) TiH_2 acts, in the bulk of the nanocomposite, as an inhibitor of Mg grain growth, which is a key property for ensuring cycling stability [410,411]. The close values of cell volume of TiH_2 (13.2 cm^3/mol) and Mg (13.8 cm^3/mol) allows for effective interface coupling between these phases [412], which limits grain growth on cycling.

Besides these effects, TiH_2 may also act as a favorable site for MgH_2 nucleation during the absorption process. Further studies will be valuable to evaluate the synergetic effects of TiH_2 and ZrH_2 mixtures as mixed additives in novel MgH_2-$ETMH_x$ nanocomposite systems.

8. Hydrogen sorption properties of low-dimensional metal hydrides

Many experimental and theoretical studies have investigated hydrogen sorption in low-dimensional materials such as nanoparticles (NPs) and thin films with the aim to understand the mechanistic effects of nanosizing and gain new tools to tailor the hydride properties. Consensus has been reached on topics such as enhanced solubility, interface enthalpy, and enhanced sorption kinetics, while several open questions and unsolved issues remain, for instance strain-induced lowering of desorption enthalpy, interfacial entropy, and enthalpy-entropy correlation [413–416]. Nanosizing is highly effective in enhancing the hydrogen sorption kinetics, while the aspiration to modify the often-unfavourable thermodynamics of hydrogen release is much more difficult to fulfil. We will discuss the fundamental mechanisms that modify the hydrogen sorption properties of low dimensional materials in light of recent progress in this field.

8.1. Surface and interface energetics

The excess free energy associated with surfaces or interfaces in a nanosized system is given by the product $A\gamma$ of the total area A by the specific free energy (surface tension) γ. If its change upon hydriding $\Delta\{A\gamma\} \equiv \{A\gamma\}_{hyd} - \{A\gamma\}_{met}$ is positive, the nanomaterial is destabilized compared to the bulk, and vice versa [417]. The free energy change $\Delta\gamma \equiv \gamma_{hyd} - \gamma_{met}$ clearly contains enthalpy and entropy terms, i.e. $\Delta\gamma = \Delta h - T\Delta s$. Systematic calculations of Δh for different binary hydrides showed that an enthalpy-driven destabilization is expected for MgH_2 and NaH, whereas VH_2, TiH_2, ScH_2, AlH_3 and LiH would all be stabilised [418]. However, the estimated enthalpy change compared to bulk is only 5 kJ/mol H_2 for Mg NPs with a diameter of 2 nm. For extremely small clusters constituted by less than 10 Mg atoms, the enthalpy change may become more

significant [419,420]. However, these ultra-small cluster sizes have eluded experimental observations until today. Experiments on Mg thin films embedded within TiH_2 layers have demonstrated that $\Delta\{A\gamma\}$ scales inversely with the film thickness, and estimated that $\Delta\gamma = 0.33\,Jm^{-2}$ [421]. In order to achieve a significant destabilization, a large positive value of $\Delta\gamma$ is required. A higher value of $0.81\,Jm^{-2}$ was reported by replacing TiH_2 with TiAl, a strategy that exploits the strongly different binding energy of Al with Mg and H [422]. Interfacial free energy was also deemed responsible for the destabilization of self-organized MgH_2 clusters within a TiH_2 matrix [423], and of MgH_2–TiH_2 composite NPs prepared by gas phase condensation [424].

8.2. Enthalpy-entropy correlation

There have been several experimental reports of altered enthalpy and entropy in small NPs due to surface/interface effects [424–428]. In some cases, the enthalpic destabilization was significantly larger than predicted by calculations for the relevant NPs size [425,427]. The puzzling aspect, though, is that the plateau pressure exhibits only small changes (if any) compared to the bulk counterparts. In part, this probably arises from some entropic compensation. On the other hand, an accurate determination of enthalpy and entropy from the slope and intercept of a van't Hoff plot requires the collection of equilibrium data over a wide temperature range, which is often not accessible in nanosized systems. Because of possible statistical phantoms [429], enthalpy-entropy compensation should be invoked with extreme caution to justify the sometimes surprising outcome of data analysis. In nanomaterials, a genuine enthalpy-entropy correlation is expected if $\Delta\{A\gamma\} \propto \Delta\gamma$, in which case systems with different morphologies and/or compositions all attain a plateau pressure equal to the bulk at $T_{comp} = \Delta h/\Delta s$ [416].

8.3. Elastic clamping

Another source of thermodynamical alteration emerges in mechanically confined nanomaterials, the paradigmatic case being thin films clamped by a rigid substrate. Wagner and Pundt have shown that the attractive H–H interaction energy in Pd thin films is reduced by up to 50% due to substrate-induced stress and microstructural refinement, strongly lowering the critical temperature for the phase separation [430]. The effects of elastic clamping in Mg-based low-dimensional materials have been modelled and experimentally investigated for thin films [431], cores-shell NPs [432] and encapsulated nanodots [433]. The enthalpic destabilization, proportional to the compressive elastic strain in the hydride phase, should attain the remarkably high value of ≈ 15– 20 kJ/ mol H_2 in Mg–MgO core-shell NPs or nanodots with diameter of about 50 nm [432,433]. In real life, however, plastic deformation develops due to high stress levels, thereby reducing the magnitude of the effect and increasing the hysteresis between absorption and desorption plateaus [432–436]. For this reason, the exploitation of mechanical constraints to raise the desorption pressure of MgH_2 has not been experimentally successful. Fig. 14 shows that, for Mg nanodots of two different sizes, the desorption pressure is size-independent whereas both the absorption pressure and the hysteresis increase in the smaller nanodots, which are subjected to higher lateral stresses. Nevertheless, the concept remains challenging and open to future developments. For instance, it was recently shown that immiscible Zr nanoclusters within an yttrium thin film induce a stable lattice compression, which increases the hydrogen pressure of $YH_2 \leftrightarrow YH_3$ both for absorption and desorption, a signature of true destabilization [437].

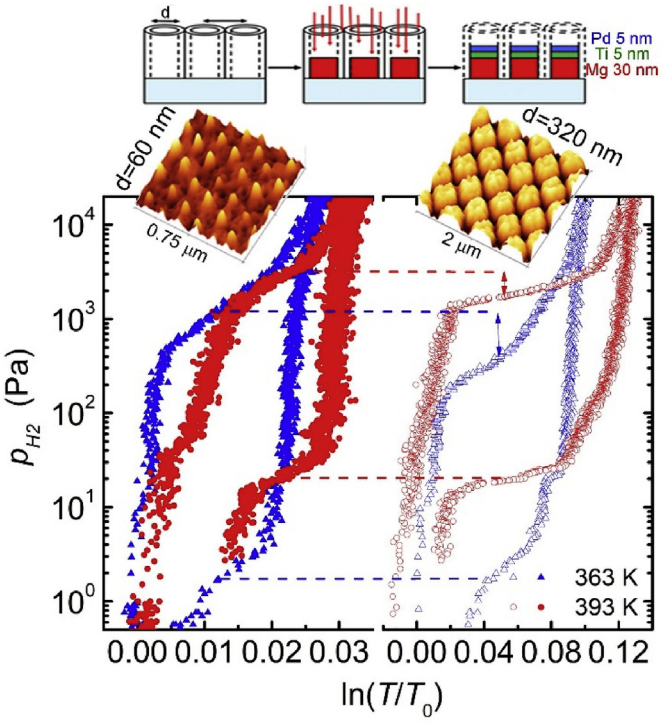

Fig. 14. Size dependent hydrogen properties in Mg(30 nm)/Ti(5 nm)/Pd(5 nm) layered nanodots with diameters of 60 nm (left) and 320 nm (right) obtained by mask-templated deposition [433].

8.4. Nanoconfinement in porous hosts

Through incorporation into porous media or polymer-based host materials, the NPs size of metal hydrides can be stabilised to 5 nm or smaller [306,438–441]. The most effective approaches have been either solution impregnation or melt infiltration using porous carbon materials, such as carbon aerogels, high surface area graphite, and carbon replicas of ordered mesoporous materials [439]. The obtained nanocomposites always display very good sorption kinetics and good cyclic stability because the confining medium reduces coarsening phenomena. The host material may modify the properties of the hydride by a combination of the previously discussed features, in particular mechanical constraints and interfacial free energy. In the case of MgH_2, however, despite greatly enhanced kinetics, only limited thermodynamic changes (if any) have been observed. A drastic change of the hydrogen-metal interaction appears in Rh NPs supported on a porous carbon host. In contrast to bulk Rh that can form a hydride phase under 4 GPa pressure, the metallic Rh NPs (~2.3 nm) absorb hydrogen and form a hydride phase at pressures below 0.1 MPa [442].

Beyond porous carbon, other host materials have gained considerable attention. Reduced graphene oxide (rGO) has been proposed as a gas-selective, hydrogen permeable, and atomically thin material suitable for the realization of multi-laminated nanocomposites, in which metal hydride NPs are encapsulated and protected against oxidation [441]. MOFs are also attractive scaffolds because their crystalline structure yields highly defined, monodisperse micropores (<2 nm). $NaAlH_4$ confined in the micropores of a titanium-functionalized Mg-MOF-74 forms clusters of several formula units and can reversibly store hydrogen with minimal loss of capacity [443]. All scaffold materials significantly decrease the overall hydrogen storage capacity by their added weight.

9. Electrochemical storage of energy

9.1. Metallic and complex hydrides as efficient materials for electrochemical storage of energy

Storage of renewable energy is an important issue in the modern energy landscape. Electrochemical storage has shown its capability to provide energy supply for both on-board and stationary applications. Different systems exist from supercapacitors to redox flow batteries. However, the present work focusses on secondary batteries that are already developed in the market, such as alkaline and Li-ion, that suffer from low energy density, high costs and safety issues. Recently, innovative research in the field of complex and metallic hydrides has shown that these materials might bring ground-breaking solutions leading to significant improvement for these electrochemical energy storage devices.

9.1.1. Metallic hydrides as anodes for Ni-MH alkaline batteries

Ni-*M*H alkaline batteries are widely used for energy storage [444–447] in varied applications from Emergency Lighting Units (ELU) to small portable devices. Despite lower performances compared to Li-ion batteries, they can withstand higher charge currents and are intrinsically safer against overheating issues [448]. Moreover, they are cheaper and can be easily recycled [449]. Therefore, they are now used in most of the hybrid electric vehicles (HEV for Toyota[1] or Honda). Recently, they have been developed for stationary applications. Indeed, Nilar, a Swedish company, has teamed up with the energy company Ferroamp to create an energy management system designed for smart storage and distribution of solar energy. In a pilot project with Nilar, Ferroamp uses Nilar energy storage integrated with a midsize solar power plant to store up to 30 kWh of energy from photovoltaic panels (Fig. 15). An EnergyHub controls the energy storage to support the three-phase grid. When the voltage drops below a certain level, energy storage kicks in to raise the voltage.

This bipolar Ni-*M*H battery technology is a new approach [450] and the EnergyHub (Fig. 15) provides the necessary energy storage, monitoring and control capability for managing the flow of energy to and from storage, with the expectation of eventually storing up to 200 kWh of energy.

9.1.2. Increasing cycle life of hydride batteries (NiMH) by utilizing gas phase reactions

NiMH chemistry is one of the simplest battery chemistries. Hydrogen atoms are shuttled between the electrodes in the form of water molecules when the battery is cycled. Both electrode reactions are solid state intercalation reactions. When the battery is charged, hydrogen is removed from the $Ni(OH)_2$ at the Ni-electrode by an OH^- ion transforming $Ni(OH)_2$ into NiOOH and forming a water molecule H_2O. At the MH-electrode another H_2O molecule donates a hydrogen atom inserting into the hydrogen storage alloy, forming another OH^- ion. When the battery is discharged, the reactions above are reversed. These simple hydrogen atom transferal reactions can also be manipulated by adding oxygen or hydrogen gas into the battery casing. This opens up possibilities to reset internal electrode balance as well as a controlled way to replenish water to a battery drying out from long time cycling in a way that no other battery chemistry can offer.[1]

The surface must contain a passivating layer in order to protect the alloy from excessive corrosion. A passivated surface can be formed by a controlled oxidation process that slows down the corrosion rate. This is important as corrosion consumes water in the electrolyte leading to an increased internal resistance, which is the main cause of cell failure. The corrosion evolves hydrogen, causing an imbalance between the anode and the cathode. This can lead to a premature internal pressure increase that can accelerate the drying out of cells, if the evolved gases are vented through the safety valve. However, the bipolar design such as in Nilar batteries makes it possible to counteract the aging process of the metal hydride. Adding oxygen causes new water-based electrolyte to form in the battery. This replaces the lost electrolyte and restores the internal electrode balance. With a suitable balance of oxygen and hydrogen, these batteries can reach a superior lifetime and the internal resistence as well as internal cell balance can be restored on old cycled batteries, Fig. 16.

The increased cycle life means that NiMH batteries will be able to store and deliver more energy throughout their lifetime than other industrial battery technologies with reduced cost per kWh. Even though NiMH batteries cannot compete with Li-ion batteries with respect to capacity, they can compete with respect to energy throughput during the lifetime of a system (i.e. battery capacity times cycle life), similar to the success of the even lower capacity Li-titanate (LTO) long cycle life batteries [451].

Current Ni-MH batteries are mainly based on $LaNi_5$-type materials as anodes. Such materials are effective, but their intrinsic capacity is restricted to 300 $mAh.g^{-1}$ [446,452–454]. The research approach to improve their energy density is by investigating new materials with larger capacity. One approach is to use stacked-structure phases. These structures are built by stacking along the *c*-axis different subunits with compositions AB_5 and AB_2 (*A*: rare earths and *B*: transition metals). By adding different slabs as $mAB_5 + 2AB_2$, various stoichiometries of the general *A*-*B* phase diagram can be described such as AB_3 ($m = 1$), A_2B_7 ($m = 2$), and A_5B_{19} ($m = 3$). Costly rare-earths can be partially replaced by additions of magnesium leading to pseudo-binary or ternary systems *A*-Mg-*B* (Fig. 17). Mg substitution has been demonstrated to be effective as it enables a lower molar mass, enhances the structural stability, and stabilizes the equilibrium pressure as well as reducing the overall cost [376,378,455–467].

Furthermore, excellent hydrogen storage performance, including improved cycle life and high electrochemical discharge capacities, attract interest to rare earth-free Zr and Ti based Laves phase intermetallics. Such multicomponent alloys have a variable ratio between Ti and Zr and also contain Ni, Mn, Fe, Co, Ni, and V transition metals together with non-transitional elements, Al and Sn. Depending on the composition, these alloys crystallize with C15 or C14 structures. Further to the structure, properties can be improved by applying a rapid solidification process with the aim of improving the performance of the AB_2-based Laves type alloys as battery anode materials; examples include $Ti_{12}Zr_{21.5}V_{10}Cr_{7.5}Mn_{8.1}Co_8Ni_{32.2}Al_{0.4}Sn_{0.3}$ as C14 [468] and $Ti_{0.15}Zr_{0.85}La_{0.03}Ni_{1.2}Mn_{0.70}V_{0.12}Fe_{0.12}$ as C15 [469] predominated alloys. After rapid solidification, both alloys achieved a significant improvement in their discharge capacities and rate performances.

Excellent discharge capacity performance including high reversible storage capacity, together with easy activation, fast charge kinetics, and low polarization, was achieved for two C15 predominated alloys including $Ti_{0.15}Zr_{0.85}La_{0.03}Ni_{1.2}Mn_{0.7}V_{0.12}Fe_{0.12}$ [470] and $Ti_{0.2}Zr_{0.8}La_xNi_{1.2}Mn_{0.7}V_{0.12}Fe_{0.12}$ ($x = 0.01–0.05$) [471]. Both alloys achieved high discharge capacities, 410 mAh/g and 420 mAh/g, respectively. 3 wt% of La was added to both alloys causing an easier activation and an increased capacity because of the catalysing effect of a secondary phase - LaNi intermetallic – on the hydrogenation.

For commercial metal hydride batteries the following range of

[1] The mention of all commercial suppliers in this paper is for clarity and does not imply the recommendation or endorsement of these suppliers by the IEA, NIST or the authors.

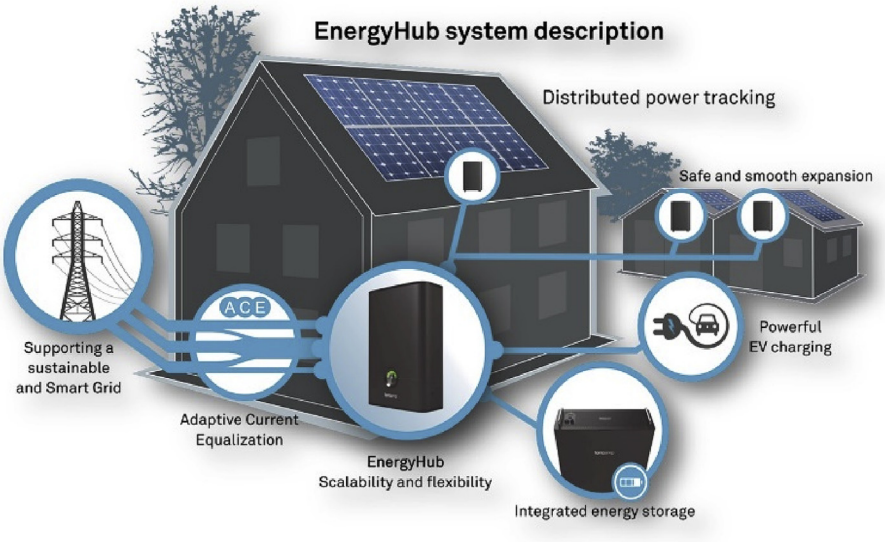

Fig. 15. Schematic of the Ferroamp EnergyHub based on Nilar's bipolar in Sweden (from http://www.nilar.com/wpcontent/uploads/2017/09/Ferroamp-Customer-Case-NIL17.pdf).

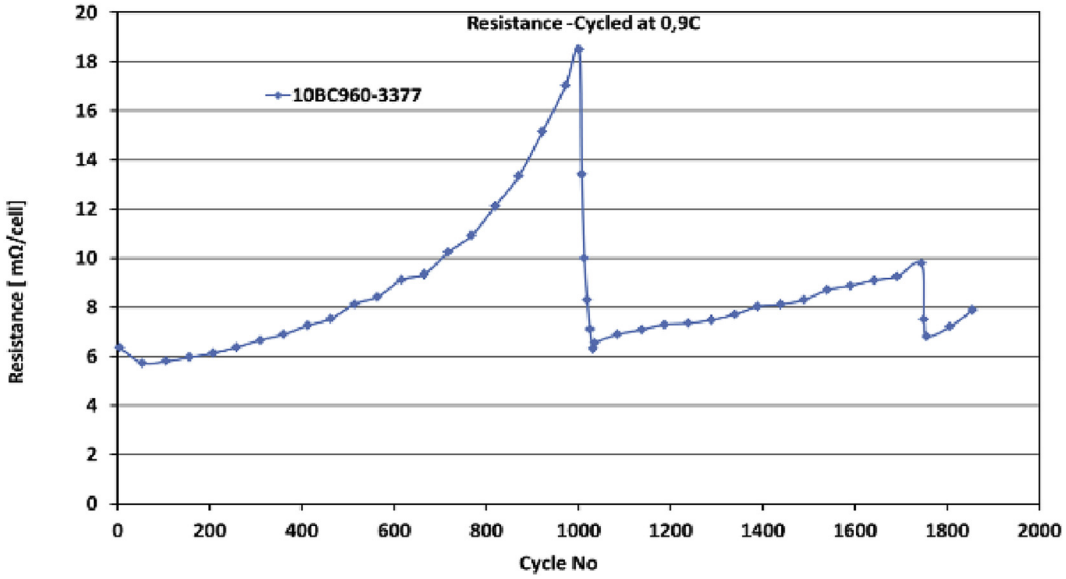

Fig. 16. Internal resistance upon cycling (0.9C rate), with additions of 5 consecutive 3L batches of oxygen gas at cycle 1000, and 2 consecutive 3L O_2 and 3L H_2 batches at cycle 1700 [451].

gravimetric/volumetric energy storage capacities and cycle stabilities is presently reached: 50 to 110 Wh/kg and 150 to 390 Wh/L depending on the materials and technology, with a cycling stability reaching 6000 cycles.

9.2. Metallic hydrides as anodes for Li-ion batteries

Li-ion batteries are dominating the battery market due to their high energy density. Though their capacities are larger than other technologies, such as alkaline batteries (by 50%), demanding applications such as EVs will need much higher energy densities to reach the specifications for long-range vehicles (by a factor of four). All components such as cathodes, electrolytes and anodes are under scrutiny. For anodes, current materials use mainly intercalation/deintercalation reactions while conversion type reations are an alternative to develop more capacitive anodes.

Among the possible materials for conversion, metallic hydrides show promise based on their intrinsic properties: low potential, low polarization, high volumetric and weight capacities and low cost [472]. The first evidence of this reaction was provided by Oumellal [450], following the general equation $MH_x + x\text{Li} \leftrightarrows x\text{LiH} + M$. From a thermodynamical point of view, the reaction is favorable for electrochemical applications as far as $\Delta G_f(MH_x)/x$ or is greater than $\Delta G_f(\text{LiH})$, opening the opportunity to investigate many hydrides with high capacities [473]. Theoretically, as shown in Fig. 18, such materials might provide volume and weight capacities ten times larger than graphite which is typically used. Indeed, most of the investigated hydrides (MgH_2 [450,473–477], TiH_2 [478,479], composites $(Mg,Ti)H_2$ [402,480], TiNiH [481], Mg_2MH_x complex hydrides (M = Fe, Co, Ni) [482–484], alane [475,485], and alanates

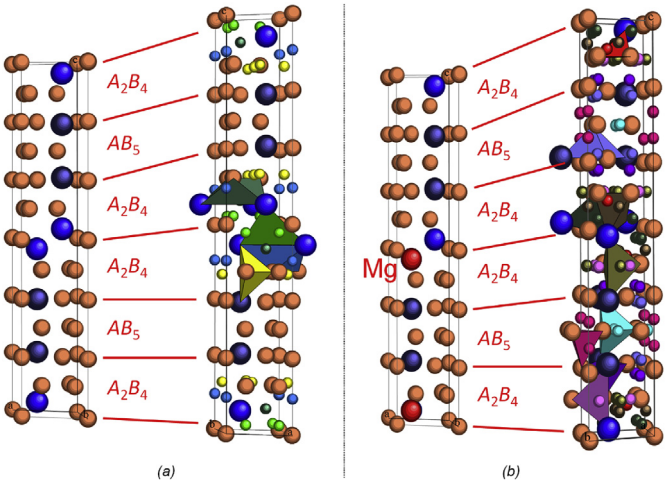

Fig. 17. Comparison of the structural properties of two intermetallics (a) La_2Ni_7 and (b) $La_{1.5}Mg_{0.5}Ni_7$ and their respective deuterides showing the different site occupancies for deuterium (from Refs. [378,458]). Reprinted from Ref. [376], Copyright (2014), with permission from Elsevier.

[485,486]), showed good ability for lithiation.

Despite successful lithiation of these hydrides, reversibility remains an issue for these systems as room temperature experiments show slow kinetics for de-lithiation, limiting the effectiveness of the reaction. Different strategies to improve the reversibility include nanosizing to enhance diffusion paths or the addition of secondary conductive phases such as carbon to improve electronic conductivity. It was demonstrated that increasing the temperature to *c.a.* 120 °C allows good reversibility of the reaction for MgH_2 [487-490], composites $(Mg,Ti)H_2$ [491], or complex hydride Mg_2FeH_6 [492]. In addition, a recent study made on a thin film of MgH_2 [493] at room temperature shows that the poor reversibility of the hydride conversion reaction is not due to electronic contact losses, neither to low conductivity of the electrode nor to cracks or voids induced by the volume expansion upon cycling, but rather to mass-transport limitations. This agrees with the enhancement of the reversibility observed at higher temperatures. Keeping low-dimensional microstructures during electrochemical cycling and utilizing the optimal operating temperature are therefore key to achieving good reversibility and cycling for the use of metal hydrides as efficient conversion anodes in Li-ion batteries.

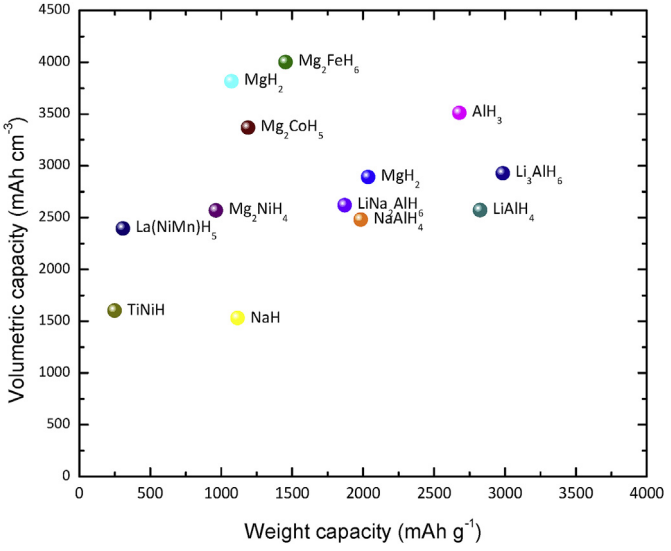

Fig. 18. Calculated capacities (by volume and by weight) for various binary and ternary hydrides using the electrochemical conversion reaction with lithium $MH_x + xLi \leftrightarrows xLiH + M$.

9.3. Complex hydrides as electrolytes for Li-ion batteries

Solid state electrolytes are a breakthrough in Li-ion technology as they allow to avoid the use of flammable liquid electrolytes while ensuring safer and more powerful batteries by preventing dendrite formation with Li metal. However, obtaining high ionic conductivities in solid materials at room temperature (above 10^{-3} S cm^{-1}), while keeping a low electronic conductivity, remains challenging. Solid electrolytes must present good stabilities in a large range of potential (typically 0–5 V) and should be compatible with the highly reactive materials composing the electrodes.

Complex hydrides were recently found to be interesting materials in this field [494,495]. Indeed, $LiBH_4$ was reported as a fast ionic conductor for lithium by the group of Matsuo et al. [496,497]. Unfortunately, this compound undergoes a structural transition at 110 °C and only the high temperature hexagonal phase is significantly conductive (10^{-3} S cm^{-1}) [497]. Various strategies have been developed to lower the transition closer to room temperature. This includes nanoconfinement in scaffold materials such as silica [498,499], partial BH_4^- anion substitution with halides (Cl^- or I^-) [496,500], solid solutions with amides (NH_2^-) [501], and synthesis of rare-earth (RE) chloride compounds $LiRE(BH_4)_3Cl$ [217], leading to some improvement but still one or two orders of magnitude below the required conductivities at RT. This illustrates the potential of other possibilities by modifying both chemistry and nanostructuration. In addition, significant ionic conductivities have been also reported with other cations such as Na^+ [502,503] in various *closo*-borate and monocarbo-*closo*-decaborates (Fig. 19) [504], paving the way to many possibilities in the field of solid state ion batteries.

9.4. Full Li-ion batteries made of complex and metallic hydrides

Based on the above reports on the attractive properties of complex and metallic hydrides as solid electrolytes or anodes, several groups have attempted to use them in full cells to demonstrate their ability for developing practical batteries [505]. All attempts were made with $LiBH_4$-type electrolytes and with temperatures ranging from 45 to 120 °C. To provide high capacities, most of the investigated batteries were using a metallic lithium anode, coupled with various cathode materials: TiS_2 [504,506–508], sulphur [509–512] and Co or Ti oxides [513]. To our knowledge, only one battery combines the complex hydride $LiBH_4$ as electrolyte and a metallic hydride as anode (MgH_2+TiH_2) [491]. Here, the device was completed with a sulphur cathode. Despite slow kinetics at room temperature, most of the batteries cited above show good cycling behaviour up to hundreds of cycles.

Metallic and complex hydrides have been mainly developed in the past for their capability to reversibly store gaseous H_2 or to serve as anodes in alkaline batteries. Recent research has demonstrated their aptitude to also play a crucial role in Li-ion technology, providing safer solid electrolytes and higher capacitive anodes to face the increasing demand for energy storage. Based on the very rich chemistry of these materials, a large field of research is open to discover new hydride materials that might bring large innovation in this field.

10. Thermal storage using metal hydrides

Thermochemical energy storage materials have higher energy

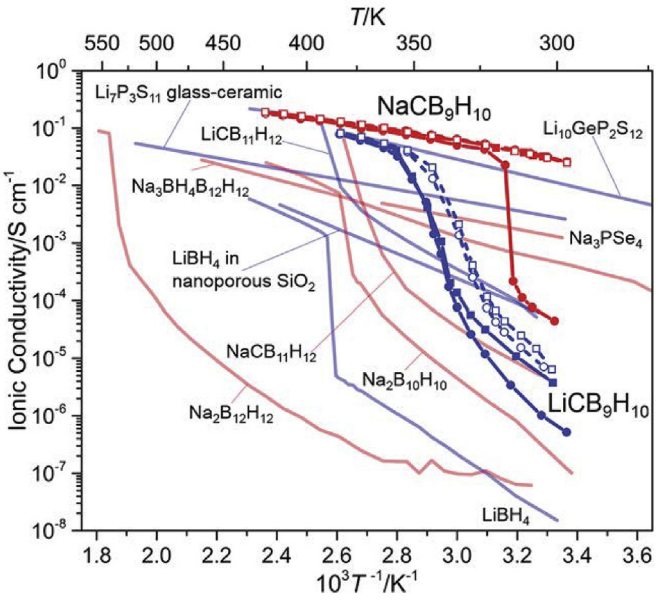

Fig. 19. Comparison of the ionic conductivities (Li^+ or Na^+) as a function of the temperature for various polycrystalline materials, suitable as solid state electrolytes, from Ref. [504].

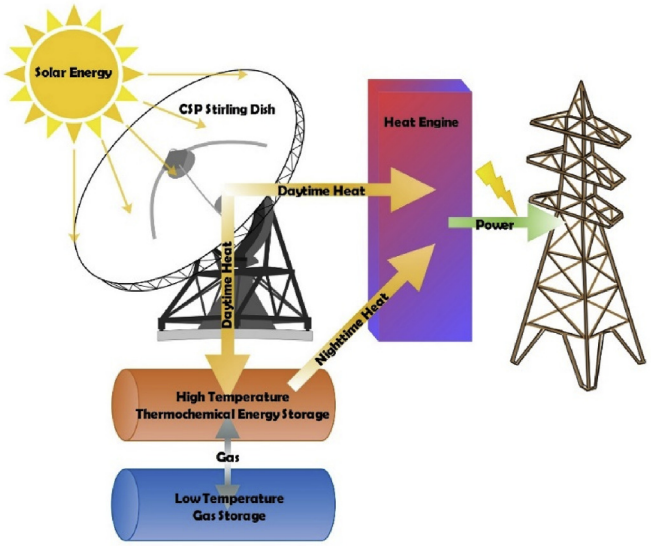

Fig. 20. Depiction of a Stirling dish concentrating solar power plant based on solid-gas thermochemical energy storage. The arrows indicate the heat, gas, and power flow.

densities compared to latent and sensible heat storage materials. Metal hydrides have properties such as high enthalpies, reversibility and cycling stability, and this makes them ideal for thermal energy storage applications in the temperature range of 25 °C–800 °C [514]. The heat source can be derived from several sources such as waste heat and concentrated solar thermal (CST).

Solar energy is the most abundant renewable energy resource and therefore logically represents the most important renewable energy resource for the future. The IEA roadmap for solar energy set a target of *ca.* 22% of global electricity production from solar energy by 2050, with 50% being produced from CST power (CSP) systems. Achieving this target will be possible only if the costs of producing electricity from solar energy are significantly reduced and cost effective energy storage technologies can be developed. A major challenge is to achieve continuous, low-variability power generation from renewable energy sources, for stand-alone applications or for integration with domestic power grids. Solar mirror collection fields can collect thermal energy during the day and run a heat engine to convert it into electricity, but cannot provide power at night. However, if some of the heat is used to remove hydrogen from a metal hydride, the reverse reaction where hydrogen absorbs back into the metal hydride can then occur at night, releasing heat for power generation (Fig. 20). This allows solar energy to provide 24 h power generation. By combining a high temperature metal hydride with a low temperature metal hydride or a compressed gas store, a coupled reversible thermochemical solar energy storage system is created [515,516]. CST coupled to a high and low temperature storage system has the potential to provide a continuous supply of electricity to remote areas around the world.

Recent, focus has widened from being devoted to the development of the metal hydride materials but also to the whole TES system [357,514,517,518]. This includes the containment material for the metal hydride material, which must not only endure temperatures of up to 800 °C, hydrogen pressures of up to 150 bar, but also hydrogen permeation and embrittlement [519]. Thermal management of the system has also been considered including the reduction of heat loss from the system, the heat transfer fluid (HTF) and thermal properties of the metal-hydride bed. Storage of the hydrogen released by the TES materials during the energy storage regime has been explored with costs simulations being carried out [520–522]. Storage options range from compression of the gas in volumetric containers or salt caverns to compression into low-temperature metal hydrides that are specifically paired to the high temperature metal hydride.

The development of new high temperature metal hydride materials has a vital role to enable maximum efficiency of the CST plant by operating at maximum temperature. A host of compounds have been developed in an effort to increase the operational temperature, while keeping the operating pressures to a minimum. Fluorine substitution for hydrogen has allowed the thermodynamic stabilization of metal hydrides including $Mg(H_{1-x}F_x)_2$, $NaH_{1-x}F_x$ and $NaMgH_{3-x}F_x$ [521,523–525]. Other potential materials developed as TES materials include $Na_2Mg_2NiH_6$, Mg_2Si, $LiBH_4$–$Ca(BH_4)_2$ Li–H–Al, Li_2NH and $CaAl_2$ [153,278,526–528,528–534]. Despite many of these materials having the required thermodynamic stability to operate at temperatures of >400 °C, reversible hydrogenation and cyclability remain a concern, and as such particle refinement additives were explored [535].

While TES materials have continued to be explored, the construction of prototype TES systems or thermal batteries has also been underway. The materials used for the prototype TES include MgH_2 and $NaMgH_3$ and over time these materials were scaled up from 19 g of MgH_2, to 40 g MgH_2 and 150 g $NaMgH_3$ [536–538]. Each of these prototypes have not only increased in dimension but also operating temperature, with the latter having an upper limit of 480 °C. In addition, thermal management has been tried with the inclusion of a HTF supply line inserted through the powder bed. The super-heated water HTF acts to supply heat during the day cycle to promote the endothermic release of H_2 and the exothermic process at night where H_2 is reabsorbed by the metal powder bed. As stated above, the operating temperature for a thermal storage system should be as high as possible, to operate as efficiently as possible. Since the solar collectors, that are the main source of heat for such systems, already deliver temperatures well in excess of 1000 °C, obtaining suitable temperatures at the beginning of the energy generation chain is not a problem. However, transferring the heat at these high temperatures is problematic and the heat transfer agent needs to be chosen with care.

To maximize steam turbine efficiencies, high temperature thermal stores from 550 to 800 °C are required. However, as mentioned above these higher temperatures put challenges on containment of metal hydride stores and pressure fittings adding significant cost. Therefore, despite the lower steam turbine efficiency, there is still interest in CSP plants that operate at economic hot oil heat transfer fluid temperatures, typically 393 °C. This temperature is the sweet spot for magnesium hydride. Its flat pressure plateau operating at ≈ 12 bar, low hysteresis and low cost of Mg (€2/kg) makes it attractive. Magnesium hydride's enthalpy of absorption of $\Delta H_{abs} = -74.06 \pm 0.42$ kJ mol^{-1}.H_2 is less than that for the higher temperature candidates, ΔH_{abs}($CaMgNiH_4$) = −129 kJ mol^{-1}.H_2 and ΔH_{abs}($Ca_4Mg_4Fe_3H_{22}$) = −122 kJ mol^{-1}.H_2 operating at 600 and 800 °C respectively [514]. Higher temperatures are limited for a practical system by not only the increased plateau pressure but excessive sintering of Mg metal powder in its de-hydrided state. If the temperature is raised above 420 °C the sintering causes increasing diffusion distances, limiting kinetics. Possible porous structures can be built utilizing lower controlled temperature-pressure cycles. An example is given in Fig. 21.

Often researchers have sought to improve the kinetics of magnesium metal hydride stores by introducing additives such as TiB_2 or Nb_2O_5 during ball milling [535,539–541] or by sputtering [542]. However, it is worth noting that above 380 °C the effect of the catalyst is minimised due to reduction of the oxides by Mg to MgO that would otherwise impede the transport of hydrogen [514,543]. Thus, a more cost-effective pure Mg (without catalysts) can be used as the kinetics are sufficient; provided the simulations and modelling of MH thermal store CSP bed performance and heat transfer is based on reliable and representative kinetic data. A problem remains in that the return oil HTF from the steam turbine is likely to be ≈ 320 °C, thus the entrance to the MH bed will be below 380 °C and suffer from poor kinetics if uncatalyzed, and this must be calculated into the CSP simulations and models.

Another strong influence that needs careful consideration if using Mg is the amount of overpressure the MH bed is subjected to. This can influence both the kinetics and capacity. A simplistic view is to think that an increase in overpressure compared to the bed plateau pressure translates to a subsequent increase in the rate of reaction. However, this is not always the case as beyond a critical overpressure (typically twice the plateau pressure) the overpressure only increases the initial reaction rate but decelerates the remainder of the reaction. One explanation is related to how fast localized regions of MgH_2 form on the surface of each Mg particle and grow together into a single continuous outer layer [544–546].

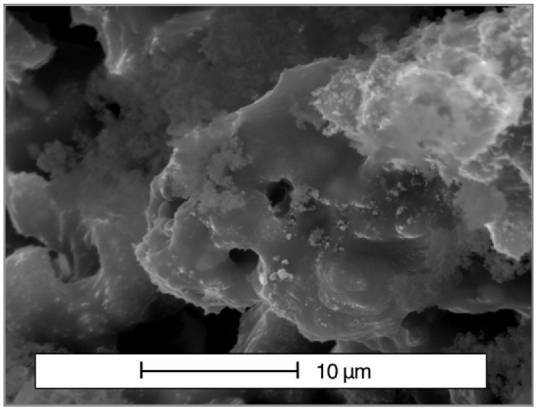

Fig. 21. Example of Porous Mg microstructure produced by partial sintering during cycling at 400 °C.

Further increases in overpressure speed up the formation of MgH_2 reducing the time it takes the outer layer to reach a thickness that will inhibit the penetration of hydrogen into the core of the particle.

At higher temperatures, one material with extremely high cycle stability is Mg_2FeH_6, working without any degradation over hundreds of cycles. This is derived from a complete separation of Mg and Fe metals during the decomposition and formation of Mg_2FeH_6 during the hydrogenation. The material has a gravimetric hydrogen content of 5.5 wt% and a volumetric hydrogen density of 150 kg m^{-3}. The reaction enthalpy was determined to be 77.4 kJ mol^{-1} H_2, slightly higher compared to pure MgH_2 with a value of 74 kJ mol^{-1} H_2. Mg_2FeH_6 can be used for heat storage applications at temperatures up to 550 °C [547]. The high working temperature makes heat transfer more difficult and molten salts must be used instead of thermo oils. This was shown in a demonstration unit with 5 kg of Mg_2FeH_6 as the heat storage material [548,549]. The heat storage unit was constructed as a tube bundle reactor with molten salt as the heat transfer medium flowing partly across and partly parallel to the tubes. During the initial experimental tests heat losses prevent stable conditions during heat storage and heat release, and values of ≈ 60% of the theoretical heat amount could be reached. This corresponds to a heat amount of 1.5 kWh.

At even higher temperatures, for short distances, heat can be transferred via heat pipes using sodium as the heat transfer agent [550]. Although sodium has also been used for longer distance heat transfer in atomic reactors [551], the complexity and safety considerations of pumping a corrosive, pyrophoric liquid metal argue against the economics of the scheme.

Two other heat transfer agent types have been suggested and tried out for heat transfer at high temperatures over distances of up to several hundred meters. One choice is in using supercritical fluids [357,552]. Both supercritical water and supercritical CO_2 are good agents concerning the fact that they boast the density of liquids and therefore also provide relatively high heat capacities and conductivities. Their drawback is the need to keep the fluids in the supercritical state, for which a certain minimum pressure is required. Especially in the case of supercritical water, this requires piping resistant to several tens of bars in pressure, which makes installation more expensive.

The other type of heat transfer agent is a gas. Both helium and air have been considered for this role [357]. Helium has the best heat transfer characteristics at the expense of a considerably higher cost than any other gas. Air is the most economical heat transfer agent, but with significantly worse heat transfer characteristics and therefore needing a higher volume flow to deliver the same performance.

Important for the construction of demonstration units is the measurement of the effective thermal conductivity (ETC) of the heat storage materials, because one drawback could be the low heat transfer capability of packed beds. ETC measurements should be done under working conditions of high temperatures and under hydrogen pressure. For the Mg/MgH_2 system strong temperature dependency in the dehydrogenated state and a significant influence of hydrogen gas pressure to heat transfer capability at higher temperatures was observed [553]. In addition, the heat transfer in a packed magnesium hydride bed is strongly influenced by repeated hydrogenation and dehydrogenation cycles. The ETC increases by 50% in the dehydrogenated state at ambient pressure and by 10% in the hydrogenated state after 16 and 18 cycles.

Since the systems being considered here are all cost-driven, having an economical heat transfer agent that combines well with the overall concept of the heat storage system is essential to make such systems successful.

11. Hydrogen energy systems – H_2 driven fork lift and metal hydride compressors

Metal hydrides that operate at or around room temperature and provide hydrogen storage capacities close to 2 wt% H (i.e. storage of 1 kg H requires approx. 50 kg of the MH material) can provide compact H_2 storage required for fuel cell driven heavy-duty utility vehicles including material handling units/forklifts where the hydrogen storage system can simultaneously serve as a ballast. Thus, the limited gravimetric hydrogen storage capacity of metallic hydrides, which is frequently considered as a major disadvantage for their use in vehicular hydrogen storage, becomes an advantage in such an application [356,554–558].

Successful integration of metal hydride hydrogen storage in Balance of Plant (BoP) of fuel cell (FC) power modules for electric forklift has been demonstrated by HySA Systems, University of the Western Cape, South Africa. The system concept, Fig. 22, is based on a distributed hybrid hydrogen storage solution [559] where a metal hydride (MH) hydrogen storage tank is connected to a compressed gas hydrogen (CGH2) tank used as a buffer to dampen H_2 pressure oscillations during the FC stack operation, as well as to provide a sufficient pressure driving force for H_2 absorption in the MH during the short periods of system refuelling. The MH tank is thermally coupled with the FC stack and the BoP components generate heat to balance the endothermic desorption of the MH. In refuelling mode, the heat released during exothermic H_2 absorption in the MH is dissipated into environment.

Fig. 23 shows the first prototype of HySA Systems MH hydrogen storage system integrated with a commercial FC power module (Plug Power, Inc.) installed in a standard 3-ton electric forklift (STILL, GmbH) [556,557]. The MH hydrogen storage extension tank is built as an assembly of 20 MH containers immersed into a water tank. The gas manifold of the tank is connected to the high-pressure side of the buffer gas cylinder of the power module (74 L composite cylinder, CGH2). Heat management of the MH tank is via a circulating waterglycol mixture driven by a circulation pump (CP), and a radiator–fan (RF) assembly and air-to-liquid heat exchanger. The containers have an optimized MH bed which provides easy activation and fast H_2 charge/discharge. The system has the same hydrogen storage capacity (~19 Nm^3 H_2 or 1.7 kg) as the CGH2 tank charged at $P = 350$ bar, but at a lower H_2 charge pressure (185 bar). The forklift with an FC power module and MH extension tank has been successfully operating at the facilities of an industrial customer (Impala Platinum Ltd, South Africa) since 2015.

A recently developed HySA Systems 15 kW FC power module, which uses a second prototype of the MH hydrogen storage tank [558], is shown in Fig. 24. Since all the BoP was bespoke, it allowed for flexibility in the integration of the MH tank into the FC system.

The tank uses a C14-AB_2-type MH alloy characterised by a hydrogen storage capacity of about 170 NL/g, a sloping plateau on pressure-composition isotherms (equilibrium H_2 pressure at RT between 5 and 10 bar) and a low absolute value of hydrogenation enthalpy ($\Delta H = -18.5$ kJ/mol H_2, $\Delta S = -78.1$ J/(mol H_2 K)), minimising the heat release during refuelling and relaxing the requirement for the heat supply during H_2 release to the FC stack. The system has 40 MH containers (total H_2 storage capacity about 1.7 kg). Additional features from the initial prototype include: (i) direct integration of the heating/cooling system of MH tank with the FC stack; (ii) counterbalancing by encasing the MH containers in melted-and-solidified lead to reach the required total weight [560], and (iii) a smaller size of the gas buffer (9 L; CGH2 in Fig. 24) as compared to the first prototype (74 L). Recently performed heavy duty tests (VDI 60/VDI 2198 standard protocol) of the forklift delivered up to 170 NL/min H_2 to the FC stack (average power about 14 kW), at 6–12 bar and by heating at temperatures up to 55 °C. The refuelling time of the MH tank at ambient temperatures - 15 and 20 °C - was between 15 and 20 min[2]. A more stable MH material, as compared to the material used in Ref. [558], enabled the maximum H_2 dispensing pressure to be lowered from 185 to 100–150 bar.

The main advantage of hydrogen storage systems utilizing MH is in a lower hydrogen storage pressure compared to the CGH2 storage option. According to a recent estimation [561], the replacement of a CGH2 storage tank with a MH one on-board an FC vehicle allows approx. 38% reduction in the refuelling costs due to a significant reduction in the costs for hydrogen compression.

The on-board MH hydrogen storage systems for forklift applications described above are characterised by an operating H_2 pressure between 30 and 50 bar (plateau pressure at $T = 25–50$ °C) for the hydrogen storage extension tank (Fig. 23) [557] and between 5 and 20 bar in the same temperature range for the MH tank integrated in HySA Systems forklift power module (Fig. 24) [558]. The higher H_2 refuelling pressures were used only to reduce the refuelling time.

The main material-related problems relevant to future developments of MH hydrogen storage systems on board FC vehicles are associated with the necessity to further decrease the H_2 refuelling pressures while shortening the refuelling time. At the same time, the pressure of hydrogen desorption from the MH at the operating temperature has to be above 1 bar to provide H_2 supply to the FC stack. In doing so, the material engineering, i.e. identification of the composition of a hydrogen storage alloy whose metal-hydrogen thermodynamic characteristics match with the pressure – temperature operating conditions of the application, will be in great demand. An approach establishing empirical correlations between hydrogen equilibrium pressures at different temperatures and elemental composition of C14-AB_2-type alloys [562] has to be developed for this, as well as other classes of hydrogen storage materials, taking into account such properties as hydrogen storage capacity, plateau slope and hysteresis. The issues of accelerating kinetics, particularly for H_2 absorption, lowering hydrogenation enthalpy, and increasing the volumetric hydrogen storage density are also of great importance.

Apart from optimising the composition of the hydrogen storage alloys, reduction of their cost is another challenging problem to be solved in the future. Medium-to-large scale manufacturing of the alloys by induction melting seems to be a viable option. Here, the main problem to be addressed is to inhibit interaction of the melt with the crucible at high temperatures thus minimising

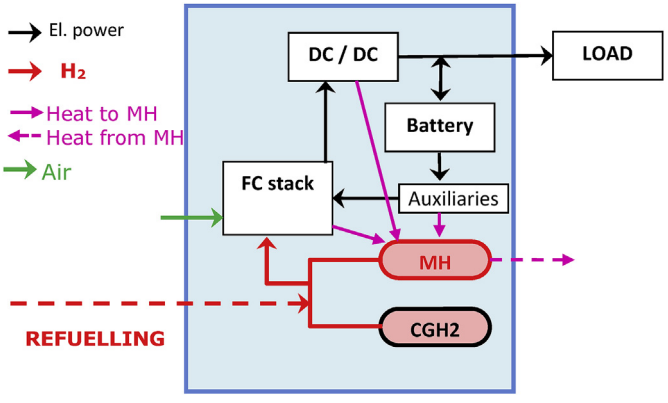

Fig. 22. Hydrogen storage on-board fuel cell powered material handling vehicle: a HySA Systems concept.

[2] Less than 10 min for 85% H_2 charge.

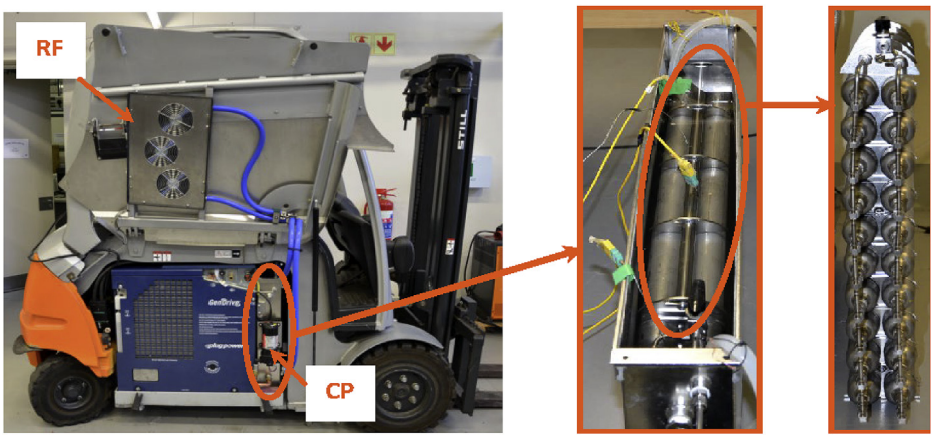

Fig. 23. Left – Electric forklift equipped with fuel cell power module and metal hydride hydrogen storage extension tank (circled). Middle – the MH tank. Right – assembly of MH containers.

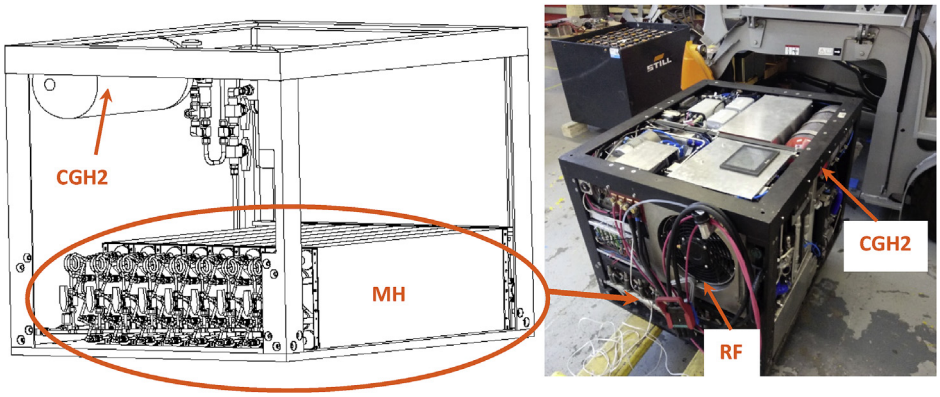

Fig. 24. MH tank with 9 L CGH2 buffer cylinder integrated in HySA Systems power module for electric forklift.

contamination of the product and prolonging the crucible service time. Corresponding approaches have been analysed for Ti-containing alloys in a recently published review [563]. Other cost-efficient methods like powder metallurgy [564], hydride combustion synthesis [565], high temperature electrolysis [566], etc., should be considered as well, with the focus on achieving high purity and homogeneity of the final alloy product.

Nearly all current technology demonstrations and commercial FC-powered vehicles store the hydrogen (H_2) fuel as a highly compressed gas up to 875 bar to enable refuelling to 700 bar systems. These pressures are achieved at fuelling stations by compressing H_2 from various initial feed sources at lower pressures [567]. Conventional mechanical compressors contribute approximately half of the station's cost, face reliability issues, and may have insufficient flow rates for a mature FCEV market [561,568,569]. Fatigue associated with their moving parts, including cracking of diaphragms and failure of seals, leads to failures exacerbated by the repeated starts and stops. The conventional lubrication of these compressors with oil is generally unacceptable at hydrogen filling stations due to potential fuel contamination. MH technology offers an excellent alternative to both conventional (mechanical) and the newly developed (i.e., electrochemical, ionic liquid pistons, etc.) methods of hydrogen compression. The advantages of MH compression include simplicity in design and operation, minimal number of moving parts, compactness, safety and reliability, and the possibility to utilize waste industrial heat for the heating of the MH compressor beds [358] offering decreased operational costs.

MH hydrogen compression utilizes a reversible heat-driven interaction of a hydride-forming metal, alloy or intermetallic compound with H_2 gas to form the MH phase and is a most promising candidate for hydrogen energy applications [356,358,570]. Metal hydride hydrogen compressor (MHHC) feasibility has been known with various laboratory experiments and demonstration as well as limited commercial units being offered for a number of years going back to the early 1970s [571].

When the hydride is cycled between a lower temperature (T_L) and a higher temperature (T_H), hydrogen pressure increases from P_L to P_H as illustrated in Fig. 25A. The extent of pressure increase follows the equilibrium of H_2 gas with H atoms within the host metal or alloy in the interstitial hydride phase when the equilibrium H_2 pressure in a plateau region of the pressure–composition isotherm is proportional to the exponent of reciprocal absolute temperature in accordance with the van 't Hoff equation. Accordingly, the pressure increase in an H_2 – MH system significantly exceeds the one taking place during thermal expansion of the gas (Fig. 25B).

The compression ratio, P_H/P_L, is strongly dependent upon the thermodynamic properties (e.g., ΔH and ΔS) for the individual hydride phase, which is restricted by the operating temperature range and structural stabilities of the hydrides [358]. Hence, practical MH compressors use generally two or more consecutive stages with different hydrides [358,570]. Only very few metal hydrides possess the ideal characteristics of broad and flat isotherms with minimal hysteresis between the absorption and desorption

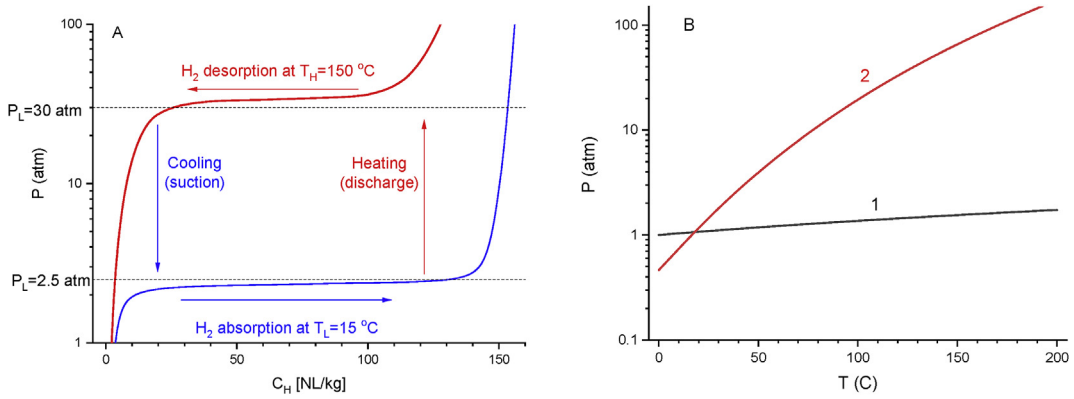

Fig. 25. A – schematic presentation of thermally driven hydrogen compression cycle using metal hydride. B – temperature dependencies of hydrogen pressure in a closed volume (1; thermal expansion) and hydrogen in equilibrium with metal hydride (2; plateau pressure). Both A and B (plot 2) show as an example $LaNi_5H_x$ ($\Delta S^o = -110.0\,J\,mol^{-1}\,H_2\,K^{-1}$; $\Delta H = -31.8\,kJ\,mol^{-1}\,H_2$).

pressures to allow efficient compression ratios [356,570]. There are usually significant variations in pressure across the plateau (sloping isotherms) as well as several other complications [358,572]. Using the desorption isotherms of the intermetallic alloys $La_{0.85}Ce_{0.15}Ni_5$ (Stage-1) and C14-Laves phase $Ti_{0.65}Zr_{0.35}(Mn,Cr,Fe,Ni)_2$ (Stage-2), Yartys et al. [570] showed a two-stage operation achieving a H_2 compression ratio 74.6 from $P_L = 3.5$ bar over the temperature range from 20 to 130 °C. The specific roles and impacts of other factors related to engineering have been described [358,570] to optimize for specific applications. Recent activities are on the materials development [562,573–579], engineering design [574,578,580–589], performance assessments [574,578,589–593], and demonstration [556,578,580,581,584,588] of MH hydrogen compressors over a range of pressures and operating conditions with some publications [578,589,593,594] including the evaluation of their commercialization. A detailed review considering materials, design, system integration aspects and operation of MH compressors with gas-gap heat switches for space applications has been recently published by Bowman [595].

MH compressors are heat engines and their efficiency is low, being limited by Carnot efficiency in a narrow temperature range [358]. Their use is especially beneficial to those applications where efficiency is not critical but safety, reliability and simplicity of operation are; examples include isotope handling, space flight missions, and thermally driven actuators and prototypes [352,557,595]. As stated above, utilization of waste industrial heat for H_2 compression makes large-scale MHHCs very promising in industries where this is available. Development of industrial-scale MH compressors is the focus of R&D activities of a number of teams; see Fig. 26 and Table 3.

Apart from proper selection of MH materials with high dissociation pressures [576–578], MHHCs have several engineering challenges. In particular, minimising void space to avoid the loss of productivity at high pressure, effective heat exchange between the MH and the heating/cooling fluid, minimising heat losses during periodic heating/cooling of the MH material and H_2 gas containment at operating pressures >500 bar. Effective heat exchange for compressors has been explored with suitable external and internal designs and multiphysics modelling [583,584].

Meeting the challenge of heat management and minimising void space is the focus of a recent prototype MHHC system within a US DoE funded project led by Sandia National Laboratories (SNL) [578]. A two-stage prototype MH compressor, providing H_2 compression from 150 to 875 bar with a productivity of 0.15 kg/h using periodic oil heating/cooling in the temperature range from 20

Fig. 26. Top – HYMEHC-10 MHHC (HYSTORSYS AS, # 1 in Table 1). Bottom – SAIAMC/UWC MHHC (# 3 in Table 3).

to 150 °C, was designed and modelled [578]. Seven alloy candidates for the two stages were selected and test samples were procured for initial volumetric characterization of their hydrogen absorption and desorption behaviour at pressures up to 1000 bar [578]. The AB_2 alloy $TiCrMn_{0.7}Fe_{0.2}V_{0.1}$ was selected for the first-stage hydride to operate from 20 to 150 °C, over a pressure range from a maximum P_L ~150 bar to $P_H > 450$ bar during desorption. For the second stage, another AB_2 alloy $Ti_{0.8}Zr_{0.2}Fe_{1.6}V_{0.4}$ was chosen. Based upon its isotherm measurements, this hydride can operate from P_L of >400 bar at a T_L of ~20 °C and produce $P_H > 875$ bar at T_H of 150 °C.

All of the components for the prototype hydride beds have been fabricated and a demonstration compressor is currently being assembled at SNL for performance testing scheduled to start during late 2019 in a dedicated high-pressure facility [578]. Stage-1

Table 3
Overview of industrial-scale metal hydride hydrogen compressors developed within last 5 years.

#	Manufacturer (type), country	P_L [bar]	P_H [bar]	Productivity [Nm^3/h]	Number of stages (types of MH material)	T_L [°C]	Cooling medium	T_H [°C]	Heating medium	References
1	HYSTORSYS AS (HYMEHC-10), Norway	10	200	10	2 (1: AB_5; 2: AB_2)	15	oil	160	oil	[578, 582]
2	HYSTORSYS AS (HYMEHC-5), Norway	5	200	5	2 (1: AB_5; 2: AB_2)	16	oil	200	oil	this work
3	SAIAMC/UWC, South Africa	3	200	5	3 (1,2: AB_5; 3: AB_2)	20	water	150	steam	[588]
4	HySA Systems/UWC, South Africa	50	200	up to 13	1 (AB_2)	20	water	130	steam	[556,580,588]
5	HYSTORE Technologies Ltd./Cyprus	7	220	up to 2.5	6 (1: AB_5; 2–6: AB_2)	10	water	80	water	[584]
6	Special Design Engineering Bureau in Electrochemistry with Experimental Factory/Russia	2–5	150–160	up to 15	2 (AB_5)	15–20	oil	150–160	oil	[581,591]

contains 25 kg of the low-pressure alloy and stage-2 has 21.7 kg of the high-pressure alloy. Fig. 27 shows design of the MH beds and MH containers. In order to enhance the thermal performance of the compressor design, configurations were numerically examined. The optimal design, which also allowed for filling and assembly of these beds with processed alloy powder in thermally enhanced compacts, was based on internal helical coil design configuration, with minimal free volumes within the hydride filled beds, to increase the pressurization and delivery efficiencies of H_2 desorbed at pressures >800 bar.

Another solution implemented by HySA Systems and its industrial partner, TF Design (South Africa), used a composite MH container (carbon fibre wound stainless steel liner which comprises a MH cartridge) designed for the conditions of hydrogen compression applications (see Fig. 28). This provides H_2 compression from 100 to 500 bar in the temperature range of 20–150 °C with dynamic performance where the low pressure H_2 absorption/high pressure H_2 desorption completes in 5–10 min [356].

As discussed above, future developments of MH hydrogen compressors will mainly address the problem of achieving high, up to 500–1000 bar, hydrogen pressures with a reasonable productivity when operating over a narrow (20–150 °C) temperature range. Furthermore, the number of hydrogen compression stages should be minimised to avoid a drop in the energy efficiency [358].

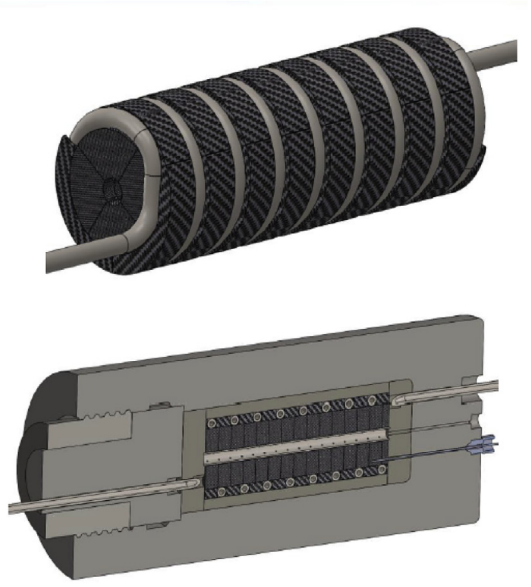

Fig. 27. Design of metal hydride bed and container for up to 875 bar H_2 compression prototype of the Sandia Project (USA) [578]. Pre-compressed pellets consisting of a mixture of MH material with expanded natural graphite (ENG) are loaded in/around the helical coil and gas distribution tube within the Teflon liner.

Mostly, solution of these problems is related to engineering issues. However, the problems of optimization of MH materials for hydrogen compression are also very important since the engineering solutions are strictly bound to the material's properties.

Generally, future activities in MH materials for hydrogen compression are expected to be similar to the ones for hydrogen storage materials outlined above in this section. They include development of hydride forming alloys (compositions and manufacturing routes) characterised by (i) well-matched operating pressure and temperature ranges, (ii) high reversible hydrogen sorption capacities at the operating pressure–temperature conditions, (iii) minimum plateau slope and hysteresis, (iv) fast kinetics of low-pressure hydrogen absorption and high pressure H_2 desorption. Additional target parameters important for H_2 compression include (v) high cycle stability during the extensive H_2 absorption and desorption implicit with these devices and (vi) minimal volume decrease upon dehydrogenation – the latter property is particularly important for high pressure hydrogen compression by allowing an increase of the MH filling density to minimise “dead space” formation within the MH containers during the hydrogen compression process.

12. Summary and future prospects

This review summarizes the work performed under the umbrella of IEA Hydrogen Task 32 “Hydrogen-based energy storage” during 2013–2018, providing the most up-to-date research results and ideas from leading experts in the field, which is the basis for

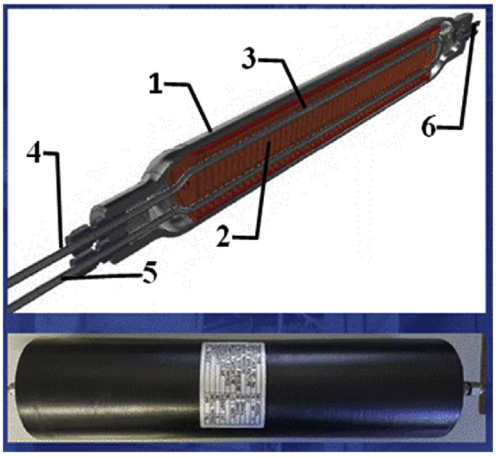

Fig. 28. Composite MH container for 100–500 bar H_2 compression developed by HySA Systems and TF Design (South Africa). Top – stainless steel liner (1) with a finned cartridge (2) filled by powdered mixture of AB_2-type MH and ENG and equipped with heating/cooling tube (3-5); (6) – H_2 input/output pipeline. Bottom – carbon fibre wound container.

ongoing research and development in this exciting field. Each section gives an insight into the latest results and aspects on research for “hydrogen-based energy storage”.

For many decades, hydrogen interactions with materials and hydrogen storage in solids were mainly of fundamental scientific interest, with some exceptions such as MH batteries at the end of the 1990s. Beginning with the 21st century the need became more urgent to convert individual transportation from internal combustion engines to emission-free FC vehicles. Hydrogen storage research was therefore driven by the goal to find a safe and efficient storage method fulfilling the strict requirements of the automotive industry concerning weight and volume. However, with the ongoing increase in renewable energy replacing more and more fossil fuels power plants, there has been increasing interest in hydrogen for chemical storage and as an energy carrier since 2010.

During this renaissance of hydrogen technologies, the spectrum of areas and topics covered within Task 32 widened compared to previous tasks on hydrogen storage in solids. Totally new areas, e.g. complex hydrides as solid-state electrolytes for novel lithium-ion batteries or heat storage in high-temperature hydrides for solar-thermal plants were initiated by experts in Task 32. Recently, liquid carriers and ammonia came back into focus for hydrogen transport in large quantities over long distances.

For hydrogen storage by physisorption, new framework materials have been developed possessing a high porosity and extremely large inner surface areas. The gravimetric hydrogen storage capacity of these novel frameworks can exceed 15 wt% on a material basis at 77 K and pressures of 50 bar. In the coming years, hydrogen storage in porous materials will focus on improving volumetric and working capacity, operating temperature, and thermal conductivity. The volumetric capacity will be increased by using interpenetrated framework structures that offer more surface area per volume, by compacting powders and preparing monoliths. Increasing the binding energies by tailoring pore volume and chemistry will raise the operating temperature. New materials, including flexible and core-shell MOFs, and porous molecular solids, such as organic cage compounds, will be investigated to optimize working capacity. Thermal conductivity will be improved by designing heat exchangers, such as fins or foams, compaction and mixing with graphite. The aim is a reversible, mobile or stationary energy-storage system with fast kinetics for power-to-hydrogen applications.

Substantial research efforts are being conducted to investigate new approaches towards the chemically based liquid hydrogen carriers. Currently, the two most prominent directions of work are focused on organic liquids containing molecules that can reversibly release and take up hydrogen, and the production of ammonia, which can be transported and stored and later cleaved back to hydrogen and nitrogen.

The chemistry of hydrogen is also very diverse, and hydrogen creates a variety of different types of chemical interactions and bonds, forming compounds with most other elements in the Periodic Table, including new varieties of compounds and solids which have been explored in the past half-decade and described in Section 4. Detailed analysis of intermetallic hydrides reveals their crystal chemistry and electronic, magnetic and hydrogen storage related properties. Sections 9 and 11 demonstrated that use of interstitial hydrides can achieve high volumetric and gravimetric H densities, and that they have excellent performance in MH batteries, in hydrogen stores utilized in hydrogen driven forklifts as well as in hydrogen gas compressors providing output pressures from 100 bar to 800 bar. Recently, alloys consisting of four or five metals have received significant focus as their higher entropy influences hydrogen release and uptake properties as discussed in Section 6. Although their volumetric hydrogen densities are high, the gravimetric densities are similar to conventional crystalline phases. However, this class of materials has a promising high stability over thousands of cycles of hydrogen release and uptake at moderate conditions, which is a very desirable trait for many applications. Further research efforts are envisaged to identify alloys offering enhanced H capacities exceeding $H/Me = 2$ and revealing the bonding mechanism of the metal-hydrogen interactions.

Magnesium-based materials have been considered for several decades and in the past few years researchers have provided Mg-containing systems with further improved kinetics of hydrogen release and uptake at more moderate working temperatures, which was covered in Section 7. Interestingly, magnesium-based systems are also considered for the concentrated solar thermal energy storage systems described in Section 10. Furthermore, Mg-based materials are utilized commercially for stationary hydrogen storage systems.

Hydrogen also forms covalent bonds to other elements, e.g. boron, aluminum and nitrogen. This behaviour has led to a very large diversity of novel materials with fascinating structures, compositions and physical and chemical properties, denoted complex hydrides. These materials often have both very high gravimetric and volumetric hydrogen densities, but reversible hydrogen release and uptake is very challenging to achieve. However, continuous improvement of the properties of reactive hydride composites has now led to a catalyzed $2LiBH_4–MgH_2$ composite, which has very promising properties. Higher borate anions, with higher thermal stability, such as closo-borates, have for a long time been considered as unwanted byproducts obtained during dehydrogenation. However, the closo-borates are now being utilized for design and synthesis of novel battery materials, such as electrolytes, owing to their relatively weak coordination to cations and dynamic disorder, which is often observed in high temperature polymorphs. Thus, complex hydrides are shown in Section 9 to have attractive properties for new applications in electrochemical storage as well as hydrogen storage. Recent progress in the design and synthesis of novel materials has opened new routes to solid state batteries and a significant potential for electrochemical energy storage.

Fundamental studies will further focus on nanostructured metal hydrides and will follow the approach described in Section 8. Within the next years, the goal is to achieve an experimental determination of the excess enthalpy and entropy associated with interfaces for a set of magnesium-based nanomaterials with different microstructural scales and compositions, in the search for a material, in which a significant enthalpic destabilization is not counteracted by entropic effects. In addition, we plan to explore the concept of elastic destabilization in nanostructures with an intermediate size range to exploit the power of long-range stress fields. Success in these research areas would promote the development of lightweight hydrides with lower desorption temperature at ambient hydrogen pressure and improved cyclic stability.

After many years of thorough research work and characterization of metal hydrides for heat storage applications, the next step towards commercialization is the up-scaling of these systems for heat storage. The Max-Planck-Institut in Mülheim an der Ruhr recently started a demonstration project together with other partners from academia and industry (IUTA Duisburg, Westphalian University of Applied Sciences, Gelsenkirchen, Martin Busch & Sohn GmbH, Schermbeck). The aim of the project is the storage of 250 kWh heat at a temperature level around 350 °C with an amount of roughly 400 kg of Mg/MgH_2. Easy handling of the storage material, a simple storage tank construction with the option for further enlargement and the operation of the system under changing conditions will be demonstrated during the project. Researchers at Western Australia's Curtin University are collaborating with TEXEL

and ITP Thermal for the development of an innovative thermal battery which will be a key component in allowing solar power systems to produce electricity overnight – a breakthrough which could allow solar systems to be used as a viable alternative to fossil fuels in commercial and heavy industries around the world. The research aims to develop new technology to integrate thermochemical energy storage via a thermal battery into a dish-Stirling system.

In 2019 the IEA recognized hydrogen as a key part of a clean and secure energy future and presented recommendations on "The Future of Hydrogen" to the G20 in Japan in June [596]. On this exciting pathway to a new, renewable energy economy, the work achieved in Task 32 is continued in Task 40 "Energy storage and conversion based on hydrogen" via eight working groups, focusing on porous materials for hydrogen storage, magnesium- and intermetallic alloys-based hydrides for energy storage, complex hydrides, ammonia and reversible liquid hydrogen carriers, catalysis, electrochemical storage of energy, hydride-based thermal energy storage, and research and development for hydrogen storage and compression.

In the present paper, we have reviewed the recent assessments on properties of a broad group of hydrogen storage materials, H storage methods and hydrogen-material interactions. Our vision is that for a sustainable energy future, hydrogen will most likely have a prominent status as an energy carrier since it has the highest energy density among all known substances, and can be readily produced from water via several processes including renewable sources [597]. Thus, an energy system based on hydrogen may have just as few steps in the chain as the presently-used methods based on fossil fuels, i.e. production of the energy carrier, storage and transportation and then a variety of possible utilizations. Importantly, hydrogen has the fastest dispersion rate in air [598], which can contribute to the safety aspects of its use in case of a leak with appropriate ventilation considerations.

In conclusion, we have presented different, safe and efficient storage methods for the future energy carrier hydrogen, which are very promising. However, prior to application they still need improvement and optimization requiring further research and development. The ultimate goal is to discover a sustainable replacement for liquid fossil fuels for transportation, for which a U.S. Department of Energy advisory group has indicated that more than 20 properties need to be simultaneously optimized [599]. This is clearly a very challenging task. However, this review reveals that fundamental science and engineering are making headway towards solving this task. Furthermore, new moderate to large scale demonstration projects are underway in 2019. For example, the HyCARE (Hydrogen CArrier for Renewable Energy Storage) project [600] aims at developing a hydrogen storage tank with a 50 kg hydrogen storage capacity through use of a metal hydride by linking hydrogen and heat storage to improve energy efficiency and to reduce the footprint of the complete system. This storage tank will be connected to a 20 kW Proton Exchange Membrane (PEM) electrolyzer as the hydrogen provider and a 10 kW PEM fuel cell as the hydrogen user. While metal hydrides have been utilized for fuel storage on-board submarines for nearly 20 years [356,554], several storage methods were recently assessed for various types of inland maritime vessels [601] and different options were proposed depending upon operating scenarios. Hence, the scope of applications utilizing hydrogen storage in different forms continues to expand.

Declaration of competing interest

The authors declare that they have no known competing financial interests or personal relationships that could have appeared to influence the work reported in this paper.

CRediT authorship contribution statement

Michael Hirscher: Writing - original draft, Supervision, Writing - review & editing. **Volodymyr A. Yartys:** Writing - original draft, Supervision, Writing - review & editing. **Marcello Baricco:** Writing - original draft. **Jose Bellosta von Colbe:** Writing - original draft. **Didier Blanchard:** Writing - original draft. **Robert C. Bowman:** Writing - original draft, Writing - review & editing. **Darren P. Broom:** Writing - original draft, Writing - review & editing. **Craig E. Buckley:** Writing - original draft. **Fei Chang:** Writing - original draft. **Ping Chen:** Writing - original draft. **Young Whan Cho:** Writing - original draft. **Jean-Claude Crivello:** Writing - original draft. **Fermin Cuevas:** Writing - original draft. **William I.F. David:** Writing - original draft. **Petra E. de Jongh:** Writing - original draft. **Roman V. Denys:** Writing - original draft. **Martin Dornheim:** Writing - original draft. **Michael Felderhoff:** Writing - original draft. **Yaroslav Filinchuk:** Writing - original draft. **George E. Froudakis:** Writing - original draft. **David M. Grant:** Writing - original draft, Writing - review & editing. **Evan MacA. Gray:** Writing - original draft. **Bjørn C. Hauback:** Writing - original draft. **Teng He:** Writing - original draft. **Terry D. Humphries:** Writing - original draft, Writing - review & editing. **Torben R. Jensen:** Writing - original draft. **Sangryun Kim:** Writing - original draft. **Yoshitsugu Kojima:** Writing - original draft. **Michel Latroche:** Writing - original draft. **Hai-Wen Li:** Writing - original draft. **Mykhaylo V. Lototskyy:** Writing - original draft, Writing - review & editing. **Joshua W. Makepeace:** Writing - original draft. **Kasper T. Møller:** Writing - original draft. **Lubna Naheed:** Writing - original draft. **Peter Ngene:** Writing - original draft. **Dag Noréus:** Writing - original draft. **Magnus Moe Nygård:** Writing - original draft. **Shinichi Orimo:** Writing - original draft. **Mark Paskevicius:** Writing - original draft. **Luca Pasquini:** Writing - original draft. **Dorthe B. Ravnsbæk:** Writing - original draft. **M. Veronica Sofianos:** Writing - original draft. **Terrence J. Udovic:** Writing - original draft. **Tejs Vegge:** Writing - original draft. **Gavin S. Walker:** Writing - original draft. **Colin J. Webb:** Writing - original draft, Writing - review & editing. **Claudia Weidenthaler:** Writing - original draft. **Claudia Zlotea:** Writing - original draft.

Acknowledgements

All authors contributed to the preparation of the draft of the manuscript and read, commented and corrected its final version.

VAY is grateful for the support this work has received from the Research Council of Norway (Project 285146 - New IEA Task ENERGY STORAGE AND CONVERSION BASED ON HYDROGEN).

Financial support from the EU HORIZON2020/RISE Program, project HYDRIDE4MOBILITY, is gratefully acknowledged by VAY, JBvC, RVD, MD and MVL.

MVL acknowledges financial support from the Department of Science and Innovation (DSI; Hydrogen South Africa/HySA Program, projects KP6–S02 and KP6–S03), as well as the National Science Foundation (NRF; grant number 109092) of Republic of South Africa.

References

[1] M. Becher, M. Haluska, M. Hirscher, A. Quintel, V. Skakalova, U. Dettlaff-Weglikovska, et al., Hydrogen storage in carbon nanotubes, Compt. Rendus Phys. 4 (9) (2003) 1055–1062.

[2] G.G. Tibbetts, G.P. Meisner, C.H. Olk, Hydrogen storage capacity of carbon nanotubes, filaments, and vapor-grown fibers, Carbon 39 (15) (2001) 2291–2301.

[3] D.P. Broom, M. Hirscher, Irreproducibility in hydrogen storage material

research, Energy Environ. Sci. 9 (11) (2016) 3368–3380.
[4] N.L. Rosi, J. Eckert, M. Eddaoudi, D.T. Vodak, J. Kim, M. O'Keeffe, et al., Hydrogen storage in microporous metal-organic frameworks, Science 300 (5622) (2003) 1127–1129.
[5] J.L.C. Rowsell, A.R. Millward, K.S. Park, O.M. Yaghi, Hydrogen sorption in functionalized metal-organic frameworks, J. Am. Chem. Soc. 126 (18) (2004) 5666–5667.
[6] M. Hirscher, Hydrogen storage by cryoadsorption in ultrahigh-porosity metal-organic frameworks, Angew. Chem. Int. Ed. 50 (3) (2011) 581–582.
[7] M. Hirscher, B. Panella, Hydrogen storage in metal–organic frameworks, Scr. Mater. 56 (10) (2007) 809–812.
[8] B. Panella, M. Hirscher, Hydrogen physisorption in metal-organic porous crystals, Adv. Mater. 17 (5) (2005) 538–541.
[9] B. Panella, M. Hirscher, H. Pütter, U. Müller, Hydrogen adsorption in metal–organic frameworks: Cu-MOFs and Zn-MOFs compared, Adv. Funct. Mater. 16 (4) (2006) 520–524.
[10] A.G. Wong-Foy, A.J. Matzger, O.M. Yaghi, Exceptional H_2 saturation uptake in microporous metal-organic frameworks, J. Am. Chem. Soc. 128 (11) (2006) 3494–3495.
[11] B. Panella, K. Hönes, U. Müller, N. Trukhan, M. Schubert, H. Pütter, et al., Desorption studies of hydrogen in metal-organic frameworks, Angew. Chem. Int. Ed. 47 (11) (2008) 2138–2142.
[12] B. Schmitz, U. Müller, N. Trukhan, M. Schubert, G. Férey, M. Hirscher, Heat of adsorption for hydrogen in microporous high-surface-area materials, ChemPhysChem 9 (15) (2008) 2181–2184.
[13] M. Dincă, J.R. Long, Hydrogen storage in microporous metal-organic frameworks with exposed metal sites, Angew. Chem. Int. Ed. 47 (36) (2008) 6766–6779.
[14] M.D. Allendorf, Z. Hulvey, T. Gennett, A. Ahmed, T. Autrey, J. Camp, et al., An assessment of strategies for the development of solid-state adsorbents for vehicular hydrogen storage, Energy Environ. Sci. 11 (10) (2018) 2784–2812.
[15] D. Dybtsev, C. Serre, B. Schmitz, B. Panella, M. Hirscher, M. Latroche, et al., Influence of $[Mo_6Br_8F_6]^{2-}$ cluster unit inclusion within the mesoporous solid MIL-101 on hydrogen storage performance, Langmuir 26 (13) (2010) 11283–11290.
[16] P. Szilágyi, D.M. Rogers, I. Zaiser, E. Callini, S. Turner, A. Borgschulte, et al., Functionalised metal-organic frameworks: a novel approach to stabilising single metal atoms, J. Mater. Chem. 5 (30) (2017) 15559–15566.
[17] P.Á. Szilágyi, I. Weinrauch, H. Oh, M. Hirscher, J. Juan-Alcañiz, P. Serra-Crespo, et al., Interplay of linker functionalization and hydrogen adsorption in the metal-organic framework MIL-101, J. Phys. Chem. C 118 (34) (2014) 19572–19579.
[18] R. Balderas-Xicohténcatl, M. Schlichtenmayer, M. Hirscher, Volumetric hydrogen storage capacity in metal–organic frameworks, Energy Technol. 6 (3) (2018) 578–582.
[19] A. Ahmed, Y. Liu, J. Purewal, L.D. Tran, A.G. Wong-Foy, M. Veenstra, et al., Balancing gravimetric and volumetric hydrogen density in MOFs, Energy Environ. Sci. 10 (11) (2017) 2459–2471.
[20] M. Schlichtenmayer, M. Hirscher, The useable capacity of porous materials for hydrogen storage, Appl. Phys. A 122 (4) (2016) 379.
[21] A. Ahmed, S. Seth, J. Purewal, A.G. Wong-Foy, M. Veenstra, A.J. Matzger, et al., Exceptional hydrogen storage achieved by screening nearly half a million metal-organic frameworks, Nat. Commun. 10 (1) (2019) 1568.
[22] J.A. Mason, J. Oktawiec, M.K. Taylor, M.R. Hudson, J. Rodriguez, J.E. Bachman, et al., Methane storage in flexible metal-organic frameworks with intrinsic thermal management, Nature 527 (7578) (2015) 357–361.
[23] D.P. Broom, C.J. Webb, Pitfalls in the characterisation of the hydrogen sorption properties of materials, Int. J. Hydrogen Energy 42 (49) (2017) 29320–29343.
[24] C.J. Webb, E.M. Gray, Analysis of the uncertainties in gas uptake measurements using the Sieverts method, Int. J. Hydrogen Energy 39 (1) (2014) 366–375.
[25] C.J. Webb, E.M.A. Gray, Misconceptions in the application of the Sieverts technique, Int. J. Hydrogen Energy 38 (33) (2013) 14281–14283.
[26] C.J. Webb, E.M. Gray, Analysis of uncertainties in gas uptake measurements using the gravimetric method, Int. J. Hydrogen Energy 39 (13) (2014) 7158–7164.
[27] C. Zlotea, P. Moretto, T. Steriotis, A Round Robin characterisation of the hydrogen sorption properties of a carbon based material, Int. J. Hydrogen Energy 34 (7) (2009) 3044–3057.
[28] P. Moretto, C. Zlotea, F. Dolci, A. Amieiro, J.L. Bobet, A. Borgschulte, et al., A Round Robin Test exercise on hydrogen absorption/desorption properties of a magnesium hydride based material, Int. J. Hydrogen Energy 38 (16) (2013) 6704–6717.
[29] K.E. Hurst, T. Gennett, J. Adams, M.D. Allendorf, R. Balderas-Xicohténcatl, M. Bielewski, et al., An international laboratory comparison study of volumetric and gravimetric hydrogen adsorption measurements, ChemPhysChem 20 (15) (2019) 1997–2009.
[30] D. Ramimoghadam, E.M.A. Gray, C.J. Webb, Review of polymers of intrinsic microporosity for hydrogen storage applications, Int. J. Hydrogen Energy 41 (2016) 16944–16965.
[31] D.S. Pyle, E.M.A. Gray, C.J. Webb, A Sieverts apparatus for measuring high-pressure hydrogen isotherms on porous materials, Int. J. Hydrogen Energy 42 (31) (2017) 20111–20119.
[32] D. Ramimoghadam, L. Naheed, S.E. Boyd, C.L. Brown, T.A. Webb, E. Maca Gray, et al., Postsynthetic modification of a network polymer of intrinsic microporosity and its hydrogen adsorption properties, J. Phys. Chem. C 123 (12) (2019) 6998–7009.
[33] D. Ramimoghadam, C.L. Brown, S.E. Boyd, E. Gray, C.J. Webb, Hydrogen uptake properties of a nanoporous PIM-1-polyaniline nanocomposite polymer, J. Mater. Chem. 123 (2019) 6998–7009.
[34] D. Ramimoghadam, S.E. Boyd, C.L. Brown, A. Mac, E. Gray, C.J. Webb, The effect of thermal treatment on the hydrogen-storage properties of PIM-1, ChemPhysChem 20 (12) (2019) 1613–1623.
[35] B. Streppel, M. Hirscher, BET specific surface area and pore structure of MOFs determined by hydrogen adsorption at 20 K, Phys. Chem. Chem. Phys. 13 (8) (2011) 3220–3222.
[36] H. Oh, D. Lupu, G. Blanita, M. Hirscher, Experimental assessment of physical upper limit for hydrogen storage capacity at 20 K in densified MIL-101 monoliths, RSC Adv. 4 (6) (2014) 2648–2651.
[37] C.I. Contescu, C.M. Brown, Y. Liu, V.V. Bhat, N.C. Gallego, Detection of hydrogen spillover in palladium-modified activated carbon fibers during hydrogen adsorption, J. Phys. Chem. C 113 (14) (2009) 5886–5890.
[38] H. Oh, T. Gennett, P. Atanassov, M. Kurttepeli, S. Bals, K.E. Hurst, et al., Hydrogen adsorption properties of platinum decorated hierarchically structured templated carbons, Microporous Mesoporous Mater. 177 (2013) 66–74.
[39] N.P. Stadie, J.J. Purewal, C.C. Ahn, B. Fultz, Measurements of hydrogen spillover in platinum doped superactivated carbon, Langmuir 26 (19) (2010) 15481–15485.
[40] S.B. Kalidindi, H. Oh, M. Hirscher, D. Esken, C. Wiktor, S. Turner, et al., Metal@COFs: covalent organic frameworks as templates for pd nanoparticles and hydrogen storage properties of Pd@COF-102 hybrid material, Chem. Eur J. 18 (35) (2012) 10848–10856.
[41] A. Malouche, C. Zlotea, P.Á. Szilágyi, Interactions of hydrogen with Pd@MOF composites, ChemPhysChem 20 (10) (2019) 1282–1295.
[42] M. Paskevicius, H.Y. Tian, D.A. Sheppard, C.J. Webb, M.P. Pitt, E.M.A. Gray, et al., Magnesium hydride formation within carbon aerogel, J. Phys. Chem. C 115 (5) (2011) 1757–1766.
[43] H.Y. Tian, C.E. Buckley, M. Paskevicius, D.A. Sheppard, S.B. Wang, C.J. Webb, et al., Nanoscale cobalt doped carbon aerogel: microstructure and isosteric heat of hydrogen adsorption, Int. J. Hydrogen Energy 36 (17) (2011) 10855–10860.
[44] M.V. Sofianos, A.L. Chaudhary, M. Paskevicius, D.A. Sheppard, T.D. Humphries, M. Dornheim, et al., Hydrogen storage properties of eutectic metal borohydrides melt-infiltrated into porous Al scaffolds, J. Alloy. Comp. 775 (2019) 474–480.
[45] E. Ianni, M.V. Sofianos, D.A. Sheppard, M.R. Rowles, T.D. Humphries, S. Liu, et al., Synthesis and characterisation of a porous Al scaffold sintered from $NaAlH_4$, J. Mater. Sci. 53 (2) (2018) 1076–1087.
[46] E. Ianni, M.V. Sofianos, M.R. Rowles, D.A. Sheppard, T.D. Humphries, C.E. Buckley, Synthesis of $NaAlH_4$/Al composites and their applications in hydrogen storage, Int. J. Hydrogen Energy 43 (36) (2018) 17309–17317.
[47] M.V. Sofianos, D.A. Sheppard, M.R. Rowles, T.D. Humphries, S. Liu, C.E. Buckley, Novel synthesis of porous Mg scaffold as a reactive containment vessel for $LiBH_4$, RSC Adv. 7 (58) (2017) 36340–36350.
[48] M. Veronica Sofianos, D.A. Sheppard, E. Ianni, T.D. Humphries, M.R. Rowles, S. Liu, et al., Novel synthesis of porous aluminium and its application in hydrogen storage, J. Alloy. Comp. 702 (2017) 309–317.
[49] M.V. Sofianos, D.A. Sheppard, D.S. Silvester, J. Lee, M. Paskevicius, T.D. Humphries, et al., Electrochemical synthesis of highly ordered porous Al scaffolds melt-infiltrated with $LiBH_4$ for hydrogen storage, J. Electrochem. Soc. 165 (2) (2018) D37–D42.
[50] E. Tylianakis, G.K. Dimitrakakis, S. Melchor, J.A. Dobado, G.E. Froudakis, Porous nanotube network: a novel 3-D nanostructured material with enhanced hydrogen storage capacity, Chem. Commun. 47 (8) (2011) 2303–2305.
[51] A. Gotzias, E. Tylianakis, G. Froudakis, T. Steriotis, Theoretical study of hydrogen adsorption in oxygen functionalized carbon slit pores, Microporous Mesoporous Mater. 154 (2012) 38–44.
[52] T. Stergiannakos, E. Tylianakis, E. Klontzas, P.N. Trikalitis, G.E. Froudakis, Hydrogen storage in novel Li-doped corrole metal-organic frameworks, J. Phys. Chem. C 116 (15) (2012) 8359–8363.
[53] A. Gotzias, E. Tylianakis, G. Froudakis, T. Steriotis, Effect of surface functionalities on gas adsorption in microporous carbons: a grand canonical Monte Carlo study, Adsorption 19 (2–4) (2013) 745–756.
[54] E. Tylianakis, G.K. Dimitrakakis, F.J. Martin-Martinez, S. Melchor, J.A. Dobado, E. Klontzas, et al., Designing novel nanoporous architectures of carbon nanotubes for hydrogen storage, Int. J. Hydrogen Energy 39 (18) (2014) 9825–9829.
[55] G.N. Kalantzopoulos, A. Enotiadis, E. Maccallini, M. Antoniou, K. Dimos, A. Policicchio, et al., Hydrogen storage in ordered and disordered phenylene-bridged mesoporous organosilicas, Int. J. Hydrogen Energy 39 (5) (2014) 2104–2114.
[56] C.Y. Wang, J.L. Gray, Q. Gong, Y. Zhao, J. Li, E. Klontzas, et al., Hydrogen storage with spectroscopic identification of chemisorption sites in Cu-TDPAT via spillover from a Pt/activated carbon catalyst, J. Phys. Chem. C 118 (46) (2014) 26750–26763.
[57] A. Gotzias, E. Tylianakis, G. Froudakis, T. Steriotis, Adsorption in micro and mesoporous slit carbons with oxygen surface functionalities, Microporous

Mesoporous Mater. 209 (2015) 141–149.
[58] L.P. Zârbo, M.A. Oancea, E. Klontzas, I.G. Grosu, G.E. Froudakis, Electrically enhanced hydrogen adsorption in metal-organic frameworks, ChemRxiv 1–19 (2019), https://doi.org/10.26434/chemrxiv.8209304.v1.
[59] I. Spanopoulos, C. Tsangarakis, E. Klontzas, E. Tylianakis, G. Froudakis, K. Adil, et al., Reticular synthesis of HKUST-like tbo-MOFs with enhanced CH_4 storage, J. Am. Chem. Soc. 138 (5) (2016) 1568–1574.
[60] I. Spanopoulos, C. Tsangarakis, S. Barnett, H. Nowell, E. Klontzas, G.E. Froudakis, et al., Directed assembly of a high surface area 2D metal-organic framework displaying the augmented "kagomé dual" (kgd-a) layered topology with high H_2 and CO_2 uptake, Inorg. Chem. Front. 4 (5) (2017) 825–832.
[61] G. Borboudakis, T. Stergiannakos, M. Frysali, E. Klontzas, I. Tsamardinos, G.E. Froudakis, Chemically intuited, large-scale screening of MOFs by machine learning techniques, NPJ Comput. Mater. 3 (1) (2017) 40.
[62] G.S. Fanourgakis, K. Gkagkas, E. Tylianakis, E. Klontzas, G. Froudakis, A robust machine learning algorithm for the prediction of methane adsorption in nanoporous materials, J. Phys. Chem. A 123 (28) (2019) 6080–6087.
[63] D.P. Broom, C.J. Webb, K.E. Hurst, P.A. Parilla, T. Gennett, C.M. Brown, et al., Outlook and challenges for hydrogen storage in nanoporous materials, Appl. Phys. As 122 (3) (2016) 1–21.
[64] D.P. Broom, C.J. Webb, G.S. Fanourgakis, G.E. Froudakis, P.N. Trikalitis, M. Hirscher, Concepts for improving hydrogen storage in nanoporous materials, Int. J. Hydrogen Energy 44 (15) (2019) 7768–7779.
[65] Strategic Innovation Promotion Program, Energy Carriers Japan, 2015.
[66] IRENA, Renewable Energy Auctions: Status and Trends beyond Price, 2019.
[67] ACIL Allen Consulting, Opportunities for Australia from Hydrogen Exports [Internet], ACIL Allen Consulting for ARENA, 2018. Available from: https://arena.gov.au/assets/2018/08/opportunities-for-australia-from-hydrogen-exports.pdf.
[68] T. Grube, L. Doré, A. Hoffrichter, L.E. Hombach, S. Raths, M. Robinius, et al., An option for stranded renewables: electrolytic-hydrogen in future energy systems, Sustain. Energy Fuels 2 (7) (2018) 1500–1515.
[69] R. Bañares-Alcántara, G. Dericks III, M. Fiaschetti, Philipp Grünewald, J.M. Lopez, E. Tsang, et al., Analysis of Islanded Ammonia-Based Energy Storage Systems, 2015. http://www2.eng.ox.ac.uk/systemseng/publications/Ammonia-based_ESS.pdf.
[70] G. Gahleitner, Hydrogen from renewable electricity: an international review of power-to-gas pilot plants for stationary applications, Int. J. Hydrogen Energy 38 (5) (2013) 2039–2061.
[71] E.M. Gray, C.J. Webb, J. Andrews, B. Shabani, P.J. Tsai, S.L.I. Chan, Hydrogen storage for off-grid power supply, Int. J. Hydrogen Energy 36 (1) (2011) 654–663.
[72] Energy Trends and Prices Statistical Release: 26 July 2018, U.K. Government Department for Business, Energy & Industrial Strategy, 2018.
[73] W.A. Amos, Costs of storing and transporting hydrogen, Other Information: PBD: 27 Jan 1999; PBD: 27 Jan 1999; PBD: 27 Jan 1999. 1999. Available from: http://www.osti.gov/bridge/servlets/purl/6574-OBMIES/webviewable/.
[74] International Energy Agency, The Future of Hydrogen: Seizing Today's Opportunities, 2019.
[75] J.W. Makepeace, T. He, C. Weidenthaler, T.R. Jensen, F. Chang, T. Vegge, et al., Reversible ammonia-based and liquid organic hydrogen carriers for high-density hydrogen storage: recent progress, Int. J. Hydrogen Energy 44 (15) (2019) 7746–7767.
[76] C.H. Christensen, T. Johannessen, R.Z. Sørensen, J.K. Nørskov, Towards an ammonia-mediated hydrogen economy? Catal. Today 111 (1–2) (2006) 140–144.
[77] P. Preuster, C. Papp, P. Wasserscheid, Liquid organic hydrogen carriers (LOHCs): toward a hydrogen-free hydrogen economy, Acc. Chem. Res. 50 (1) (2017) 74–85.
[78] P.T. Aakko-Saksa, C. Cook, J. Kiviaho, T. Repo, Liquid organic hydrogen carriers for transportation and storing of renewable energy – review and discussion, J. Power Sources 396 (2018) 803–823.
[79] A. Klerke, C.H. Christensen, J.K. Nørskov, T. Vegge, Ammonia for hydrogen storage: challenges and opportunities, J. Mater. Chem. 18 (20) (2008) 2304–2310.
[80] J.S. Yoo, R. Christensen, T. Vegge, J.K. Nørskov, F. Studt, Theoretical insight into the trends that guide the electrochemical reduction of carbon dioxide to formic acid, ChemSusChem 9 (4) (2016) 358–363.
[81] S. Bruce, M. Temminghoff, J. Hayward, E. Schmidt, C. Munnings, D. Palfreyman, et al., National hydrogen roadmap, Available from: https://www.csiro.au/en/Do-business/Futures/Reports/Hydrogen-Roadmap, 2018.
[82] Y. Mizuno, Y. Ishimoto, S. Sakai, K. Sakata, Economic analysis on international hydrogen energy carrier supply chains, J. Jpn. Soc. Energy Resour. 38 (3) (2016) 11–17. Available from: http://www.jser.gr.jp/journal/journal_pdf/2017/journal201705_2.pdf.
[83] M. Aziz, T. Oda, T. Kashiwagi, Comparison of liquid hydrogen, methylcyclohexane and ammonia on energy efficiency and economy, Energy Procedia 158 (2019) 4086–4091.
[84] Ministry of Economy Trade and Industry, Study of Master Plan for Creating a Low-Carbon Energy System in Saudi Arabia, 2018.
[85] T. He, P. Pachfule, H. Wu, Q. Xu, P. Chen, Hydrogen carriers, Nat. Rev. Mater. 1 (12) (2016) 1–17.
[86] M. van der Van, Y. Kobayashi, R. Diercks, Technology roadmap: energy and GHG reductions in the chemical industry via catalytic processes, Energy Technol. Perspect. (2013). Available from: https://www.iea.org/publications/freepublications/publication/TechnologyRoadmapEnergyandGHGReductionsintheChemicalIndustryviaCatalyticProcesses.pdf.
[87] G.P. Pez, A.R. Scott, A.C. Cooper, H. Cheng, F.C. Wilhelm, A.H. Abdourazak, Hydrogen Storage by Reversible Hydrogenation of Pi-Conjugated Substrates, US7101530B2, U.S., 2008.
[88] E. Clot, O. Eisenstein, R.H. Crabtree, Computational structure-activity relationships in H_2 storage: how placement of N atoms affects release temperatures in organic liquid storage materials, Chem. Commun. (22) (2007) 2231–2233.
[89] Y. Cui, S. Kwok, A. Bucholtz, B. Davis, R.A. Whitney, P.G. Jessop, The effect of substitution on the utility of piperidines and octahydroindoles for reversible hydrogen storage, New J. Chem. 32 (6) (2008) 1027–1037.
[90] A. Moores, M. Poyatos, Y. Luo, R.H. Crabtree, Catalysed low temperature H_2 release from nitrogen heterocycles, New J. Chem. 30 (11) (2006) 1675–1678.
[91] K.M. Eblagon, D. Rentsch, O. Friedrichs, A. Remhof, A. Zuettel, A.J. Ramirez-Cuesta, et al., Hydrogenation of 9-ethylcarbazole as a prototype of a liquid hydrogen carrier, Int. J. Hydrogen Energy 35 (20) (2010) 11609–11621.
[92] J. Chen, G. Wu, Z. Xiong, H. Wu, Y.S. Chua, W. Zhou, et al., Synthesis, thermal behavior, and dehydrogenation kinetics study of lithiated ethylenediamine, Chem. Eur J. 20 (42) (2014) 13636–13643.
[93] J. Chen, H. Wu, G. Wu, Z. Xiong, R. Wang, H. Fan, et al., Lithiated primary amine - a new material for hydrogen storage, Chem. Eur J. 20 (22) (2014) 6632–6635.
[94] Y. Yu, T. He, A. Wu, Q. Pei, A. Karkamkar, T. Autrey, et al., Reversible hydrogen uptake/release over a sodium phenoxide–cyclohexanolate pair, Angew. Chem. Int. Ed. 58 (10) (2019) 3102–3107.
[95] A. Bourane, M. Elanany, T.V. Pham, S.P. Katikaneni, An overview of organic liquid phase hydrogen carriers, Int. J. Hydrogen Energy 41 (48) (2016) 23075–23091.
[96] T. He, L. Liu, G. Wu, P. Chen, Covalent triazine framework-supported palladium nanoparticles for catalytic hydrogenation of N-heterocycles, J. Mater. Chem. A. 3 (31) (2015) 16235–16241.
[97] Z. Wang, J. Belli, C.M. Jensen, Homogeneous dehydrogenation of liquid organic hydrogen carriers catalyzed by an iridium PCP complex, Faraday Discuss 151 (2011) 297–305.
[98] Z. Wang, I. Tonks, J. Belli, C.M. Jensen, Dehydrogenation of N-ethyl perhydrocarbazole catalyzed by PCP pincer iridium complexes: evaluation of a homogenous hydrogen storage system, J. Organomet. Chem. 694 (17) (2009) 2854–2857.
[99] J.W. Erisman, M.A. Sutton, J. Galloway, Z. Klimont, W. Winiwarter, How a century of ammonia synthesis changed the world, Nat. Geosci. 1 (10) (2008) 636–639.
[100] C. Loos-Neskovic, M.H. Dierkes, E. Jackwerth, M. Fedoroff, E. Garnier, Fixation of palladium on insoluble simple or complex cyano compounds, Hydrometallurgy 32 (3) (1993) 345–363.
[101] S. Mukherjee, S.V. Devaguptapu, A. Sviripa, C.R.F. Lund, G. Wu, Low-temperature ammonia decomposition catalysts for hydrogen generation, Appl. Catal. B Environ. 226 (2018) 162–181.
[102] S.F. Yin, B.Q. Xu, X.P. Zhou, C.T. Au, A mini-review on ammonia decomposition catalysts for on-site generation of hydrogen for fuel cell applications, Appl. Catal. A Gen. 277 (1–2) (2004) 1–9.
[103] Y.Q. Gu, X.P. Fu, P.P. Du, D. Gu, Z. Jin, Y.Y. Huang, et al., In situ X-ray diffraction study of Co-Al nanocomposites as catalysts for ammonia decomposition, J. Phys. Chem. C 119 (30) (2015) 17102–17110.
[104] V. Tagliazucca, K. Schlichte, F. Schüth, C. Weidenthaler, Molybdenum-based catalysts for the decomposition of ammonia: in situ X-ray diffraction studies, microstructure, and catalytic properties, J. Catal. 305 (2013) 277–289.
[105] M. Feyen, C. Weidenthaler, R. Güttel, K. Schlichte, U. Holle, A.H. Lu, et al., High-temperature stable, iron-based core-shell catalysts for ammonia decomposition, Chem. Eur. J. 17 (2) (2011) 598–605.
[106] J.C. Tseng, D. Gu, C. Pistidda, C. Horstmann, M. Dornheim, J. Ternieden, et al., Tracking the active catalyst for iron-based ammonia decomposition by in situ synchrotron diffraction studies, ChemCatChem 10 (19) (2018) 4465–4472.
[107] T.J. Wood, J.W. Makepeace, W.I.F. David, Neutron diffraction and gravimetric study of the manganese nitriding reaction under ammonia decomposition conditions, Phys. Chem. Chem. Phys 20 (13) (2018) 8547–8553.
[108] W.I.F. David, J.W. Makepeace, S.K. Callear, H.M.A. Hunter, J.D. Taylor, T.J. Wood, et al., Hydrogen production from ammonia using sodium amide, J. Am. Chem. Soc. 136 (38) (2014) 13082–13085.
[109] J. Guo, P. Wang, G. Wu, A. Wu, D. Hu, Z. Xiong, et al., Lithium imide synergy with 3d transition-metal nitrides leading to unprecedented catalytic activities for ammonia decomposition, Angew. Chem. Int. Ed. 54 (10) (2015) 2950–2954.
[110] J.W. Makepeace, T.J. Wood, H.M.A. Hunter, M.O. Jones, W.I.F. David, Ammonia decomposition catalysis using non-stoichiometric lithium imide, Chem Sci. 6 (7) (2015) 3805–3815.
[111] J.W. Makepeace, H.M.A. Hunter, T.J. Wood, R.I. Smith, C.A. Murray, W.I.F. David, Ammonia decomposition catalysis using lithium-calcium imide, Faraday Discuss. 188 (2016) 525–544.
[112] J. Guo, Z. Chen, A. Wu, F. Chang, P. Wang, D. Hu, et al., Electronic promoter or reacting species? The role of $LiNH_2$ on Ru in catalyzing NH_3 decomposition, Chem. Commun. 51 (82) (2015) 15161–15164.
[113] P. Yu, J. Guo, L. Liu, P. Wang, F. Chang, H. Wang, et al., Effects of alkaline earth

metal amides on Ru in catalytic ammonia decomposition, J. Phys. Chem. C 120 (5) (2016) 2822–2828.
[114] J. Guo, F. Chang, P. Wang, D. Hu, P. Yu, G. Wu, et al., Highly active MnN-Li_2NH composite catalyst for producing CO_x-free hydrogen, ACS Catal. 5 (5) (2015) 2708–2713.
[115] H. Cao, J. Guo, F. Chang, C. Pistidda, W. Zhou, X. Zhang, et al., Transition and alkali metal complex ternary amides for ammonia synthesis and decomposition, Chem. Eur J. 23 (41) (2017) 9766–9771.
[116] P.L. Bramwell, S. Lentink, P. Ngene, P.E. De Jongh, Effect of pore confinement of $LiNH_2$ on ammonia decomposition catalysis and the storage of hydrogen and ammonia, J. Phys. Chem. C 120 (48) (2016) 27212–27220.
[117] T.J. Wood, J.W. Makepeace, W.I.F. David, Isotopic studies of the ammonia decomposition reaction using lithium imide catalyst, Phys. Chem. Chem. Phys. 19 (6) (2017) 4719–4724.
[118] J.W. Makepeace, T.J. Wood, P.L. Marks, R.I. Smith, C.A. Murray, W.I.F. David, Bulk phase behavior of lithium imide-metal nitride ammonia decomposition catalysts, Phys. Chem. Chem. Phys. 20 (35) (2018) 22689–22697.
[119] C.D. Zeinalipour-Yazdi, J.S.J. Hargreaves, C.R.A. Catlow, Nitrogen activation in a Mars-van Krevelen mechanism for ammonia synthesis on Co_3Mo_3N, J. Phys. Chem. C 119 (51) (2015) 28368–28376.
[120] P. Wang, F. Chang, W. Gao, J. Guo, G. Wu, T. He, et al., Breaking scaling relations to achieve low-temperature ammonia synthesis through LiH-mediated nitrogen transfer and hydrogenation, Nat. Chem. 9 (1) (2017) 64–70.
[121] W. Gao, P. Wang, J. Guo, F. Chang, T. He, Q. Wang, et al., Barium hydride-mediated nitrogen transfer and hydrogenation for ammonia synthesis: a case study of cobalt, ACS Catal. 7 (5) (2017) 3654–3661.
[122] W. Gao, J. Guo, P. Wang, Q. Wang, F. Chang, Q. Pei, et al., Production of ammonia via a chemical looping process based on metal imides as nitrogen carriers, Nat. Energy 3 (12) (2018) 1067–1075.
[123] V. Kyriakou, I. Garagounis, E. Vasileiou, A. Vourros, M. Stoukides, Progress in the electrochemical synthesis of ammonia, Catal. Today 286 (2017) 2–13.
[124] S.Z. Andersen, V. Čolić, S. Yang, J.A. Schwalbe, A.C. Nielander, J.M. McEnaney, et al., A rigorous electrochemical ammonia synthesis protocol with quantitative isotope measurements, Nature 570 (7762) (2019) 504–508.
[125] B.H.R. Suryanto, H.L. Du, D. Wang, J. Chen, A.N. Simonov, D.R. MacFarlane, Challenges and prospects in the catalysis of electroreduction of nitrogen to ammonia, Nat. Catal. 2 (4) (2019) 290–296.
[126] Y. Abghoui, A.L. Garden, J.G. Howalt, T. Vegge, E. Skúlason, Electroreduction of N_2 to ammonia at ambient conditions on mononitrides of Zr, Nb, Cr, and V: a DFT guide for experiments, ACS Catal. 6 (2) (2016) 635–646.
[127] J.G. Howalt, T. Vegge, Electrochemical ammonia production on molybdenum nitride nanoclusters, Phys. Chem. Chem. Phys. 15 (48) (2013) 20957–20965.
[128] J.G. Howalt, T. Bligaard, J. Rossmeisl, T. Vegge, DFT based study of transition metal nano-clusters for electrochemical NH_3 production, Phys. Chem. Chem. Phys. 15 (20) (2013) 7785–7795.
[129] E. Skúlason, T. Bligaard, S. Gudmundsdóttir, F. Studt, J. Rossmeisl, F. Abild-Pedersen, et al., A theoretical evaluation of possible transition metal electrocatalysts for N_2 reduction, Phys. Chem. Chem. Phys. 14 (3) (2012) 1235–1245.
[130] S. Guthrie, F. Dunkerley, H. Tabaqchali, A. Harshfield, B. Ioppolo, C. Manville, Impact of Ammonia Emissions from Agriculture on Biodiversity: an Evidence Synthesis, RAND Corporation, Santa Monica, Calif., and Cambridge, UK, 2018.
[131] F.A. Uribe, S. Gottesfeld, T.A. Zawodzinski, Effect of ammonia as potential fuel impurity on proton exchange membrane fuel cell performance, J. Electrochem. Soc. 149 (3) (2002) A293.
[132] B.A. Van Hassel, J.R. Karra, J. Santana, S. Saita, A. Murray, D. Goberman, et al., Ammonia sorbent development for on-board H_2 purification, Sep. Purif. Technol. 142 (2015) 215–226.
[133] H. Miyaoka, H. Miyaoka, T. Ichikawa, T. Ichikawa, Y. Kojima, Highly purified hydrogen production from ammonia for PEM fuel cell, Int. J. Hydrogen Energy 43 (31) (2018) 14486–14492.
[134] K.E. Lamb, D.M. Viano, M.J. Langley, S.S. Hla, M.D. Dolan, High-purity H_2 produced from NH_3 via a ruthenium-based decomposition catalyst and vanadium-based membrane, Ind. Eng. Chem. Res. 57 (23) (2018) 7811–7816.
[135] R.Z. Sørensen, J.S. Hummelshøj, A. Klerke, J.B. Reves, T. Vegge, J.K. Nørskov, et al., Indirect, reversible high-density hydrogen storage in compact metal ammine salts, J. Am. Chem. Soc. 130 (27) (2008) 8660–8668.
[136] C.H. Christensen, R.Z. Sørensen, T. Johannessen, U.J. Quaade, K. Honkala, T.D. Elmøe, et al., Metal ammine complexes for hydrogen storage, J. Mater. Chem. 15 (38) (2005) 4106–4108.
[137] H.S. Jacobsen, H.A. Hansen, J.W. Andreasen, Q. Shi, A. Andreasen, R. Feidenhans'l, et al., Nanoscale structural characterization of $Mg(NH_3)_6Cl_2$ during NH_3 desorption: an *in situ* small angle X-ray scattering study, Chem. Phys. Lett. 441 (4–6) (2007) 255–260.
[138] R.E. Johnsen, P.B. Jensen, P. Norby, T. Vegge, Temperature- and pressure-induced changes in the crystal structure of $Sr(NH_3)_8Cl_2$, J. Phys. Chem. C 118 (42) (2014) 24349–24356.
[139] P.B. Jensen, A. Bialy, D. Blanchard, S. Lysgaard, A.K. Reumert, U.J. Quaade, et al., Accelerated DFT-based design of materials for ammonia storage, Chem. Mater. 27 (13) (2015) 4552–4561.
[140] S. Lysgaard, A.L. Ammitzbøll, R.E. Johnsen, P. Norby, U.J. Quaade, T. Vegge, Resolving the stability and structure of strontium chloride amines from equilibrium pressures, XRD and DFT, Int. J. Hydrogen Energy 37 (24) (2012) 18927–18936.
[141] P.B. Jensen, S. Lysgaard, U.J. Quaade, T. Vegge, Designing mixed metal halide ammines for ammonia storage using density functional theory and genetic algorithms, Phys. Chem. Chem. Phys. 16 (36) (2014) 19732–19740.
[142] A. Tekin, J.S. Hummelshøj, H.S. Jacobsen, D. Sveinbjörnsson, D. Blanchard, J.K. Nørskov, et al., Ammonia dynamics in magnesium ammine from DFT and neutron scattering, Energy Environ. Sci. 3 (4) (2010) 448–456.
[143] A. Bialy, P.B. Jensen, D. Blanchard, T. Vegge, U.J. Quaade, Solid solution barium-strontium chlorides with tunable ammonia desorption properties and superior storage capacity, J. Solid State Chem. 221 (2015) 32–36.
[144] A.L. Ammitzboll, S. Lysgaard, A. Klukowska, T. Vegge, U.J. Quaade, Surface adsorption in strontium chloride ammines, J. Chem. Phys. 138 (16) (2013), 164701-1.
[145] M. Paskevicius, L.H. Jepsen, P. Schouwink, R. Černý, D.B. Ravnsbæk, Y. Filinchuk, et al., Metal borohydrides and derivatives-synthesis, structure and properties, Chem. Soc. Rev. 46 (5) (2017) 1565–1634.
[146] L.H. Jepsen, M.B. Ley, Y.S. Lee, Y.W. Cho, M. Dornheim, J.O. Jensen, et al., Boron-nitrogen based hydrides and reactive composites for hydrogen storage, Mater. Today 17 (3) (2014) 129–135.
[147] G. Soloveichik, J.H. Her, P.W. Stephens, Y. Gao, J. Rijssenbeek, M. Andrus, et al., Ammine magnesium borohydride complex as a new material for hydrogen storage: structure and properties of $Mg(BH_4)_2 \cdot 2NH_3$, Inorg. Chem. 47 (10) (2008) 4290–4298.
[148] L.H. Jepsen, M.B. Ley, Y. Filinchuk, F. Besenbacher, T.R. Jensen, Tailoring the properties of ammine metal borohydrides for solid-state hydrogen storage, ChemSusChem 8 (8) (2015) 1452–1463.
[149] L.H. Jepsen, Y.S. Lee, R. Černý, R.S. Sarusie, Y.W. Cho, F. Besenbacher, et al., Amine calcium and strontium borohydrides: syntheses, structures, and properties, ChemSusChem 8 (20) (2015) 3472–3482.
[150] K. Yvon, G. Renaudin, Hydrides: solid state transition metal complexes, in: Encyclopedia of Inorganic and Bioinorganic Chemistry, John Wiley & Sons, Ltd, 2011, p. 1.
[151] T.D. Humphries, D.A. Sheppard, C.E. Buckley, Recent advances in the 18-electron complex transition metal hydrides of Ni, Fe, Co and Ru, Coord. Chem. Rev. 342 (2017) 19–33.
[152] T.D. Humphries, M. Matsuo, G. Li, S.I. Orimo, Complex transition metal hydrides incorporating ionic hydrogen: thermal decomposition pathway of $Na_2Mg_2FeH_8$ and $Na_2Mg_2RuH_8$, Phys. Chem. Chem. Phys. 17 (12) (2015) 8276–8282.
[153] T.D. Humphries, D.A. Sheppard, G. Li, M.R. Rowles, M. Paskevicius, M. Matsuo, et al., Complex hydrides as thermal energy storage materials: characterisation and thermal decomposition of $Na_2Mg_2NiH_6$, J. Mater. Chem. 6 (19) (2018) 9099–9108.
[154] S. Takagi, S.I. Orimo, Recent progress in hydrogen-rich materials from the perspective of bonding flexibility of hydrogen, Scr. Mater. 109 (2015) 1–5.
[155] T.D. Humphries, D.A. Sheppard, C.E. Buckley, Complex transition metal hydrides: linear correlation of countercation electronegativity versus T-D bond lengths, Chem. Commun. 51 (56) (2015) 11248–11251.
[156] J. Puszkiel, F. Gennari, P.A. Larochette, F. Karimi, C. Pistidda, R. Gosalawit-Utke, et al., Sorption behavior of the MgH_2-Mg_2FeH_6 hydride storage system synthesized by mechanical milling followed by sintering, Int. J. Hydrogen Energy 38 (34) (2013) 14618–14630.
[157] M. Polanski, T.K. Nielsen, I. Kunce, M. Norek, T. Płociński, L.R. Jaroszewicz, et al., Mg_2NiH_4 synthesis and decomposition reactions, Int. J. Hydrogen Energy 38 (10) (2013) 4003–4010.
[158] M. Polanski, T.K. Nielsen, Y. Cerenius, J. Bystrzycki, T.R. Jensen, Synthesis and decomposition mechanisms of Mg_2FeH_6 studied by *in-situ* synchrotron X-ray diffraction and high-pressure DSC, Int. J. Hydrogen Energy 35 (8) (2010) 3578–3582.
[159] M. Norek, T.K. Nielsen, M. Polanski, I. Kunce, T. Płociński, L.R. Jaroszewicz, et al., Synthesis and decomposition mechanisms of ternary Mg_2CoH_5 studied using *in situ* synchrotron X-ray diffraction, Int. J. Hydrogen Energy 36 (17) (2011) 10760–10770.
[160] T.D. Humphries, S. Takagi, G. Li, M. Matsuo, T. Sato, M.H. Sørby, et al., Complex transition metal hydrides incorporating ionic hydrogen: synthesis and characterization of $Na_2Mg_2FeH_8$ and $Na_2Mg_2RuH_8$, J. Alloy. Comp. 645 (S1) (2015) S347–S352.
[161] M. Matsuo, H. Saitoh, A. Machida, R. Sato, S. Takagi, K. Miwa, et al., Formation of an Fe-H complex anion in YFe_2: adjustment of imbalanced charge by using additional Li as an electron donor, RSC Adv. 3 (4) (2013) 1013–1016.
[162] K. Miwa, T. Sato, M. Matsuo, K. Ikeda, T. Otomo, S. Deledda, et al., Metallic intermediate hydride phase of $LaMg_2Ni$ with Ni-H covalent bonding: precursor state for complex hydride formation, J. Phys. Chem. C 120 (11) (2016) 5926–5931.
[163] K. Miwa, S. Takagi, M. Matsuo, S.I. Orimo, Thermodynamical stability of complex transition metal hydrides M_2FeH_6, J. Phys. Chem. C 117 (16) (2013) 8014–8019.
[164] H. Saitoh, S. Takagi, M. Matsuo, Y. Iijima, N. Endo, K. Aoki, et al., Li_4FeH_6: iron-containing complex hydride with high gravimetric hydrogen density, APL. Mater. 2 (7) (2014), 076103.
[165] T. Sato, S. Takagi, M. Matsuo, K. Aoki, S. Deledda, B.C. Hauback, et al., Raman and infrared spectroscopic studies on Li_4RuH_6 combined with first-principles calculations, Mater. Trans. 55 (8) (2014) 1117–1121.
[166] S. Takagi, T.D. Humphries, K. Miwa, S.I. Orimo, Enhanced tunability of thermodynamic stability of complex hydrides by the incorporation of H- anions, Appl. Phys. Lett. 104 (20) (2014) 203901.

[167] S. Takagi, Y. Iijima, T. Sato, H. Saitoh, K. Ikeda, T. Otomo, et al., True boundary for the formation of homoleptic transition-metal hydride complexes, Angew. Chem. Int. Ed. 54 (19) (2015) 5650–5653.

[168] E. Callini, K.F. Aguey-Zinsou, R. Ahuja, J.R. Ares, S. Bals, N. Biliškov, et al., Nanostructured materials for solid-state hydrogen storage: a review of the achievement of COST Action MP1103, Int. J. Hydrogen Energy 41 (32) (2016) 14404–14428.

[169] E. Callini, Z.Ö.K. Atakli, B.C. Hauback, S. Orimo, C. Jensen, M. Dornheim, et al., Complex and liquid hydrides for energy storage, Appl. Phys. A. 122 (4) (2016) 353.

[170] L.H. Jepsen, M.B. Ley, Y.S. Lee, Y.W. Cho, M. Dornheim, J.O. Jensen, et al., Boron-nitrogen based hydrides and reactive composites for hydrogen storage, Mater. Today 17 (3) (2014) 129–135.

[171] M.B. Ley, L.H. Jepsen, Y.S. Lee, Y.W. Cho, J.M. Bellosta Von Colbe, M. Dornheim, et al., Complex hydrides for hydrogen storage - new perspectives, Mater. Today 17 (3) (2014) 122–128.

[172] M. Paskevicius, L.H. Jepsen, P. Schouwink, R. Černý, D.B. Ravnsbæk, Y. Filinchuk, et al., Metal borohydrides and derivatives-synthesis, structure and properties, Chem. Soc. Rev. 46 (5) (2017) 1565–1634.

[173] K.T. Møller, T.R. Jensen, E. Akiba, Li H. wen, Hydrogen - a sustainable energy carrier, Prog. Nat. Sci. Mater. Int. 27 (1) (2017) 34–40.

[174] K.T. Møller, D. Sheppard, D.B. Ravnsbæk, C.E. Buckley, E. Akiba, H.W. Li, et al., Complex metal hydrides for hydrogen, thermal and electrochemical energy storage, Energies 10 (10) (2017) 1645.

[175] J. Huot, F. Cuevas, S. Deledda, K. Edalati, Y. Filinchuk, T. Grosdidier, et al., Mechanochemistry of metal hydrides: recent advances, Materials 12 (17) (2019) 2778.

[176] J. Huot, D.B. Ravnsbæk, J. Zhang, F. Cuevas, M. Latroche, T.R. Jensen, Mechanochemical synthesis of hydrogen storage materials, Prog. Mater. Sci. 58 (1) (2013) 30–75.

[177] B. Richter, J.B. Grinderslev, K.T. Møller, M. Paskevicius, T.R. Jensen, From metal hydrides to metal borohydrides, Inorg. Chem. 57 (17) (2018) 10768–10780.

[178] X.R. Liu, X.M. Chen, J. Zhang, T.R. Jensen, X. Chen, The interconversion between THF·B_3H_7 and $B_3H_8^-$: an efficient synthetic method for MB_3H_8 (M═Li and Na), Dalton Trans. 48 (16) (2019) 5140–5143.

[179] M.B. Ley, M. Paskevicius, P. Schouwink, B. Richter, D.A. Sheppard, C.E. Buckley, et al., Novel solvates $M(BH_4)_3S(CH_3)_2$ and properties of halide-free $M(BH_4)_3$ (M═y or Gd), Dalton Trans. 43 (35) (2014) 13333–13342.

[180] J.B. Grinderslev, K.T. Møller, M. Bremholm, T.R. Jensen, Trends in synthesis, crystal structure, and thermal and magnetic properties of rare-earth metal borohydrides, Inorg. Chem. 58 (9) (2019) 5503–5517.

[181] R. Černý, P. Schouwink, The crystal chemistry of inorganic metal borohydrides and their relation to metal oxides, Acta Crystallogr. B. 71 (6) (2015) 619–640.

[182] J.E. Olsen, C. Frommen, M.H. Sørby, B.C. Hauback, Crystal structures and properties of solvent-free $LiYb(BH_4)_{4-x}Cl_x$, $Yb(BH_4)_3$ and $Yb(BH_4)_{2-x}Cl_x$, RSC Adv. 3 (27) (2013) 10764–10774.

[183] T.D. Humphries, M.B. Ley, C. Frommen, K.T. Munroe, T.R. Jensen, B.C. Hauback, Crystal structure and *in situ* decomposition of $Eu(BH_4)_2$ and $Sm(BH_4)_2$, J. Mater. Chem. 3 (2) (2015) 691–698.

[184] D.B. Ravnsbæk, E.A. Nickels, R. Černý, C.H. Olesen, W.I.F. David, P.P. Edwards, et al., Novel alkali earth borohydride $Sr(BH_4)_2$ and borohydride-chloride $Sr(BH_4)Cl$, Inorg. Chem. 52 (19) (2013) 10877–10885.

[185] L.H. Rude, M. Corno, P. Ugliengo, M. Baricco, Y.S. Lee, Y.W. Cho, et al., Synthesis and structural investigation of $Zr(BH_4)_4$, J. Phys. Chem. C 116 (38) (2012) 20239–20245.

[186] D.B. Ravnsbæk, Y. Filinchuk, R. Černý, M.B. Ley, D. Haase, H.J. Jakobsen, et al., Thermal polymorphism and decomposition of $Y(BH_4)_3$, Inorg. Chem. 49 (8) (2010) 3801–3809.

[187] N.A. Tumanov, E. Roedern, Z. Łodziana, D.B. Nielsen, T.R. Jensen, A.V. Talyzin, et al., High-pressure study of $Mn(BH_4)_2$ reveals a stable polymorph with high hydrogen density, Chem. Mater. 28 (1) (2016) 274–283.

[188] B. Richter, D.B. Ravnsbæk, N. Tumanov, Y. Filinchuk, T.R. Jensen, Manganese borohydride; Synthesis and characterization, Dalton Trans. 44 (9) (2015) 3988–3996.

[189] Y. Filinchuk, B. Richter, T.R. Jensen, V. Dmitriev, D. Chernyshov, H. Hagemann, Porous and dense magnesium borohydride frameworks: synthesis, stability, and reversible absorption of guest species, Angew. Chem. Int. Ed. 50 (47) (2011) 11162–11166.

[190] N.A. Tumanov, D.A. Safin, B. Richter, Z. Łodziana, T.R. Jensen, Y. Garcia, et al., Challenges in the synthetic routes to $Mn(BH_4)_2$: insight into intermediate compounds, Dalton Trans. 44 (14) (2015) 6571–6580.

[191] L.H. Rude, T.K. Nielsen, D.B. Ravnsbæk, U. Bösenberg, M.B. Ley, B. Richter, et al., Tailoring properties of borohydrides for hydrogen storage: a review, Phys. Status Solidi Appl. Mater. Sci. 208 (8) (2011) 1754–1773.

[192] D.B. Ravnsbœk, L.H. Sørensen, Y. Filinchuk, F. Besenbacher, T.R. Jensen, Screening of metal borohydrides by mechanochemistry and diffraction, Angew. Chem. Int. Ed. 51 (15) (2012) 3582–3586.

[193] E. Roedern, T.R. Jensen, Amine-stabilized transition-metal borohydrides of iron, cobalt, and chromium: synthesis and characterization, Inorg. Chem. 54 (21) (2015) 10477–10482.

[194] E. Roedern, T.R. Jensen, Synthesis, structures and dehydrogenation properties of zinc borohydride ethylenediamine complexes, ChemistrySelect 1 (4) (2016) 752–755.

[195] D.B. Ravnsbæk, C. Frommen, D. Reed, Y. Filinchuk, M. Sørby, B.C. Hauback, et al., Structural studies of lithium zinc borohydride by neutron powder diffraction, Raman and NMR spectroscopy, J. Alloy. Comp. 509 (SUPPL. 2) (2011) S698–S704.

[196] D. Ravnsbœk, Y. Filinchuk, Y. Cerenius, H.J. Jakobsen, F. Besenbacher, J. Skibsted, et al., A series of mixed-metal borohydrides, Angew. Chem. Int. Ed. 48 (36) (2009) 6659–6663.

[197] R. Černý, D.B. Ravnsbæk, P. Schouwink, Y. Filinchuk, N. Penin, J. Teyssier, et al., Potassium zinc borohydrides containing triangular $[Zn(BH_4)_3]^-$ and tetrahedral $[Zn(BH_4)_xCl_{4-x}]^{2-}$ anions, J. Phys. Chem. C 116 (1) (2012) 1563–1571.

[198] R. Černý, D.B. Ravnsbæk, G. Severa, Y. Filinchuk, V. D'Anna, H. Hagemann, et al., Structure and characterization of $KSc(BH_4)_4$, J. Phys. Chem. C 114 (45) (2010) 19540–19549.

[199] C. Milanese, T.R. Jensen, B.C. Hauback, C. Pistidda, M. Dornheim, H. Yang, et al., Complex hydrides for energy storage, Int. J. Hydrogen Energy 44 (15) (2019) 7860–7874.

[200] R. Černý, G. Severa, D.B. Ravnsbæk, Y. Filinchuk, V. D'Anna, H. Hagemann, et al., $NaSc(BH_4)_4$: a novel scandium-based borohydride, J. Phys. Chem. C 114 (2) (2010) 1357–1364.

[201] P. Schouwink, M.B. Ley, A. Tissot, H. Hagemann, T.R. Jensen, Smrčok ubomír, et al., Structure and properties of complex hydride perovskite materials, Nat. Commun. 5 (5706) (2014) 1.

[202] K.T. Møller, M.B. Ley, P. Schouwink, R. Černý, T.R. Jensen, Synthesis and thermal stability of perovskite alkali metal strontium borohydrides, Dalton Trans. 45 (2) (2016) 831–840.

[203] K.T. Møller, M. Jørgensen, A.S. Fogh, T.R. Jensen, Perovskite alkali metal samarium borohydrides: crystal structures and thermal decomposition, Dalton Trans. 46 (35) (2017) 11905–11912.

[204] R. Černý, P. Schouwink, Y. Sadikin, K. Stare, L. Smrčok, B. Richter, et al., Trimetallic borohydride $Li_3MZn_5(BH_4)_{15}$ (M = Mg, Mn) containing two weakly interconnected frameworks, Inorg. Chem. 52 (17) (2013) 9941–9947.

[205] H. Hagemann, M. Longhini, J.W. Kaminski, T.A. Wesolowski, R. Černý, N. Penin, et al., $LiSc(BH_4)_4^+$: a novel salt of Li and discrete $Sc(BH_4)_4$ Complex anions, J. Phys. Chem. A 112 (33) (2008) 7551–7555.

[206] P. Schouwink, V. D'Anna, M.B. Ley, L.M. Lawson Daku, B. Richter, T.R. Jensen, et al., Bimetallic borohydrides in the system $M(BH_4)_2$-KBH_4 (*M* = Mg, Mn): on the structural diversity, J. Phys. Chem. C 116 (20) (2012) 10829–10840.

[207] C. Frommen, N. Aliouane, S. Deledda, J.E. Fonneløp, H. Grove, K. Lieutenant, et al., Crystal structure, polymorphism, and thermal properties of yttrium borohydride $Y(BH_4)_3$, J. Alloy. Comp. 496 (1–2) (2010) 710–716.

[208] J.E. Olsen, C. Frommen, T.R. Jensen, M.D. Riktor, M.H. Sørby, B.C. Hauback, Structure and thermal properties of composites with RE-borohydrides (RE = La, Ce, Pr, Nd, Sm, Eu, Gd, Tb, Er, Yb or Lu) and $LiBH_4$, RSC Adv. 4 (4) (2014) 1570–1582.

[209] C. Frommen, M.H. Sørby, M. Heere, T.D. Humphries, J.E. Olsen, B.C. Hauback, Rare earth borohydrides - crystal structures and thermal properties, Energies 10 (12) (2017) 2115.

[210] P. Schouwink, M.B. Ley, T.R. Jensen, L. Smrčok, Černý R. Borohydrides, From sheet to framework topologies, Dalton Trans. 43 (21) (2014) 7726–7733.

[211] S. Payandeh Gharibdoust, D.B. Ravnsbæk, R. Černý, T.R. Jensen, Synthesis, structure and properties of bimetallic sodium rare-earth (RE) borohydrides, $NaRE(BH_4)_4$, RE = Ce, Pr, Er or Gd, Dalton Trans. 46 (39) (2017) 13421–13431.

[212] M.B. Ley, M. Jørgensen, R. Černý, Y. Filinchuk, T.R. Jensen, From $M(BH_4)_3$ (M═La, Ce) borohydride frameworks to controllable synthesis of porous hydrides and ion conductors, Inorg. Chem. 55 (19) (2016) 9748–9756.

[213] E. Roedern, Y.S. Lee, M.B. Ley, K. Park, Y.W. Cho, J. Skibsted, et al., Solid state synthesis, structural characterization and ionic conductivity of bimetallic alkali-metal yttrium borohydrides $MY(BH_4)_4$ (M═Li and Na), J. Mater. Chem. 4 (22) (2016) 8793–8802.

[214] Y. Sadikin, K. Stare, P. Schouwink, M. Brix Ley, T.R. Jensen, A. Meden, et al., Alkali metal - yttrium borohydrides: the link between coordination of small and large rare-earth, J. Solid State Chem. 225 (2015) 231–239.

[215] Y.S. Lee, M.B. Ley, T.R. Jensen, Y.W. Cho, Lithium ion disorder and conduction mechanism in $LiCe(BH_4)_3Cl$, J. Phys. Chem. C 120 (34) (2016) 19035–19042.

[216] M.B. Ley, D.B. Ravnsbæk, Y. Filinchuk, Y.S. Lee, R. Janot, Y.W. Cho, et al., $LiCe(BH_4)_3Cl$, a new lithium-ion conductor and hydrogen storage material with isolated tetranuclear anionic clusters, Chem. Mater. 24 (9) (2012) 1654–1663.

[217] M.B. Ley, S. Boulineau, R. Janot, Y. Filinchuk, T.R. Jensen, New li ion conductors and solid state hydrogen storage materials: $LiM(BH_4)_3Cl$, M═La, Gd, J. Phys. Chem. C 116 (40) (2012) 21267–21276.

[218] S.H.P. GharibDoust, M. Brighi, Y. Sadikin, D.B. Ravnsbæk, R. Černý, J. Skibsted, et al., Synthesis, structure, and Li-ion conductivity of $LiLa(BH_4)_3X$, X═Cl, Br, I, J. Phys. Chem. C 121 (35) (2017) 19010–19021.

[219] A.V. Skripov, A.V. Soloninin, M.B. Ley, T.R. Jensen, Y. Filinchuk, Nuclear magnetic resonance studies of BH_4 reorientations and Li diffusion in $LiLa(BH_4)_3Cl$, J. Phys. Chem. C 117 (29) (2013) 14965–14972.

[220] D.B. Ravnsbæk, L.H. Sørensen, Y. Filinchuk, D. Reed, D. Book, H.J. Jakobsen, et al., Mixed-anion and mixed-cation borohydride $KZn(BH_4)Cl_2$: synthesis, structure and thermal decomposition, Eur. J. Inorg. Chem. 2010 (11) (2010) 1608–1612.

[221] D.B. Ravnsbæk, M.B. Ley, Y.S. Lee, H. Hagemann, V. D'Anna, Y.W. Cho, et al., A mixed-cation mixed-anion borohydride $NaY(BH_4)_2Cl_2$, Int. J. Hydrogen

Energy 37 (10) (2012) 8428–8438.
[222] B. Richter, D.B. Ravnsbæk, M. Sharma, A. Spyratou, H. Hagemann, T.R. Jensen, Fluoride substitution in $LiBH_4$; Destabilization and decomposition, Phys. Chem. Chem. Phys. 19 (44) (2017) 30157–30165.
[223] L.H. Rude, U. Filsø, V. D'Anna, A. Spyratou, B. Richter, S. Hino, et al., Hydrogen-fluorine exchange in $NaBH_4$-$NaBF_4$, Phys. Chem. Chem. Phys. 15 (41) (2013) 18185–18194.
[224] H. Grove, L.H. Rude, T.R. Jensen, M. Corno, P. Ugliengo, M. Baricco, et al., Halide substitution in $Ca(BH_4)_2$, RSC Adv. 4 (9) (2014) 4736–4742.
[225] S. Hino, J.E. Fonneløp, M. Corno, O. Zavorotynska, A. Damin, B. Richter, et al., Halide substitution in magnesium borohydride, J. Phys. Chem. C 116 (23) (2012) 12482–12488.
[226] L.H. Rude, E. Groppo, L.M. Arnbjerg, D.B. Ravnsbæk, R.A. Malmkjær, Y. Filinchuk, et al., Iodide substitution in lithium borohydride, $LiBH_4$-LiI, J. Alloy. Comp. 509 (33) (2011) 8299–8305.
[227] L.H. Rude, O. Zavorotynska, L.M. Arnbjerg, D.B. Ravnsbæk, R.A. Malmkjær, H. Grove, et al., Bromide substitution in lithium borohydride, $LiBH_4$-LiBr, Int. J. Hydrogen Energy 36 (24) (2011) 15664–15672.
[228] D.B. Ravnsbæk, L.H. Rude, T.R. Jensen, Chloride substitution in sodium borohydride, J. Solid State Chem. 184 (7) (2011) 1858–1866.
[229] E. Grube, C.H. Olesen, D.B. Ravnsbæk, T.R. Jensen, Barium borohydride chlorides: synthesis, crystal structures and thermal properties, Dalton Trans. 45 (19) (2016) 8291–8299.
[230] J.B. Grinderslev, K.T. Møller, Y. Yan, X.M. Chen, Y. Li, H.W. Li, et al., Potassium octahydridotriborate: diverse polymorphism in a potential hydrogen storage material and potassium ion conductor, Dalton Trans. 48 (24) (2019) 8872–8881.
[231] M.P. Pitt, P.E. Vullum, M.H. Sørby, H. Emerich, M. Paskevicius, C.E. Buckley, et al., Crystalline Al_{1-x} Ti_x phases in the hydrogen cycled $NaAlH_4$ + $0.02TiCl_3$ system, Philos. Mag. 93 (9) (2013) 1080–1094.
[232] T.D. Humphries, J.W. Makepeace, S. Hino, W.I.F. David, B.C. Hauback, Regeneration of sodium alanate studied by powder in situ neutron and synchrotron X-ray diffraction, J. Mater. Chem. 2 (39) (2014) 16594–16600.
[233] T.D. Humphries, D. Birkmire, B.C. Hauback, G.S. McGrady, C.M. Jensen, *In situ* high pressure NMR study of the direct synthesis of $LiAlH_4$, J. Mater. Chem. 1 (9) (2013) 2974–2977.
[234] T.D. Humphries, D. Birkmire, G.S. McGrady, B.C. Hauback, C.M. Jensen, Regeneration of $LiAlH_4$ at sub-ambient temperatures studied by multinuclear NMR spectroscopy, J. Alloy. Comp. 723 (2017) 1150–1154.
[235] M.P. Pitt, P.E. Vullum, M.H. Sorby, H. Emerich, M. Paskevicius, C.J. Webb, et al., Hydrogen absorption kinetics and structural features of $NaAlH_4$ enhanced with transition-metal and Ti-based nanoparticles, Int. J. Hydrogen Energy 37 (20) (2012) 15175–15186.
[236] S. Chumphongphan, U. Filsø, M. Paskevicius, D.A. Sheppard, T.R. Jensen, C.E. Buckley, Nanoconfinement degradation in $NaAlH_4$/CMK-1, Int. J. Hydrogen Energy 39 (21) (2014) 11103–11109.
[237] D.A. Sheppard, L.H. Jepsen, T.R. Jensen, M. Paskevicius, C.E. Buckley, New directions for hydrogen storage: sulphur destabilised sodium aluminium hydride, J. Mater. Chem. 1 (41) (2013) 12775–12781.
[238] A.E. Finholt, A.C. Bond, H.I. Schlesinger, Lithium aluminum hydride, aluminum hydride and lithium gallium hydride, and some of their applications in organic and inorganic chemistry, J. Am. Chem. Soc. 69 (5) (1947) 1199–1203.
[239] B. Bogdanović, M. Schwickardi, Ti-doped alkali metal aluminium hydrides as potential novel reversible hydrogen storage materials, J. Alloy. Comp. 253–254 (1997) 1–9.
[240] A. Pommerin, A. Wosylus, M. Felderhoff, F. Schüth, C. Weidenthaler, Synthesis, crystal structures, and hydrogen storage properties of $Eu(AlH_4)_2$ and $Sr(AlH_4)_2$ and of their decomposition intermediates, $EuAlH_5$ and $SrAlH_5$, Inorg. Chem. 51 (7) (2012) 4143–4150.
[241] L.M. Arnbjerg, T.R. Jensen, New compounds in the potassium-aluminium-hydrogen system observed during release and uptake of hydrogen, Int. J. Hydrogen Energy 37 (1) (2012) 345–356.
[242] T. Sato, S. Takagi, M.H. Sørby, S. Deledda, B.C. Hauback, S.I. Orimo, Crystal structural determination of $SrAlD_5$ with corner-sharing AlD_6 octahedron chains by x-ray and neutron diffraction, Crystals 8 (2) (2018) 89.
[243] D. Krech, B. Zibrowius, C. Weidenthaler, M. Felderhoff, On the preparation and structure of caesium aluminium tetrahydride, Eur. J. Inorg. Chem. 2014 (33) (2014) 5683–5688.
[244] T. Bernert, D. Krech, W. Kockelmann, M. Felderhoff, T.J. Frankcombe, C. Weidenthaler, Crystal structure relation between tetragonal and orthorhombic $CsAlD_4$: DFT and time-of-flight neutron powder diffraction studies, Eur. J. Inorg. Chem. 2015 (33) (2015) 5545–5550.
[245] C. Weidenthaler, M. Felderhoff, T. Bernert, M.H. Sørby, B.C. Hauback, D. Krech, Synthesis, crystal structure analysis and decomposition of $RbALH_4$, Crystals 8 (2) (2018) 103.
[246] A.L. Golovanova, Interaction of titanium and iron halides with lithium aluminum hydride in diethyl ether, Bull. Acad. Sci. USSR. Chem. Sci. 24 (5) (1975) 905–907.
[247] C. Weidenthaler, A. Pommerin, M. Felderhoff, W. Sun, C. Wolverton, B. Bogdanović, et al., Complex rare-earth aluminum hydrides: mechanochemical preparation, crystal structure and potential for hydrogen storage, J. Am. Chem. Soc. 131 (46) (2009) 16735–16743.
[248] A.I. Golovanova, M.E. Kost, V.I. Mikheeva, Interaction of tantalum halides with lithium aluminum hydride in ether, Bull. Acad. Sci. USSR. Chem. Sci. 22 (7) (1973) 1410–1413.
[249] Z. Cao, L. Ouyang, H. Wang, J. Liu, M. Felderhoff, M. Zhu, Reversible hydrogen storage in yttrium aluminum hydride, J. Mater. Chem. 5 (13) (2017) 6042–6046.
[250] I. Dovgaliuk, V. Ban, Y. Sadikin, R. Černý, L. Aranda, N. Casati, et al., The first halide-free bimetallic aluminum borohydride: synthesis, structure, stability, and decomposition pathway, J. Phys. Chem. C 118 (1) (2014) 145–153.
[251] I. Dovgaliuk, D.A. Safin, N.A. Tumanov, F. Morelle, A. Moulai, R. Černý, et al., Solid aluminum borohydrides for prospective hydrogen storage, ChemSusChem 10 (23) (2017) 4725–4734.
[252] O.A. Babanova, R.V. Skoryunov, A.V. Soloninin, I. Dovgaliuk, A.V. Skripov, Y. Filinchuk, Nuclear magnetic resonance study of hydrogen dynamics in $Al(BH_4)_4$-based hypersalts $M[Al(BH_4)_4]$ (M=Na, K, Rb, Cs), J. Alloy. Comp. 745 (2018) 179–186.
[253] Q. Gu, Z. Wang, Y. Filinchuk, J.A. Kimpton, H.E.A. Brand, Q. Li, et al., Aluminum borohydride complex with ethylenediamine: crystal structure and dehydrogenation mechanism studies, J. Phys. Chem. C 120 (19) (2016) 10192–10198.
[254] I. Dovgaliuk, K.T. Møller, K. Robeyns, V. Louppe, T.R. Jensen, Y. Filinchuk, Complexation of ammonia boranes with Al^{3+}, Inorg. Chem. 58 (8) (2019) 4753–4760.
[255] A. Gradišek, L.H. Jepsen, T.R. Jensen, M.S. Conradi, Nuclear magnetic resonance study of molecular dynamics in ammine metal borohydride $Sr(BH_4)_2(NH_3)_2$, J. Phys. Chem. C 120 (43) (2016) 24646–24654.
[256] L.H. Jepsen, M.B. Ley, R. Černý, Y.S. Lee, Y.W. Cho, D. Ravnsbæk, et al., Trends in syntheses, structures, and properties for three series of ammine rare-earth metal borohydrides, $M(BH_4)_3 \cdot nNH_3$ (M=Y, Gd, and Dy), Inorg. Chem. 54 (15) (2015) 7402–7414.
[257] L.H. Jepsen, M.B. Ley, Y. Filinchuk, F. Besenbacher, T.R. Jensen, Tailoring the properties of ammine metal borohydrides for solid-state hydrogen storage, ChemSusChem 8 (8) (2015) 1452–1463.
[258] I. Dovgaliuk, C.S. Le Duff, K. Robeyns, M. Devillers, Y. Filinchuk, Mild dehydrogenation of ammonia borane complexed with aluminum borohydride, Chem. Mater. 27 (3) (2015) 768–777.
[259] I. Dovgaliuk, Y. Filinchuk, Aluminium complexes of B- and N-based hydrides: synthesis, structures and hydrogen storage properties, Int. J. Hydrogen Energy 41 (34) (2016) 15489–15504.
[260] I. Dovgaliuk, L.H. Jepsen, D.A. Safin, Z. Łodziana, V. Dyadkin, T.R. Jensen, et al., A composite of complex and chemical hydrides yields the first Al-based amidoborane with improved hydrogen storage properties, Chem. Eur J. 21 (41) (2015) 14562–14570.
[261] K.T. Møller, M. Jørgensen, J.G. Andreasen, J. Skibsted, Z. Łodziana, Y. Filinchuk, et al., Synthesis and thermal decomposition of potassium tetraamidoboranealuminate, $K[Al(NH_2BH_3)_4]$, Int. J. Hydrogen Energy 43 (1) (2018) 311–321.
[262] S. Hino, T. Ichikawa, Y. Kojima, M.H. Sørby, B.C. Hauback, A new complex alkali metal aluminium amide borohydride, $Li_2Al(ND_2)_4BH_4$: synthesis, thermal analysis and crystal structure, RSC Adv. 6 (34) (2016) 28761–28766.
[263] J. Yang, P.R. Beaumont, T.D. Humphries, C.M. Jensen, X. Li, Efficient synthesis of an aluminum amidoborane ammoniate, Energies 8 (9) (2015) 9107–9116.
[264] T.D. Humphries, K.T. Munroe, A. Decken, G.S. McGrady, Lewis base complexes of AlH_3: structural determination of monomeric and polymeric adducts by X-ray crystallography and DFT calculations, Dalton Trans. 42 (19) (2013) 6953–6964.
[265] T.D. Humphries, K.T. Munroe, A. Decken, G.S. McGrady, Lewis base complexes of AlH_3: prediction of preferred structure and stoichiometry, Dalton Trans. 42 (19) (2013) 6965–6978.
[266] J. Ortmeyer, A. Bodach, L. Sandig-Predzymirska, B. Zibrowius, F. Mertens, M. Felderhoff, Direct hydrogenation of aluminum via stabilization with triethylenediamine: a mechanochemical approach to synthesize the triethylenediamine • AlH_3 adduct, ChemPhysChem 20 (10) (2019) 1360–1368.
[267] N. Saunders, A.P. Miodownik, in: W. Cahn (Ed.), Calculation of Phase Diagrams, 1998. ISBN-10: 0-08-042129-6., Pergamon Materials Series.
[268] H.L. Lukas, S.G. Fries, B. Sundman, in: 1st ed.Computational Thermodynamics: The Calphad Method, Cambridge University Press, New York, NY, USA, 2007, pp. 1–313, 9780521868.
[269] P.E.A. Turchi, I.A. Abrikosov, B. Burton, S.G. Fries, G. Grimvall, L. Kaufman, et al., Interface between quantum-mechanical-based approaches, experiments, and CALPHAD methodology, Calphad 31 (1) (2007) 4–27.
[270] A. El Kharbachi, E. Pinatel, I. Nuta, M. Baricco, A thermodynamic assessment of $LiBH_4$, Calphad 39 (2012) 80–90.
[271] E.M. Dematteis, E.R. Pinatel, M. Corno, T.R. Jensen, M. Baricco, Phase diagrams of the $LiBH_4$-$NaBH_4$-KBH_4 system, Phys. Chem. Chem. Phys. 19 (36) (2017) 25071–25079.
[272] E.R. Pinatel, E. Albanese, B. Civalleri, M. Baricco, Thermodynamic modelling of $Mg(BH_4)_2$, J. Alloy. Comp. 645 (S1) (2015) S64–S68.
[273] M. Palumbo, F.J. Torres, J.R. Ares, C. Pisanie, J.F. Fernandez, M. Baricco, Thermodynamic and ab initio investigation of the Al-H-Mg system, Calphad 31 (3) (2007) 457–467, https://doi.org/10.1016/j.calphad.2007.04.005.
[274] D. Pottmaier, E.R. Pinatel, J.G. Vitillo, S. Garroni, M. Orlova, M.D. Baró, et al., Structure and thermodynamic properties of the $NaMgH_3$ perovskite: a comprehensive study, Chem. Mater. 23 (9) (2011) 2317–2326.
[275] A. Wolczyk, E.R. Pinatel, M.R. Chierotti, C. Nervi, R. Gobetto, M. Baricco, Solid-state NMR and thermodynamic investigations on $LiBH_4$–$LiNH_2$ system, Int. J. Hydrogen Energy 41 (32) (2016) 14475–14483.

[276] Y. Nakamori, K. Miwa, A. Ninomiya, H. Li, N. Ohba, S.I. Towata, et al., Correlation between thermodynamical stabilities of metal borohydrides and cation electronegativites: first-principles calculations and experiments, Phys. Rev. B. 74 (4) (2006), 045126.

[277] P. Javadian, D.A. Sheppard, C.E. Buckley, T.R. Jensen, Hydrogen storage properties of nanoconfined $LiBH_4$-$Ca(BH_4)_2$, Nanoenergy 121 (11) (2015) 96–103.

[278] P. Javadian, D.A. Sheppard, C.E. Buckley, T.R. Jensen, Hydrogen storage properties of nanoconfined $LiBH_4$-$NaBH_4$, Int. J. Hydrogen Energy 40 (43) (2015) 14916–14924.

[279] P. Javadian, D.A. Sheppard, C.E. Buckley, T.R. Jensen, Hydrogen desorption properties of bulk and nanoconfined $LiBH_4$-$NaAlH_4$, Crystals 6 (6) (2016) 70.

[280] M. Paskevicius, M.B. Ley, D.A. Sheppard, T.R. Jensen, C.E. Buckley, Eutectic melting in metal borohydrides, Phys. Chem. Chem. Phys. 15 (45) (2013) 19774–19789.

[281] E. Roedern, B.R.S. Hansen, M.B. Ley, T.R. Jensen, Effect of eutectic melting, reactive hydride composites, and nanoconfinement on decomposition and reversibility of $LiBH_4$-KBH_4, J. Phys. Chem. C 119 (46) (2015) 25818–25825.

[282] S.R.H. Jensen, L.H. Jepsen, J. Skibsted, T.R. Jensen, Phase diagram for the $NaBH_4$-KBH_4 system and the stability of a $Na_{1-x}K_xBH_4$ solid solution, J. Phys. Chem. C 119 (50) (2015) 27919–27929.

[283] M.B. Ley, E. Roedern, P.M.M. Thygesen, T.R. Jensen, Melting behavior and thermolysis of $NaBH_4$-$Mg(BH_4)_2$ and $NaBH_4$-$Ca(BH_4)_2$ composites, Energies 8 (4) (2015) 2701–2713.

[284] M.B. Ley, E. Roedern, T.R. Jensen, Eutectic melting of $LiBH_4$-KBH_4, Phys. Chem. Chem. Phys. 16 (44) (2014) 24194–24199.

[285] I. Saldan, S. Hino, T.D. Humphries, O. Zavorotynska, M. Chong, C.M. Jensen, et al., Structural changes observed during the reversible hydrogenation of $Mg(BH_4)_2$ with Ni-based additives, J. Phys. Chem. C 118 (40) (2014) 23376–23384.

[286] O. Zavorotynska, I. Saldan, S. Hino, T.D. Humphries, S. Deledda, B.C. Hauback, Hydrogen cycling in γ-$Mg(BH_4)_2$ with cobalt-based additives, J. Mater. Chem. 3 (12) (2015) 6592–6602.

[287] O. Zavorotynska, S. Deledda, J.G. Vitillo, I. Saldan, M.N. Guzik, M. Baricco, et al., Combined X-ray and Raman studies on the effect of cobalt additives on the decomposition of magnesium borohydride, Energies 8 (9) (2015) 9173–9190.

[288] I. Saldan, C. Frommen, I. Llamas-Jansa, G.N. Kalantzopoulos, S. Hino, B. Arstad, et al., Hydrogen storage properties of γ-$Mg(BH_4)_2$ modified by MoO_3 and TiO_2, Int. J. Hydrogen Energy 40 (36) (2015) 12286–12293.

[289] O. Zavorotynska, S. Deledda, B.C. Hauback, Kinetics studies of the reversible partial decomposition reaction in $Mg(BH_4)_2$, Int. J. Hydrogen Energy 41 (23) (2016) 9885–9892.

[290] O. Zavorotynska, A. El-Kharbachi, S. Deledda, B.C. Hauback, Recent progress in magnesium borohydride $Mg(BH_4)_2$: fundamentals and applications for energy storage, Int. J. Hydrogen Energy 41 (32) (2016) 14387–14403.

[291] E. Roedern, T.R. Jensen, Thermal decomposition of $Mn(BH_4)_2$-$M(BH_4)_x$ and $Mn(BH_4)_2$-MH_x composites with M=i, Na, Mg, and Ca, J. Phys. Chem. C 118 (41) (2014) 23567–23574.

[292] C. Pistidda, F. Karimi, S. Garroni, A. Rzeszutek, C. Bonatto Minella, C. Milanese, et al., Effect of the partial replacement of CaH_2 with CaF_2 in the mixed system $CaH_2 + MgB_2$, J. Phys. Chem. C 118 (49) (2014) 28409–28417.

[293] M. Paskevicius, B. Richter, M. Polański, S.P. Thompson, T.R. Jensen, Sulfurized metal borohydrides, Dalton Trans. 45 (2) (2016) 639–645.

[294] T.D. Humphries, G.N. Kalantzopoulos, I. Llamas-Jansa, J.E. Olsen, B.C. Hauback, Reversible hydrogenation studies of $NaBH_4$ milled with Ni-containing additives, J. Phys. Chem. C 117 (12) (2013) 6060–6065.

[295] O. Zavorotynska, S. Deledda, G. Li, M. Matsuo, S.I. Orimo, B.C. Hauback, Isotopic exchange in porous and dense magnesium borohydride, Angew. Chem. Int. Ed. 54 (36) (2015) 10592–10595.

[296] B.R.S. Hansen, K.T. Møller, M. Paskevicius, A.C. Dippel, P. Walter, C.J. Webb, et al., *In situ* X-ray diffraction environments for high-pressure reactions, J. Appl. Crystallogr. 48 (4) (2015) 1234–1241.

[297] K.T. Møller, B.R.S. Hansen, A.C. Dippel, J.E. Jørgensen, T.R. Jensen, Characterization of gas-solid reactions using in situ powder X-ray diffraction, Z. Anorg. Allg. Chem. 640 (15) (2014) 3029–3043.

[298] V. D'Anna, A. Spyratou, M. Sharma, H. Hagemann, FT-IR spectra of inorganic borohydrides, Spectrochim. Acta Part A Mol Biomol Spectrosc. 128 (2014) 902–906.

[299] D.B. Ravnsbæk, Y. Filinchuk, R. Černý, T.R. Jensen, Powder diffraction methods for studies of borohydride-based energy storage materials, Z. Krist. 225 (12) (2010) 557–569.

[300] T.R. Jensen, T.K. Nielsen, Y. Filinchuk, J.E. Jørgensen, Y. Cerenius, E.M.A. Gray, et al., Versatile in situ powder X-ray diffraction cells for solid-gas investigations, J. Appl. Crystallogr. 43 (6) (2010) 1456–1463.

[301] S.R.H. Jensen, M. Paskevicius, B.R.S. Hansen, A.S. Jakobsen, K.T. Møller, J.L. White, et al., Hydrogenation properties of lithium and sodium hydride-*closo* -borate, $[B_{10}H_{10}]^{2-}$ and $[B_{12}H_{12}]^{2-}$, composites, Phys. Chem. Chem. Phys. 20 (23) (2018) 16266–16275.

[302] E. Callini, P. Szilágyi, M. Paskevicius, N.P. Stadie, J. Réhault, C.E. Buckley, et al., Stabilization of volatile $Ti(BH_4)_3$ by nano-confinement in a metal-organic framework, Chem. Sci. 7 (1) (2016) 666–672.

[303] S. Thiangviriya, P. Plerdsranoy, N. Wiset, P. Javadian, T.R. Jensen, R. Utke, Hydrogen sorption and reaction mechanisms of nanoconfined $2LiBH_4$-$NaAlH_4$, J. Alloy. Comp. 633 (2015) 484–493.

[304] P. Javadian, C. Zlotea, C.M. Ghimbeu, M. Latroche, T.R. Jensen, Hydrogen storage properties of nanoconfined $LiBH_4$-Mg_2NiH_4 reactive hydride composites, J. Phys. Chem. C 119 (11) (2015) 5819–5826.

[305] P. Plerdsranoy, P. Javadian, N.D. Jensen, U.G. Nielsen, T.R. Jensen, R. Utke, Compaction of $LiBH_4$-$LiAlH_4$ nanoconfined in activated carbon nanofibers: dehydrogenation kinetics, reversibility, and mechanical stability during cycling, Int. J. Hydrogen Energy 42 (2) (2017) 1036–1047.

[306] T.K. Nielsen, F. Besenbacher, T.R. Jensen, Nanoconfined hydrides for energy storage, Nanoscale 3 (5) (2011) 2086–2098.

[307] T.K. Nielsen, U. Bösenberg, R. Gosalawit, M. Dornheim, Y. Cerenius, F. Besenbacher, et al., A reversible nanoconfined chemical reaction, ACS Nano 4 (7) (2010) 3903–3908.

[308] R. Gosalawit-Utke, S. Thiangviriya, P. Javadian, D. Laipple, C. Pistidda, N. Bergemann, et al., Effective nanoconfinement of $2LiBH_4$-MgH_2 via simply MgH_2 premilling for reversible hydrogen storages, Int. J. Hydrogen Energy 39 (28) (2014) 15614–15626.

[309] P. Javadian, T.R. Jensen, Enhanced hydrogen reversibility of nanoconfined $LiBH_4$-$Mg(BH_4)_2$, Int. J. Hydrogen Energy 39 (18) (2014) 9871–9876.

[310] T.K. Nielsen, P. Javadian, M. Polanski, F. Besenbacher, J. Bystrzycki, J. Skibsted, et al., Nanoconfined $NaAlH_4$: prolific effects from increased surface area and pore volume, Nanoscale 6 (1) (2014) 599–607.

[311] R. Gosalawit-Utke, C. Milanese, P. Javadian, J. Jepsen, D. Laipple, F. Karmi, et al., Nanoconfined $2LiBH_4$-MgH_2-$TiCl_3$ in carbon aerogel scaffold for reversible hydrogen storage, Int. J. Hydrogen Energy 38 (8) (2013) 3275–3282.

[312] A. Ampoumogli, G. Charalambopoulou, P. Javadian, B. Richter, T.R. Jensen, T. Steriotis, Hydrogen desorption and cycling properties of composites based on mesoporous carbons and a $LiBH_4$-$Ca(BH_4)_2$ eutectic mixture, J. Alloy. Comp. 645 (S1) (2015) S480–S484.

[313] M.P. Pitt, C.J. Webb, M. Paskevicius, D. Sheptyakov, C.E. Buckley, E.M.A. Gray, *In situ* neutron diffraction study of the deuteration of isotopic $Mg^{11}B_2$, J. Phys. Chem. C 115 (45) (2011) 22669–22679.

[314] P. Chen, Z. Xiong, J. Luo, J. Lin, K. Lee Tan, Interaction of hydrogen with metal nitrides and imides, Nature 420 (6913) (2002) 302–304.

[315] Z. Xiong, J. Hu, G. Wu, P. Chen, W. Luo, K. Gross, et al., Thermodynamic and kinetic investigations of the hydrogen storage in the Li-Mg-N-H system, J. Alloy. Comp. 398 (1–2) (2005) 235–239.

[316] K.T. Møller, A.S. Fogh, M. Paskevicius, J. Skibsted, T.R. Jensen, Metal borohydride formation from aluminium boride and metal hydrides, Phys. Chem. Chem. Phys. 18 (39) (2016) 27545–27553.

[317] B.R.S. Hansen, D.B. Ravnsbæk, J. Skibsted, T.R. Jensen, Hydrogen reversibility of $LiBH_4$-MgH_2-Al composites, Phys. Chem. Chem. Phys. 16 (19) (2014) 8970–8980.

[318] L.H. Jepsen, D.B. Ravnsbæk, C. Grundlach, F. Besenbacher, J. Skibsted, T.R. Jensen, A novel intermediate in the $LiAlH_4$-$LiNH_2$ hydrogen storage system, Dalton Trans. 43 (8) (2014) 3095–3103.

[319] B.R.S. Hansen, D.B. Ravnsbæk, D. Reed, D. Book, C. Gundlach, J. Skibsted, et al., Hydrogen storage capacity loss in a $LiBH_4$-Al composite, J. Phys. Chem. C 117 (15) (2013) 7423–7432.

[320] J. Puszkiel, F.C. Gennari, P. Arneodo Larochette, H.E. Troiani, F. Karimi, C. Pistidda, et al., Hydrogen storage in Mg-$LiBH_4$ composites catalyzed by FeF_3, J. Power Sources 267 (2014) 799–811.

[321] D.B. Ravnsbæk, T.R. Jensen, Mechanism for reversible hydrogen storage in $LiBH_4$-Al, J. Appl. Phys. 111 (11) (2012) 112621.

[322] I. Saldan, R. Gosalawit-Utke, C. Pistidda, U. Bösenberg, M. Schulze, T.R. Jensen, et al., Influence of stoichiometry on the hydrogen sorption behavior in the LiF-MgB_2 system, J. Phys. Chem. C 116 (12) (2012) 7010–7015.

[323] G. Barkhordarian, T. Klassen, M. Dornheim, R. Bormann, Unexpected kinetic effect of MgB_2 in reactive hydride composites containing complex borohydrides, J. Alloy. Comp. 440 (1–2) (2007) L18–L21.

[324] H. Wang, G. Wu, H. Cao, C. Pistidda, A.L. Chaudhary, S. Garroni, et al., Near ambient condition hydrogen storage in a synergized tricomponent hydride system, Adv. Energy Mater. 7 (13) (2017) 1602456.

[325] C. Frommen, M. Heere, M.D. Riktor, M.H. Sørby, B.C. Hauback, Hydrogen storage properties of rare earth (RE) borohydrides (RE=La, Er) in composite mixtures with $LiBH_4$ and LiH, J. Alloy. Comp. 645 (S1) (2015) S155–S159.

[326] M. Heere, S.H. Payandeh GharibDoust, C. Frommen, T.D. Humphries, M.B. Ley, M.H. Sørby, et al., The influence of LiH on the rehydrogenation behavior of halide free rare earth (RE) borohydrides (RE=Pr, Er), Phys. Chem. Chem. Phys. 18 (35) (2016) 24387–24395.

[327] M. Heere, S.H.P. GharibDoust, M. Brighi, C. Frommen, M.H. Sørby, R. Černý, et al., Hydrogen sorption in erbium borohydride composite mixtures with $LiBH_4$ and/or LiH, Inorganics 5 (2) (2017) 31.

[328] M. Paskevicius, A.S. Jakobsen, M. Bregnhøj, B.R.S. Hansen, K.T. Møller, P.R. Ogilby, et al., Comment on "bi-functional $Li_2B_{12}H_{12}$ for energy storage and conversion applications: solid-state electrolyte and luminescent down-conversion dye" by J. A. Teprovich Jr, H. Colón-Mercado, A. L. Washington II, P. A. Ward, S. Greenway, D. M. Missimer, H, J. Mater. Chem. 7 (8) (2019) 4185–4187.

[329] S. Payandeh Gharibdoust, M. Heere, C. Nervi, M.H. Sørby, B.C. Hauback, T.R. Jensen, Synthesis, structure, and polymorphic transitions of praseodymium(iii) and neodymium(iii) borohydride, $Pr(BH_4)_3$ and $Nd(BH_4)_3$, Dalton Trans. 47 (25) (2018) 8307–8319.

[330] B.R.S. Hansen, M. Paskevicius, H.W. Li, E. Akiba, T.R. Jensen, Metal boranes: progress and applications, Coord. Chem. Rev. 323 (2016) 60–70.

[331] M. Paskevicius, B.R.S. Hansen, M. Jørgensen, B. Richter, T.R. Jensen,

Multifunctionality of silver closo-boranes, Nat. Commun. 8 (2017) 15136.
[332] M. Paskevicius, M.P. Pitt, D.H. Brown, D.A. Sheppard, S. Chumphongphan, C.E. Buckley, First-order phase transition in the $Li_2B_{12}H_{12}$ system, Phys. Chem. Chem. Phys. 15 (38) (2013) 15825–15828.
[333] B.R.S. Hansen, M. Paskevicius, M. Jørgensen, T.R. Jensen, Halogenated sodium-closo-dodecaboranes as solid-state ion conductors, Chem. Mater. 29 (8) (2017) 3423–3430.
[334] K.T. Møller, M. Paskevicius, J.G. Andreasen, J. Lee, N. Chen-Tan, J. Overgaard, et al., Molten metal closo-borate solvates, Chem. Commun. 55 (23) (2019) 3410–3413.
[335] V.A. Yartys, O. Gutfleisch, V.V. Panasyuk, I.R. Harris, Desorption characteristics of rare earth (R) hydrides (R=Y, Ce, Pr, Nd, Sm, Gd and Tb) in relation to the HDDR behaviour of R-Fe-based-compounds, J. Alloy. Comp. 253–254 (20) (1997) 128–133.
[336] V.E. Antonov, Phase transformations, crystal and magnetic structures of high-pressure hydrides of d-metals, J. Alloy. Comp. 330–332 (2002) 110–116.
[337] G.G. Libowitz, H.F. Hayes, T.R.P. Gibb, The system zirconium-nickel and hydrogen, J. Phys. Chem. 62 (1) (1958) 76–79.
[338] J. Bergsma, J.A. Goedkoop, J.H.N. van Vucht, Neutron diffraction investigation of solid solutions $AlTh_2Dn$, Acta Crystallogr. 14 (3) (1961) 223–228.
[339] M.H. Sørby, H. Fjellvåg, B.C. Hauback, A.J. Maeland, V.A. Yartys, Crystal structure of Th_2Al deuterides, J. Alloy. Comp. 309 (1–2) (2000) 154–164.
[340] J.H.N. Van Vucht, F. Kuijpers, H.C.A.M. Bruning, Reversible room-temperature absorption of large quantities of hydrogen by intermetallic compounds, Philips Res. Rep. 25 (2) (1970) 133–140.
[341] J.J.G. Willems, K.H.J. Buschow, From permanent magnets to rechargeable hydride electrodes, J. Less Common. Met. 129 (C) (1987) 13–30.
[342] K.H.J. Buschow, P.A. Naastepad, F.F. Westendorf, Preparation of $SmCo_5$ Permanent magnets, J. Appl. Phys. 40 (1969) 4029–4032.
[343] J.H.N. van Vucht, F. Kuijpers, RCo_5-H and related systems, Philips Res. Rep. 2 (1973) 102.
[344] T. Sakai, K. Oguro, H. Miyamura, N. Kuriyama, A. Kato, H. Ishikawa, et al., Some factors affecting the cycle lives of $LaNi_5$-based alloy electrodes of hydrogen batteries, J. Less Common. Met. 161 (2) (1990) 193–202.
[345] G. Bronoel, J. Sarradin, M. Bonnemay, A. Percheron, J.C. Achard, L. Schlapbach, A new hydrogen storage electrode, Int. J. Hydrogen Energy 1 (3) (1976) 251–254.
[346] S.A. Willems, Metal Hydride Electrodes Stability of $LaNi_5$-Related Compounds, Technische Hogeschool Eindhoven, 1984.
[347] J.J.G. Willems, Metal hydride electrodes: stability of $LaNi_5$-related compounds, Z. Phys. Chem. 147 (1–2) (1986) 231.
[348] A.R. Miedema, K.H.J. Buschow, H.H. Van Mal, Which intermetallic compounds of transition metals form stable hydrides? J. Less Common. Met. 49 (C) (1976) 463–472.
[349] K.H.J. Buschow, P.C.P. Bouten, A.R. Miedema, Hydrides formed from intermetallic compounds of two transition metals: a special class of ternary alloys, Rep. Prog. Phys. 45 (9) (1982) 937–1039.
[350] K.H.J. Buschow, H.H. Van Mal, A.R. Miedema, Hydrogen absorption in intermetallic compounds of thorium, J. Less Common. Met. 42 (2) (1975) 163–178.
[351] I.R. Harris, P.J. McGuiness, D.G.R. Jones, J.S. Abell, Nd-Fe-B permanent Magnets : hydrogen absorption/desorption studies (HADS) on Nd_{16} Fe_{76} B_8 and Nd_2, Fe_{14}, B, Phys. Scr. T19B (1987) 435–440.
[352] O. Gutfleisch, M.A. Willard, E. Brück, C.H. Chen, S.G. Sankar, J.P. Liu, Magnetic materials and devices for the 21st century: stronger, lighter, and more energy efficient, Adv. Mater. 23 (7) (2011) 821–842.
[353] O. Gutfleisch, I.R. Harris, Fundamental and practical aspects of the hydrogenation, disproportionate, desorption and recombination process, J. Phys. D Appl. Phys. 29 (9) (1996) 2255–2265.
[354] O. Gutfleisch, Controlling the properties of high energy density permanent magnetic materials by different processing routes, J. Phys. D Appl. Phys. 33 (17) (2000) R157.
[355] W. Liu, C.J. Webb, E.M.A. Gray, Review of hydrogen storage in AB_3 alloys targeting stationary fuel cell applications, Int. J. Hydrogen Energy 41 (5) (2016) 3485–3507.
[356] J. Bellosta von Colbe, J.R. Ares, J. Barale, M. Baricco, C. Buckley, G. Capurso, et al., Application of hydrides in hydrogen storage and compression: achievements, outlook and perspectives, Int. J. Hydrogen Energy 44 (15) (2019) 7780–7808.
[357] D.A. Sheppard, M. Paskevicius, T.D. Humphries, M. Felderhoff, G. Capurso, J. Bellosta von Colbe, et al., Metal hydrides for concentrating solar thermal power energy storage, Appl. Phys. A. 122 (4) (2016) 395.
[358] M.V. Lototskyy, V.A. Yartys, B.G. Pollet, R.C. Bowman, Metal hydride hydrogen compressors: a review, in: International Journal of Hydrogen Energy, 2014, pp. 5818–5851.
[359] D.G. Ivey, D.O. Northwood, Storing energy in metal hydrides: a review of the physical metallurgy, J. Mater. Sci. 18 (1983) 321–347.
[360] B. Sakintuna, F. Lamari-Darkrim, M. Hirscher, Metal hydride materials for solid hydrogen storage: a review, Int. J. Hydrogen Energy 32 (9) (2007) 1121–1140.
[361] J.C. Crivello, B. Dam, R.V. Denys, M. Dornheim, D.M. Grant, J. Huot, et al., Review of magnesium hydride-based materials: development and optimisation, Appl. Phys. A 122 (2) (2016) 1–20.
[362] V.A. Yartys, M.V. Lototskyy, E. Akiba, R. Albert, V.E. Antonov, J.R. Ares, et al., Magnesium based materials for hydrogen based energy storage: past, present and future, Int. J. Hydrogen Energy 44 (15) (2019) 7809–7859.
[363] J. Graetz, J.J. Reilly, V.A. Yartys, J.P. Maehlen, B.M. Bulychev, V.E. Antonov, et al., Aluminum hydride as a hydrogen and energy storage material: past, present and future, J. Alloy. Comp. 509 (2011) S517–S528.
[364] M. Paskevicius, J. Webb, M.P. Pitt, T.P. Blach, B.C. Hauback, E.M.A. Gray, et al., Mechanochemical synthesis of aluminium nanoparticles and their deuterium sorption properties to 2 kbar, J. Alloy. Comp. 481 (1–2) (2009) 595–599.
[365] V.A. Yartys, V.V. Burnasheva, K.N. Semenenko, N.V. Fadeeva, S.P. Solov'ev, Crystal chemistry of $RT_5H(D)_x$, $RT_2H(D)_x$ and $RT_3H(D)_x$ hydrides based on intermetallic compounds of $CaCu_5$, $MgCu_2$, $MgZn_2$ and $PuNi_3$ structure types, Int. J. Hydrogen Energy 7 (12) (1982) 957–965.
[366] V.A. Yartys, V.V. Burnasheva, K.N. Semenenko, Structural chemistry of hydrides of intermetallic compounds, Russ. Chem. Rev. 52 (4) (1983) 299–317.
[367] V.A. Yartys, New aspects on the structural chemistry of hydrides of intermetallic compounds, Z. Phys. Chem. 1 (1) (1992) 183–192.
[368] V.A. Yartys, A.B. Riabov, M.V. Lototskyy, in: Materials Science and Structural Chemistry of Intermetallic Hydrides, Lviv: Spolom, 2006, p. 286.
[369] H. Smithson, C.A. Marianetti, D. Morgan, A. Van Der Ven, A. Predith, G. Ceder, First-principles study of the stability and electronic structure of metal hydrides, Phys. Rev. B 66 (14) (2002) 1–10.
[370] M. Gupta, Electronic properties of $LaNi_5$ and $LaNi_5H_7$, J. Less Common. Met. 130 (C) (1987) 219–228.
[371] J.C. Crivello, M. Gupta, Relationship between compressibility and hydrogen absorption in some Haucke compounds, J. Alloy. Comp. 404–406 (2005) 565–569.
[372] Y. Khan, Variation of period with valence electron concentration in RT_y one-dimensional long-period superstructures, Phys. Status Solidi 23 (2) (1974) 425–434.
[373] K. Kadir, T. Sakai, I. Uehara, Synthesis and structure determination of a new series of hydrogen storage alloys; RMg_2 Ni_9 (R=La, Ce, Pr, Nd, Sm and Gd) built from $MgNi_2$ laves-type layers alternating with AB_5 layers, J. Alloy. Comp. 257 (1–2) (1997) 115–121.
[374] E. Akiba, H. Hayakawa, T. Kohno, Crystal structures of novel La-Mg-Ni hydrogen absorbing alloys, J. Alloy. Comp. 408–412 (2006) 280–283.
[375] R.V. Denys, V.A. Yartys, E.M.A. Gray, C.J. Webb, $LaNi_5$-assisted hydrogenation of $MgNi_2$ in the hybrid structures of $La_{1.09}Mg_{1.91}Ni_9D_{9.5}$ and $La_{0.91}Mg_{2.09}Ni_9D_{9.4}$, Energies 8 (4) (2015) 3198–3211.
[376] J.C. Crivello, M. Gupta, M. Latroche, First principles calculations of $(La,Mg)_2Ni_7$ hydrides, J. Alloy. Comp. 645 (S1) (2015) S5–S8.
[377] J.-C. Crivello, N. Madern, J. Zhang, J. Monnier, M. Latroche, Experimental and theoretical investigations on the influence of *A* on the hydrogen sorption properties of ANi_y compounds, *A*={Y, Sm, Gd}, J. Phys. Chem. C 123 (38) (2019) 23334–23341.
[378] R.V. Denys, A.B. Riabov, V.A. Yartys, M. Sato, R.G. Delaplane, Mg substitution effect on the hydrogenation behaviour, thermodynamic and structural properties of the La_2Ni_7-$H(D)_2$ system, J. Solid State Chem. 181 (4) (2008) 812–821.
[379] V.A. Yartys, O. Isnard, A.B. Riabov, L.G. Akselrud, Unusual effects on hydrogenation: anomalous expansion and volume contraction, J. Alloy. Comp. 356–357 (2003) 109–113.
[380] R.V. Denys, V.A. Yartys, M. Sato, A.B. Riabov, R.G. Delaplane, Crystal chemistry and thermodynamic properties of anisotropic $Ce_2Ni_7H_{4.7}$ hydride, J. Solid State Chem. 180 (9) (2007) 2566–2576.
[381] V.A. Yartys, P. Vajeeston, A.B. Riabov, P. Ravindran, R.V. Denys, J.P. Maehlen, et al., Crystal chemistry and metal-hydrogen bonding in anisotropic and interstitial hydrides of intermetallics of rare earth (R) and transition metals (T), RT_3 and R_2T_7, Z. Krist. 223 (10) (2008) 674–689.
[382] Havela L. Magnetism ofintermetallic hydrides. J. Alloy. Comp. In preparation.
[383] J.W. Yeh, S.K. Chen, S.J. Lin, J.Y. Gan, T.S. Chin, T.T. Shun, et al., Nanostructured high-entropy alloys with multiple principal elements: novel alloy design concepts and outcomes, Adv. Eng. Mater. 6 (5) (2004) 299–303.
[384] D.B. Miracle, O.N. Senkov, A critical review of high entropy alloys and related concepts, Acta Mater. 122 (Supplement C) (2017) 448–511.
[385] Y.F. Ye, Q. Wang, J. Lu, C.T. Liu, Y. Yang, High-entropy alloy: challenges and prospects, Mater. Today 19 (6) (2016) 349–362.
[386] O.N. Senkov, D.B. Miracle, K.J. Chaput, J.P. Couzinie, Development and exploration of refractory high entropy alloys - a review, J. Mater. Res. 33 (19) (2018) 3092–3128.
[387] M.C. Gao, D.B. Miracle, D. Maurice, X. Yan, Y. Zhang, J.A. Hawk, High-entropy functional materials, J. Mater. Res. 33 (19) (2018) 3138–3155.
[388] M. Sahlberg, D. Karlsson, C. Zlotea, U. Jansson, Superior hydrogen storage in high entropy alloys, Sci. Rep. 6 (2016) 36770.
[389] D. Karlsson, G. Ek, J. Cedervall, C. Zlotea, K.T. Møller, T.C. Hansen, et al., Structure and hydrogenation properties of a HfNbTiVZr high-entropy alloy, Inorg. Chem. 57 (4) (2018) 2103–2110.
[390] M.M. Nygård, G. Ek, D. Karlsson, M. Sahlberg, M.H. Sørby, B.C. Hauback, Hydrogen storage in high-entropy alloys with varying degree of local lattice strain, Int. J. Hydrogen Energy 44 (55) (2019) 29140–29149.
[391] M.M. Nygård, G. Ek, D. Karlsson, M.H. Sørby, M. Sahlberg, B.C. Hauback, Counting electrons - a new approach to tailor the hydrogen sorption properties of high-entropy alloys, Acta Mater. 175 (2019) 121–129.
[392] G. Zepon, D.R. Leiva, R.B. Strozi, A. Bedoch, S.J.A. Figueroa, T.T. Ishikawa, et al., Hydrogen-induced phase transition of $MgZrTiFe_{0.5}Co_{0.5}Ni_{0.5}$ high entropy

alloy, Int. J. Hydrogen Energy 43 (3) (2018) 1702–1708.
[393] C. Zlotea, M.A. Sow, G. Ek, J.P. Couzinié, L. Perrière, I. Guillot, et al., Hydrogen sorption in TiZrNbHfTa high entropy alloy, J. Alloy. Comp. 775 (2019) 667–674.
[394] H. Shen, J. Zhang, J. Hu, J. Zhang, Y. Mao, H. Xiao, et al., A novel TiZrHfMoNb high-entropy alloy for solar thermal energy storage, Nanomaterials 9 (2) (2019) E248.
[395] J. Montero, C. Zlotea, G. Ek, J.-C. Crivello, L. Laversenne, M. Sahlberg, TiVZrNb multi-principal-element alloy: synthesis optimization, structural, and hydrogen sorption properties, Molecules 24 (15) (2019) 2799.
[396] A. Percheron-Guegan, C. Lartigue, J.C. Achard, P. Germi, F. Tasset, Neutron and X-ray diffraction profile analyses and structure of $LaNi_5$, $LaNi_{5-x}Al_x$ and $LaNi_{5-x}Mn_x$ intermetallics and their hydrides (deuterides), J. Less Common. Met. 74 (1) (1980) 1–12.
[397] L. Gal, V. Charbonnier, J. Zhang, L. Goubault, P. Bernard, M. Latroche, Optimization of the la substitution by Mg in the La_2Ni_7 hydride-forming system for use as negative electrode in Ni-MH battery, Int. J. Hydrogen Energy 40 (47) (2015) 17017–17020.
[398] A. Férey, F. Cuevas, M. Latroche, B. Knosp, P. Bernard, Elaboration and characterization of magnesium-substituted La_5Ni_{19} hydride forming alloys as active materials for negative electrode in Ni-MH battery, Electrochim. Acta 54 (6) (2009) 1710–1714.
[399] J.C. Crivello, R.V. Denys, M. Dornheim, M. Felderhoff, D.M. Grant, J. Huot, et al., Mg-based compounds for hydrogen and energy storage, Appl. Phys. A 122 (2) (2016) 1–17.
[400] H.G. Schimmel, J. Huot, L.C. Chapon, F.D. Tichelaar, F.M. Mulder, Hydrogen cycling of niobium and vanadium catalyzed nanostructured magnesium, J. Am. Chem. Soc. 127 (41) (2005) 14348–14354.
[401] J. Lu, J.C. Young, Z.F. Zhigang, Y.S. Hong, E. Rönnebro, Hydrogen storage properties of nanosized MgH_2-0.1TiH_2 prepared by ultrahigh-energy-high-pressure milling, J. Am. Chem. Soc. 131 (43) (2009) 15843–15852.
[402] F. Cuevas, D. Korablov, M. Latroche, Synthesis, structural and hydrogenation properties of Mg-rich MgH_2-TiH_2 nanocomposites prepared by reactive ball milling under hydrogen gas, Phys. Chem. Chem. Phys. 14 (3) (2012) 1200–1211.
[403] C.J. Webb, A review of catalyst-enhanced magnesium hydride as a hydrogen storage material, J. Phys. Chem. Solids 84 (1) (2015) 96–106.
[404] K. Alsabawi, T.A. Webb, E.M. Gray, C.J. Webb, The effect of C_{60} additive on magnesium hydride for hydrogen storage, Int. J. Hydrogen Energy 40 (33) (2015) 10508–10515.
[405] K. Alsabawi, T.A. Webb, E.M.A. Gray, C.J. Webb, Kinetic enhancement of the sorption properties of MgH_2 with the additive titanium isopropoxide, Int. J. Hydrogen Energy 42 (8) (2017) 5227–5234.
[406] T.A. Webb, C.J. Webb, A.K. Dahle, E.M.A. Gray, In-situ neutron powder diffraction study of Mg-Zn alloys during hydrogen cycling, Int. J. Hydrogen Energy 40 (25) (2015) 8106–8109.
[407] T. Liu, C. Chen, F. Wang, X. Li, Enhanced hydrogen storage properties of magnesium by the synergic catalytic effect of $TiH_{1.971}$ and $TiH_{1.5}$ nanoparticles at room temperature, J. Power Sources 267 (2014) 69–77.
[408] K. Asano, H. Kim, K. Sakaki, K. Jimura, S. Hayashi, Y. Nakamura, et al., Structural variation of self-organized Mg hydride nanoclusters in immiscible Ti matrix by hydrogenation, Inorg. Chem. 57 (18) (2018) 11831–11838.
[409] U. Kaess, G. Majer, M. Stoll, D.T. Peterson, R.G. Barnes, Hydrogen and deuterium diffusion in titanium dihydrides/dideuterides, J. Alloy. Comp. 259 (1–2) (1997) 74–82.
[410] M. Ponthieu, F. Cuevas, J.F. Fernández, L. Laversenne, F. Porcher, M. Latroche, Structural properties and reversible deuterium loading of MgD_2-TiD_2 nanocomposites, J. Phys. Chem. C 117 (37) (2013) 18851–18862.
[411] M. Ponthieu, M. Calizzi, L. Pasquini, J.F. Fernández, F. Cuevas, Synthesis by reactive ball milling and cycling properties of MgH_2-TiH_2 nanocomposites: kinetics and isotopic effects, Int. J. Hydrogen Energy 39 (18) (2014) 9918–9923.
[412] A. Baldi, R. Gremaud, D.M. Borsa, C.P. Baldé, A.M.J. van der Eerden, G.L. Kruijtzer, et al., Nanoscale composition modulations in $Mg_yTi_{1-y}H_x$ thin film alloys for hydrogen storage, Int. J. Hydrogen Energy 34 (3) (2009) 1450–1457.
[413] A. Schneemann, J.L. White, S. Kang, S. Jeong, L.F. Wan, E.S. Cho, et al., Nanostructured metal hydrides for hydrogen storage, Chem. Rev. 118 (22) (2018) 10775–10839.
[414] P.E. De Jongh, P. Adelhelm, Nanosizing and nanoconfinement: new strategies towards meeting hydrogen storage goals, ChemSusChem 3 (12) (2010) 1332–1348.
[415] V. Bérubé, G. Radtke, M. Dresselhaus, G. Chen, Size effects on the hydrogen storage properties of nanostructured metal hydrides: a review, Int. J. Energy Res. 31 (6–7) (2007) 637–663.
[416] L. Pasquini, The effects of nanostructure on the hydrogen sorption properties of magnesium-based metallic compounds: a review, Crystals 8 (2) (2018) 106.
[417] V. Berube, G. Chen, M.S. Dresselhaus, Impact of nanostructuring on the enthalpy of formation of metal hydrides, Int. J. Hydrogen Energy 33 (15) (2008) 4122–4131.
[418] K.C. Kim, B. Dai, J. Karl Johnson, D.S. Sholl, Assessing nanoparticle size effects on metal hydride thermodynamics using the Wulff construction, Nanotechnology 20 (20) (2009) 204001.
[419] R.W.P. Wagemans, J.H. Van Lenthe, P.E. De Jongh, A.J. Van Dillen, K.P. De Jong, Hydrogen storage in magnesium clusters: quantum chemical study, J. Am. Chem. Soc. 127 (47) (2005) 16675–16680.
[420] S.A. Shevlin, Z.X. Guo, MgH_2 dehydrogenation thermodynamics: nanostructuring and transition metal doping, J. Phys. Chem. C 117 (21) (2013) 10883–10891.
[421] L.P.A. Mooij, A. Baldi, C. Boelsma, K. Shen, M. Wagemaker, Y. Pivak, et al., Interface energy controlled thermodynamics of nanoscale metal hydrides, Adv. Energy Mater. 1 (5) (2011) 754–758.
[422] P. Kalisvaart, B. Shalchi-Amirkhiz, R. Zahiri, B. Zahiri, X. Tan, M. Danaie, et al., Thermodynamically destabilized hydride formation in “bulk” Mg-AlTi multilayers for hydrogen storage, Phys. Chem. Chem. Phys. 15 (39) (2013) 16432–16436.
[423] K. Asano, R.J. Westerwaal, A. Anastasopol, L.P.A. Mooij, C. Boelsma, P. Ngene, et al., Destabilization of Mg hydride by self-organized nanoclusters in the immiscible Mg-Ti system, J. Phys. Chem. C 119 (22) (2015) 12157–12164.
[424] N. Patelli, M. Calizzi, A. Migliori, V. Morandi, L. Pasquini, Hydrogen desorption below 150 °c in MgH_2-TiH_2 composite nanoparticles: equilibrium and kinetic properties, J. Phys. Chem. C 121 (21) (2017) 11166–11177.
[425] Z. Zhao-Karger, J. Hu, A. Roth, D. Wang, C. Kübel, W. Lohstroh, et al., Altered thermodynamic and kinetic properties of MgH_2 infiltrated in microporous scaffold, Chem. Commun. 46 (44) (2010) 8353–8355.
[426] A. Anastasopol, T.V. Pfeiffer, J. Middelkoop, U. Lafont, R.J. Canales-Perez, A. Schmidt-Ott, et al., Reduced enthalpy of metal hydride formation for Mg-Ti nanocomposites produced by spark discharge generation, J. Am. Chem. Soc. 135 (21) (2013) 7891–7900.
[427] W. Liu, K.F. Aguey-Zinsou, Size effects and hydrogen storage properties of Mg nanoparticles synthesised by an electroless reduction method, J. Mater. Chem. 2 (25) (2014) 9718–9726.
[428] Y. Sun, K.F. Aguey-Zinsou, Dual-tuning the thermodynamics and kinetics: magnesium-naphthalocyanine nanocomposite for low temperature hydrogen cycling, Int. J. Hydrogen Energy 43 (10) (2018) 5089–5097.
[429] A. Cornish-Bowden, Enthalpy-entropy compensation: a phantom phenomenon, J. Biosci. 27 (2) (2002) 121–126.
[430] S. Wagner, A. Pundt, Quasi-thermodynamic model on hydride formation in palladium-hydrogen thin films: impact of elastic and microstructural constraints, Int. J. Hydrogen Energy 41 (4) (2016) 2727–2738.
[431] A. Baldi, M. Gonzalez-Silveira, V. Palmisano, B. Dam, R. Griessen, Destabilization of the Mg-H system through elastic constraints, Phys. Rev. Lett. 102 (22) (2009) 1–4.
[432] L. Pasquini, M. Sacchi, M. Brighi, C. Boelsma, S. Bals, T. Perkisas, et al., Hydride destabilization in core-shell nanoparticles, Int. J. Hydrogen Energy 39 (5) (2014) 2115–2123.
[433] A. Molinari, F. D'Amico, M. Calizzi, Y. Zheng, C. Boelsma, L. Mooij, et al., Interface and strain effects on the H-sorption thermodynamics of size-selected Mg nanodots, Int. J. Hydrogen Energy 41 (23) (2016) 9841–9851.
[434] A. Baldi, L. Mooij, V. Palmisano, H. Schreuders, G. Krishnan, B.J. Kooi, et al., Elastic versus alloying effects in Mg-based hydride films, Phys. Rev. Lett. 121 (25) (2018) 255503.
[435] Y. Pivak, H. Schreuders, B. Dam, Thermodynamic properties, hysteresis behavior and stress-strain analysis of MgH_2 thin films, studied over a wide temperature range, Crystals 2 (2) (2012) 710–729.
[436] L. Mooij, B. Dam, Hysteresis and the role of nucleation and growth in the hydrogenation of Mg nanolayers, Phys. Chem. Chem. Phys. 15 (8) (2013) 2782–2792.
[437] P. Ngene, A. Longo, L. Mooij, W. Bras, B. Dam, Metal-hydrogen systems with an exceptionally large and tunable thermodynamic destabilization, Nat. Commun. 8 (1) (2017) 1846.
[438] C. Zlotea, Y. Oumellal, S.J. Hwang, C.M. Ghimbeu, P.E. De Jongh, M. Latroche, Ultrasmall MgH_2 nanoparticles embedded in an ordered microporous carbon exhibiting rapid hydrogen sorption kinetics, J. Phys. Chem. C 119 (32) (2015) 18091–18098.
[439] P.E. De Jongh, M. Allendorf, J.J. Vajo, C. Zlotea, Nanoconfined light metal hydrides for reversible hydrogen storage, MRS Bull. 38 (6) (2013) 488–494.
[440] K.J. Jeon, H.R. Moon, A.M. Ruminski, B. Jiang, C. Kisielowski, R. Bardhan, et al., Air-stable magnesium nanocomposites provide rapid and high-capacity hydrogen storage without using heavy-metal catalysts, Nat. Mater. 10 (4) (2011) 286–290.
[441] E.S. Cho, A.M. Ruminski, S. Aloni, Y.S. Liu, J. Guo, J.J. Urban, Graphene oxide/metal nanocrystal multilaminates as the atomic limit for safe and selective hydrogen storage, Nat. Commun. 7 (2016) 10804.
[442] C. Zlotea, Y. Oumellal, M. Msakni, J. Bourgon, S. Bastide, C. Cachet-Vivier, et al., First evidence of Rh nano-hydride formation at low pressure, Nano Lett. 15 (7) (2015) 4752–4757.
[443] V. Stavila, R.K. Bhakta, T.M. Alam, E.H. Majzoub, M.D. Allendorf, Reversible hydrogen storage by $NaAlH_4$ confined within a titanium-functionalized MOF-74(Mg) nanoreactor, ACS Nano 6 (11) (2012) 9807–9817.
[444] F. Cuevas, J.M. Joubert, M. Latroche, A. Percheron-Guégan, Intermetallic compounds as negative electrodes of Ni/MH batteries, Appl. Phys. A 72 (2) (2001) 225–238.
[445] F. Feng, M. Geng, D.O. Northwood, Electrochemical behaviour of intermetallic-based metal hydrides used in Ni/metal hydride (MH) batteries: a review, Int. J. Hydrogen Energy 26 (7) (2001) 725–734.
[446] P.H.L. Notten, M. Latroche, Secondary batteries: nickel batteries metal hydride alloys, in: J. Garche (Ed.), Encyclopedia of Electrochemical Power Sources, Elsevier, Amsterdam, 2009, pp. 502–521.

[447] P.H.L. Notten, Rechargeable nickel-metal hydride batteries: a successful new concept, in: F. Grandjean, G.J. Long, K.H.J. Buschow (Eds.), Interstitial Intermetallic Alloys, vol. 281, Kluwer Academic Publishers, Dordrecht, Boston, London, 1995, pp. 150–194. NATO ASI Series.

[448] G. Guo, P. Xu, Z. Bai, S. Zhou, G. Xu, B. Cao, Optimization of Ni-MH battery fast charging in electric vehicles using dynamic data mining and ANFIS, in: Lecture Notes in Computer Science, 5227 LNAI, SPRINGER-VERLAG BERLIN, 2008, pp. 468–475.

[449] K. Korkmaz, M. Alemrajabi, Rasmuson Å, K. Forsberg, Recoveries of valuable metals from spent nickel metal hydride vehicle batteries via sulfation, selective roasting, and water leaching, J. Sustain. Metall. 4 (3) (2018) 313–325.

[450] Z. Ye, D. Noréus, J.R. Howlett, Metal hydrides for high-power batteries, MRS Bull. 38 (6) (2013) 504–508.

[451] Y. Shen, D. Noréus, S. Starborg, Increasing NiMH battery cycle life with oxygen, Int. J. Hydrogen Energy 43 (40) (2018) 18626–18631.

[452] T.K. Ying, X.P. Gao, W.K. Hu, F. Wu, D. Noréus, Studies on rechargeable NiMH batteries, Int. J. Hydrogen Energy 31 (4) (2006) 525–530.

[453] M. Armand, J.-M. Tarascon, Building Better Batteries, Nature 451 (7179) (2008) 652–657.

[454] V. Yartys, D. Noréus, M. Latroche, Metal hydrides as negative electrode materials for Ni–MH batteries, Appl. Phys. A 122 (1) (2016) 1–11.

[455] M. Latroche, F. Cuevas, W.K. Hu, D. Sheptyakov, R.V. Denys, V.A. Yartys, Mechanistic and kinetic study of the electrochemical charge and discharge of La_2MgNi_9 by in situ powder neutron diffraction, J. Phys. Chem. C 118 (23) (2014) 12162–12169.

[456] V. Serin, J. Zhang, C. Magén, R. Serra, M.J. Hÿtch, L. Lemort, et al., Identification of the atomic scale structure of the $La_{0.65}Nd_{0.15}Mg_{0.20}Ni_{3.5}$ alloy synthesized by spark plasma sintering, Intermetallics 32 (2013) 103–108.

[457] J. Zhang, M. Latroche, C. Magen, V. Serin, M.J. Hÿtch, B. Knosp, et al., Investigation of the phase occurrence, H sorption properties, and electrochemical behavior in the composition ranges $La_{0.75-0.80}Mg_{0.30-0.38}Ni_{3.67}$, J. Phys. Chem. C 118 (48) (2014) 27808–27814.

[458] V.A. Yartys, A.B. Riabov, R.V. Denys, M. Sato, R.G. Delaplane, Novel intermetallic hydrides, J. Alloy. Comp. 408–412 (2006) 273–279.

[459] J. Monnier, H. Chen, S. Joiret, J. Bourgon, M. Latroche, Identification of a new pseudo-binary hydroxide during calendar corrosion of $(La, Mg)_2Ni_7$-type hydrogen storage alloys for Nickel-Metal Hydride batteries, J. Power Sources 266 (2014) 162–169.

[460] R.V. Denys, V.A. Yartys, Effect of magnesium on the crystal structure and thermodynamics of the $La_{3-x}Mg_xNi_9$ hydrides, J. Alloy. Comp. 509 (SUPPL. 2) (2011) S540–S548.

[461] R.V. Denys, V.A. Yartys, C.J. Webb, Hydrogen in $La_2MgNi_9D_{13}$: the role of magnesium, Inorg. Chem. 51 (7) (2012) 4231–4238.

[462] V.A. Yartys, R.V. Denys, Thermodynamics and crystal chemistry of the $RE_2MgNi_9H_{12-13}$, Chem. Met. Alloy 7 (2014) 1–8.

[463] V. Yartys, R. Denys, Structure-properties relationship in $RE_{3-x}Mg_xNi_9H_{10-13}$ (RE=La,Pr,Nd) hydrides for energy storage, J. Alloy. Comp. 645 (S1) (2015) 5412–5418.

[464] W.K. Hu, R.V. Denys, C.C. Nwakwuo, T. Holm, J.P. Maehlen, J.K. Solberg, et al., Annealing effect on phase composition and electrochemical properties of the Co-free La_2MgNi_9 anode for Ni-metal hydride batteries, Electrochim. Acta 96 (2013) 27–33.

[465] C.C. Nwakwuo, T. Holm, R.V. Denys, W. Hu, J.P. Maehlen, J.K. Solberg, et al., Effect of magnesium content and quenching rate on the phase structure and composition of rapidly solidified La_2MgNi_9 metal hydride battery electrode alloy, J. Alloy. Comp. 555 (2013) 201–208.

[466] A.A. Volodin, R.V. Denys, G.A. Tsirlina, B.P. Tarasov, M. Fichtner, V.A. Yartys, Hydrogen diffusion in $La_{1.5}Nd_{0.5}MgNi_9$ alloy electrodes of the Ni/MH battery, J. Alloy. Comp. 645 (S1) (2015) S288–S291.

[467] I.E. Gabis, E.A. Evard, A.P. Voyt, V.G. Kuznetsov, B.P. Tarasov, J.C. Crivello, et al., Modeling of metal hydride battery anodes at high discharge current densities and constant discharge currents, Electrochim. Acta 147 (2014) 73–81.

[468] I.D. Wijayanti, L. Mølmen, R.V. Denys, J. Nei, S. Gorsse, K. Young, et al., The electrochemical performance of melt-spun C14-Laves type Ti–Zr-based alloy, Int. J. Hydrogen Energy 45 (2020) 1297–1303.

[469] I.D. Wijayanti, L. Mølmen, R.V. Denys, J. Nei, S. Gorsse, M.N. Guzik, et al., Studies of Zr-based C15 type metal hydride battery anode alloys prepared by rapid solidification, J. Alloy. Comp. 804 (2019) 527–537.

[470] A.A. Volodin, R.V. Denys, C Bin Wan, I.D. Wijayanti, Suwarno, B.P. Tarasov, et al., Study of hydrogen storage and electrochemical properties of AB_2-type $Ti_{0.15}Zr_{0.85}La_{0.03}Ni_{1.2}Mn_{0.7}V_{0.12}Fe_{0.12}$ alloy, J. Alloy. Comp. 793 (2019) 564–575, https://doi.org/10.1016/j.jallcom.2019.03.134.

[471] Chubin Wan, R.V. Denys, M. Lelis, D. Milčius, V.A. Yartys, Electrochemical studies and phase-structural characterization of a high-capacity La-doped AB_2 Laves type alloy and its hydride, J. Power Sources 418 (2027) (2019) 193–201, https://doi.org/10.1016/j.jpowsour.2019.02.044.

[472] S. Sartori, F. Cuevas, M. Latroche, Metal hydrides used as negative electrode materials for Li-ion batteries, Appl. Phys. A 122 (2) (2016) 1–7.

[473] S. Brutti, G. Mulas, E. Piciollo, S. Panero, P. Reale, Magnesium hydride as a high capacity negative electrode for lithium ion batteries, J. Mater. Chem. 29 (2012) 14531–14537, https://doi.org/10.1039/c2jm90181a. Erratum: Magnesium hydride as a high capacity negative electrode for lithium ion batteries (Journal of Materials Chemistry (2012) 22 (14531-14537) DOI: 10.1039/C2JM31827J).

[474] W. Zaïdi, Y. Oumellal, J.P. Bonnet, J. Zhang, F. Cuevas, M. Latroche, et al., Carboxymethylcellulose and carboxymethylcellulose-formate as binders in MgH_2-carbon composites negative electrode for lithium-ion batteries, J. Power Sources 196 (5) (2011) 2854–2857.

[475] N. Hanada, A. Kamura, H. Suzuki, K. Takai, T. Ichikawa, Y. Kojima, Electrochemical charge and discharge properties for the formation of magnesium and aluminum hydrides, J. Alloy. Comp. 509 (SUPPL. 2) (2011) S584–S587.

[476] S. Ikeda, T. Ichikawa, K. Kawahito, K. Hirabayashi, H. Miyaoka, Y. Kojima, Anode properties of magnesium hydride catalyzed with niobium oxide for an all solid-state lithium-ion battery, Chem. Commun. 49 (64) (2013) 7174–7176.

[477] Y. Oumellal, C. Zlotea, S. Bastide, C. Cachet-Vivier, E. Léonel, S. Sengmany, et al., Bottom-up preparation of MgH_2 nanoparticles with enhanced cycle life stability during electrochemical conversion in Li-ion batteries, Nanoscale 6 (23) (2014) 14459–14466.

[478] Y. Oumellal, A. Rougier, J.M. Tarascon, L. Aymard, 2LiH + M (M=Mg, Ti): new concept of negative electrode for rechargeable lithium-ion batteries, J. Power Sources 192 (2) (2009) 698–702.

[479] Y. Oumellal, W. Zaïdi, J.P. Bonnet, F. Cuevas, M. Latroche, J. Zhang, et al., Reactivity of TiH_2 hydride with lithium ion: evidence for a new conversion mechanism, Int. J. Hydrogen Energy 37 (9) (2012) 7831–7835.

[480] L. Huang, L. Aymard, J.P. Bonnet, MgH_2 -TiH_2 mixture as an anode for lithium-ion batteries: synergic enhancement of the conversion electrode electrochemical performance, J. Mater. Chem. 3 (29) (2015) 15091–15096.

[481] M. Bououdina, Y. Oumellal, L. Dupont, L. Aymard, H. Al-Gharni, A. Al-Hajry, et al., Lithium storage in amorphous TiNi hydride: electrode for rechargeable lithium-ion batteries, Mater. Chem. Phys. 141 (1) (2013) 348–354.

[482] W. Zaïdi, J.P. Bonnet, J. Zhang, F. Cuevas, M. Latroche, S. Couillaud, et al., Reactivity of complex hydrides Mg_2FeH_6, Mg_2CoH_5 and Mg_2NiH_4 with lithium ion: far from equilibrium electrochemically driven conversion reactions, Int. J. Hydrogen Energy 38 (11) (2013) 4798–4808.

[483] K. Provost, J. Zhang, W. Zaïdi, V. Paul-Boncour, J.P. Bonnet, F. Cuevas, et al., X-ray absorption spectroscopy and X-ray diffraction studies of the thermal and li-driven electrochemical dehydrogenation of nanocrystalline complex hydrides Mg_2MH_x (M=Co, Ni), J. Phys. Chem. C 118 (51) (2014) 29554–29567.

[484] J. Zhang, W. Zaïdi, V. Paul-Boncour, K. Provost, A. Michalowicz, F. Cuevas, et al., XAS investigations on nanocrystalline Mg_2FeH_6 used as a negative electrode of Li-ion batteries, J. Mater. Chem. 1 (15) (2013) 4706–4717.

[485] J.A. Teprovich, J. Zhang, H. Colón-Mercado, F. Cuevas, B. Peters, S. Greenway, et al., Li-driven electrochemical conversion reactions of AlH_3, $LiAlH_4$, and $NaAlH_4$, J. Phys. Chem. C 119 (9) (2015) 4666–4674.

[486] L. Silvestri, S. Forgia, L. Farina, D. Meggiolaro, S. Panero, A. LaBarbera, et al., Lithium alanates as negative electrodes in lithium-ion batteries, ChemElectroChem 2 (6) (2015) 877–886.

[487] A. El Kharbachi, H. Uesato, H. Kawai, S. Wenner, H. Miyaoka, M.H. Sørby, et al., MgH_2-CoO: a conversion-type composite electrode for $LiBH_4$-based all-solid-state lithium ion batteries, RSC Adv. 8 (41) (2018) 23468–23474.

[488] K. Kawahito, L. Zeng, T. Ichikawa, H. Miyaoka, Y. Kojima, Electrochemical performance of titanium hydride for bulk-type all-solid-state lithium-ion batteries, Mater. Trans. 57 (5) (2016) 755–757.

[489] L. Zeng, T. Ichikawa, K. Kawahito, H. Miyaoka, Y. Kojima, Bulk-Type all-solid-state lithium-ion batteries: remarkable performances of a carbon nanofiber-supported MgH_2 composite electrode, ACS Appl. Mater. Interfaces 9 (3) (2017) 2261–2266.

[490] L. Zeng, K. Kawahito, S. Ikeda, T. Ichikawa, H. Miyaoka, Y. Kojima, Metal hydride-based materials towards high performance negative electrodes for all-solid-state lithium-ion batteries, Chem. Commun. 51 (48) (2015) 9773–9776.

[491] P. López-Aranguren, N. Berti, H.A. Dao, J. Zhang, F. Cuevas, M. Latroche, et al., An all-solid-state metal hydride – sulfur lithium-ion battery, J. Power Sources 357 (2017) 56–60.

[492] P. Huen, D.B. Ravnsbæk, All-solid-state lithium batteries – the Mg_2FeH_6-electrode $LiBH_4$-electrolyte system, Electrochem. Commun. 87 (2018) 81–85.

[493] N. Berti, E. Hadjixenophontos, F. Cuevas, J. Zhang, A. Lacoste, P. Dubot, et al., Thin films as model system for understanding the electrochemical reaction mechanisms in conversion reaction of MgH_2 with lithium, J. Power Sources 402 (2018) 99–106.

[494] A. Unemoto, M. Matsuo, S.I. Orimo, Complex hydrides for electrochemical energy storage, Adv. Funct. Mater. 24 (16) (2014) 2267–2279.

[495] P.E. de Jongh, D. Blanchard, M. Matsuo, T.J. Udovic, S. Orimo, Complex hydrides as room-temperature solid electrolytes for rechargeable batteries, Appl. Phys. A 122 (3) (2016) 251.

[496] M. Matsuo, S.I. Orimo, Lithium fast-ionic conduction in complex hydrides: review and prospects, Adv. Energy Mater. 1 (2) (2011) 161–172.

[497] M. Matsuo, Y. Nakamori, S.I. Orimo, H. Maekawa, H. Takamura, Lithium superionic conduction in lithium borohydride accompanied by structural transition, Appl. Phys. Lett. 91 (22) (2007) 224103.

[498] P. Ngene, P. Adelhelm, A.M. Beale, K.P. De Jong, P.E. De Jongh, $LiBH_4$/SBA-15 nanocomposites prepared by melt infiltration under hydrogen pressure: synthesis and hydrogen sorption properties, J. Phys. Chem. C 114 (13) (2010) 6163–6168.

[499] D. Blanchard, A. Nale, D. Sveinbjörnsson, T.M. Eggenhuisen, M.H.W. Verkuijlen, Suwarno, et al., Nanoconfined $LiBH_4$ as a fast lithium ion conductor, Adv. Funct. Mater. 25 (2) (2015) 184–192.

[500] J.S.G. Myrdal, D. Blanchard, D. Sveinbjörnsson, T. Vegge, Li-ion conduction in the $LiBH_4$:LiI system from density functional theory calculations and quasi-elastic neutron scattering, J. Phys. Chem. C 117 (18) (2013) 9084–9091.
[501] M. Matsuo, A. Remhof, P. Martelli, R. Caputo, M. Ernst, Y. Miura, et al., Complex hydrides with $(BH_4)^-$ and $(NH_2)^-$ anions as new lithium fast-ion conductors, J. Am. Chem. Soc. 131 (2009) 16389–16391.
[502] T.J. Udovic, M. Matsuo, A. Unemoto, N. Verdal, V. Stavila, A.V. Skripov, et al., Sodium superionic conduction in $Na_2B_{12}H_{12}$, Chem. Commun. 50 (28) (2014) 3750–3752.
[503] T.J. Udovic, M. Matsuo, W.S. Tang, H. Wu, V. Stavila, A.V. Soloninin, et al., Exceptional superionic conductivity in disordered sodium decahydro-closo-decaborate, Adv. Mater. 26 (45) (2014) 7622–7626.
[504] W.S. Tang, M. Matsuo, H. Wu, V. Stavila, W. Zhou, A.A. Talin, et al., Liquid-like ionic conduction in solid lithium and sodium monocarba-closo-decaborates near or at room temperature, Adv. Energy Mater. 6 (8) (2016) 1502237.
[505] M. Latroche, D. Blanchard, F. Cuevas, A. El Kharbachi, B.C. Hauback, T.R. Jensen, et al., Full-cell hydride-based solid-state Li batteries for energy storage, Int. J. Hydrogen Energy 44 (15) (2019) 7875–7887.
[506] A. El Kharbachi, Y. Hu, M.H. Sørby, J.P. Mæhlen, P.E. Vullum, H. Fjellvåg, et al., Reversibility of metal-hydride anodes in all-solid-state lithium secondary battery operating at room temperature, Solid State Ion. 317 (2018) 263–267.
[507] A. Unemoto, T. Ikeshoji, S. Yasaku, M. Matsuo, V. Stavila, T.J. Udovic, et al., Stable interface formation between TiS_2 and $LiBH_4$ in bulk-type All-solid-state lithium batteries, Chem. Mater. 27 (15) (2015) 5407–5416.
[508] S. Kim, N. Toyama, H. Oguchi, T. Sato, S. Takagi, T. Ikeshoji, et al., Fast lithium-ion conduction in atom-deficient closo-type complex hydride solid electrolytes, Chem. Mater. 30 (2) (2018) 386–391.
[509] S. Das, P. Ngene, P. Norby, T. Vegge, P.E. De Jongh, D. Blanchard, All-solid-state lithium-sulfur battery based on a nanoconfined $LiBH_4$ electrolyte, J. Electrochem. Soc. 163 (9) (2016) A2029–A2034.
[510] A. Unemoto, S. Yasaku, G. Nogami, M. Tazawa, M. Taniguchi, M. Matsuo, et al., Development of bulk-type all-solid-state lithium-sulfur battery using $LiBH_4$ electrolyte, Appl. Phys. Lett. 105 (8) (2014), 083901.
[511] A. Unemoto, C. Chen, Z. Wang, M. Matsuo, T. Ikeshoji, S. Orimo, Pseudo-binary electrolyte, $LiBH_4$–LiCl, for bulk-type all-solid-state lithium-sulfur battery, Nanotechnology 26 (25) (2015) 254001.
[512] J. Nguyen, B. Fleutot, R. Janot, Investigation of the stability of metal borohydrides-based compounds $LiM(BH_4)_3Cl$ (M=La, Ce, Gd) as solid electrolytes for Li-S batteries, Solid State Ion. 315 (2018) 26–32.
[513] K. Takahashi, K. Hattori, T. Yamazaki, K. Takada, M. Matsuo, S. Orimo, et al., All-solid-state lithium battery with $LiBH_4$ solid electrolyte, J. Power Sources 226 (2013) 61–64.
[514] K. Manickam, P. Mistry, G. Walker, D. Grant, C.E. Buckley, T.D. Humphries, et al., Future perspectives of thermal energy storage with metal hydrides, Int. J. Hydrogen Energy 44 (15) (2019) 7738–7745.
[515] M. Fellet, C.E. Buckley, M. Paskevicius, D.A. Sheppard, Research on metal hydrides revived for next-generation solutions to renewable energy storage, MRS Bull. 38 (12) (2013) 1012–1013.
[516] D.N. Harries, M. Paskevicius, D.A. Sheppard, T.E.C. Price, C.E. Buckley, Concentrating solar thermal heat storage using metal hydrides, Proc. IEEE 100 (2) (2012) 539–549.
[517] D.A. Sheppard, T.D. Humphries, C.E. Buckley, Sodium-based hydrides for thermal energy applications, Appl. Phys. A 122 (4) (2016) 406.
[518] P.A. Ward, C. Corgnale, J.A. Teprovich, T. Motyka, B. Hardy, D. Sheppard, et al., Technical challenges and future direction for high-efficiency metal hydride thermal energy storage systems, Appl. Phys. A 122 (4) (2016) 462.
[519] D.A. Sheppard, M. Paskevicius, P. Javadian, I.J. Davies, C.E. Buckley, Methods for accurate high-temperature Sieverts-type hydrogen measurements of metal hydrides, J. Alloy. Comp. 787 (2019) 1225–1237.
[520] D.A. Sheppard, C.E. Buckley, The potential of metal hydrides paired with compressed hydrogen as thermal energy storage for concentrating solar power plants, Int. J. Hydrogen Energy 44 (18) (2019) 9143–9163.
[521] D.A. Sheppard, C. Corgnale, B. Hardy, T. Motyka, R. Zidan, M. Paskevicius, et al., Hydriding characteristics of $NaMgH_2F$ with preliminary technical and cost evaluation of magnesium-based metal hydride materials for concentrating solar power thermal storage, RSC Adv. 4 (51) (2014) 26552–26562.
[522] C. Corgnale, B. Hardy, T. Motyka, R. Zidan, J. Teprovich, B. Peters, Screening analysis of metal hydride based thermal energy storage systems for concentrating solar power plants, Renew. Sustain. Energy Rev. 38 (2014) 821–833.
[523] T.D. Humphries, D.A. Sheppard, M.R. Rowles, M.V. Sofianos, C.E. Buckley, Fluoride substitution in sodium hydride for thermal energy storage applications, J. Mater. Chem. A 4 (31) (2016) 12170–12178.
[524] D.A. Sheppard, T.D. Humphries, C.E. Buckley, What is old is new again, Mater. Today 18 (8) (2015) 414–415.
[525] M.S. Tortoza, T.D. Humphries, D.A. Sheppard, M. Paskevicius, M.R. Rowles, M.V. Sofianos, et al., Thermodynamics and performance of the Mg-H-F system for thermochemical energy storage applications, Phys. Chem. Chem. Phys. 20 (4) (2018) 2274–2283.
[526] P.A. Ward, J.A. Teprovich, Y. Liu, J. He, R. Zidan, High temperature thermal energy storage in the $CaAl_2$ system, J. Alloy. Comp. 735 (2018) 2611–2615.
[527] P. Javadian, D.A. Sheppard, C.E. Buckley, T.R. Jensen, Hydrogen storage properties of nanoconfined $LiBH_4$-$NaBH_4$, Int. J. Hydrogen Energy 40 (43) (2015) 14916–14924.
[528] A.L. Chaudhary, D.A. Sheppard, M. Paskevicius, C. Pistidda, M. Dornheim, C.E. Buckley, Reaction kinetic behaviour with relation to crystallite/grain size dependency in the Mg-Si-H system, Acta Mater. 95 (2015) 244–253.
[529] A.L. Chaudhary, D.A. Sheppard, M. Paskevicius, C.J. Webb, E.M. Gray, C.E. Buckley, Mg_2Si nanoparticle synthesis for high pressure hydrogenation, J. Phys. Chem. C 118 (2) (2014) 1240–1247.
[530] A.L. Chaudhary, M. Paskevicius, D.A. Sheppard, C.E. Buckley, Thermodynamic destabilisation of MgH_2 and $NaMgH_3$ using Group IV elements Si, Ge or Sn, J. Alloy. Comp. 623 (2015) 109–116.
[531] K. Kadir, D. Noréus, A new synthetic route to $Mg_2Na_2NiH_6$ where a $[NiH_4]$ complex is for the first time stabilized by alkali metal counterions, Inorg. Chem. 46 (6) (2007) 2220–2223.
[532] P. Javadian, S.H.P. Gharibdoust, H.W. Li, D.A. Sheppard, C.E. Buckley, T.R. Jensen, Reversibility of $LiBH_4$ facilitated by the $LiBH_4$-$Ca(BH_4)_2$ eutectic, J. Phys. Chem. C 121 (34) (2017) 18439–18449.
[533] P. Javadian, D.A. Sheppard, T.R. Jensen, C.E. Buckley, Destabilization of lithium hydride and the thermodynamic assessment of the Li-Al-H system for solar thermal energy storage, RSC Adv. 6 (97) (2016) 94927–94933.
[534] T.T. Nguyen, D.A. Sheppard, C.E. Buckley, Lithium imide systems for high temperature heat storage in concentrated solar thermal systems, J. Alloy. Comp. 716 (2017) 291–298.
[535] M.P. Pitt, M. Paskevicius, C.J. Webb, D.A. Sheppard, C.E. Buckley, E.M. Gray, The synthesis of nanoscopic Ti based alloys and their effects on the MgH_2 system compared with the $MgH_2 + 0.01Nb_2O_5$ benchmark, Int. J. Hydrogen Energy 37 (5) (2012) 4227–4237.
[536] D. Dong, T.D. Humphries, D.A. Sheppard, B. Stansby, M. Paskevicius, M.V. Sofianos, et al., Thermal optimisation of metal hydride reactors for thermal energy storage applications, Sustain. Energy Fuels 1 (8) (2017) 1820–1829.
[537] M. Paskevicius, D.A. Sheppard, K. Williamson, C.E. Buckley, Metal hydride thermal heat storage prototype for concentrating solar thermal power, Energy 88 (2015) 469–477.
[538] L. Poupin, T.D. Humphries, M. Paskevicius, C.E. Buckley, A thermal energy storage prototype using sodium magnesium hydride, Sustain. Energy Fuels 3 (4) (2019) 985–995.
[539] K.F. Aguey-Zinsou, T. Nicolaisen, J.R. Ares Fernandez, T. Klassen, R. Bormann, Effect of nanosized oxides on MgH_2 (de)hydriding kinetics, J. Alloy. Comp. 434–435 (2007) 738–742.
[540] G. Barkhordarian, T. Klassen, R.U. Bormann, Effect of Nb_2O_5 content on hydrogen reaction kinetics of Mg, J. Alloy. Comp. 364 (1–2) (2004) 242–246.
[541] K. Alsabawi, E.M.A. Gray, C.J. Webb, The effect of ball-milling gas environment on the sorption kinetics of MgH_2 with/without additives for hydrogen storage, Int. J. Hydrogen Energy 44 (5) (2019) 2976–2980, https://doi.org/10.1016/j.ijhydene.2018.12.026.
[542] P.C. Mistry, D.M. Grant, A.D. Stuart, K. Manickam, G.S. Walker, Evolution of catalyst coated atomised magnesium spheres – an alternative thermal storage medium for concentrated solar power applications, Int. J. Hydrogen Energy 42 (47) (2017) 28453–28463.
[543] P.A. Huhn, M. Dornheim, T. Klassen, R. Bormann, Thermal stability of nanocrystalline magnesium for hydrogen storage, J. Alloy. Comp. 404–406 (2005) 499–502.
[544] H.Y. Tien, M. Tanniru, C.Y. Wu, F. Ebrahimi, Effect of hydride nucleation rate on the hydrogen capacity of Mg, Int. J. Hydrogen Energy 34 (15) (2009) 6343–6349.
[545] G. Friedlmeier, M. Groll, Experimental analysis and modelling of the hydriding kinetics of Ni-doped and pure Mg, J. Alloy. Comp. 253–254 (1997) 550–555.
[546] I. Konstanchuk, K. Gerasimov, J.L. Bobet, Cooperative effects at formation and decomposition of magnesium hydride in powders, J. Alloy. Comp. 509 (SUPPL. 2) (2011) S576–S579.
[547] A. Reiser, B. Bogdanović, K. Schlichte, Application of Mg-based metal-hydrides as heat energy storage systems, Int. J. Hydrogen Energy 25 (5) (2000) 425–430.
[548] R. Urbanczyk, M. Meggouh, R. Moury, K. Peinecke, S. Peil, M. Felderhoff, Demonstration of Mg_2FeH_6 as heat storage material at temperatures up to 550 °C, Appl. Phys. A 122 (2016) 315.
[549] R. Urbanczyk, K. Peinecke, S. Peil, M. Felderhoff, Development of a heat storage demonstration unit on the basis of Mg_2FeH_6 as heat storage material and molten salt as heat transfer media, Int. J. Hydrogen Energy 42 (19) (2017) 13818–13826.
[550] P. Marocco, D. Ferrero, A. Lanzini, M. Santarelli, Benefits from heat pipe integration in H_2/H_2O fed SOFC systems, Appl. Energy 241 (2019) 472–482.
[551] P. Du, J. Shan, B. Zhang, L.K.H. Leung, Thermal-hydraulics analysis of flow blockage events for fuel assembly in a sodium-cooled fast reactor, Int. J. Heat Mass Transf. 138 (2019) 496–507.
[552] L.F. González-Portillo, J. Muñoz-Antón, J.M. Martínez-Val, Thermodynamic mapping of power cycles working around the critical point, Energy Convers. Manag. 192 (2019) 359–373.
[553] R. Albert, M. Felderhoff, R. Urbanczyk, Thermal conductivity measurements of magnesium hydride powder beds under operating conditions for heat storage applications, Int. J. Hydrogen Energy 44 (55) (2019) 29273–29281.
[554] M.V. Lototskyy, I. Tolj, L. Pickering, C. Sita, F. Barbir, V. Yartys, The use of metal hydrides in fuel cell applications, Prog. Nat. Sci.: Mater. Int. 27 (2017) 3–20.
[555] D. Brayton, A. Narvaez, Low cost, metal hydride based hydrogen storage system for forklift applications (phase II), in: US DOE Ann Merit Rev Meeting,

2013. https://www.hydrogen.energy.gov/pdfs/review14/st09.
[556] M.V. Lototskyy, I. Tolj, M.W. Davids, Y.V. Klochko, A. Parsons, D. Swanepoel, et al., Metal hydride hydrogen storage and supply systems for electric forklift with low-temperature proton exchange membrane fuel cell power module, Int. J. Hydrogen Energy 41 (31) (2016) 13831–13842.
[557] M.V. Lototskyy, I. Tolj, A. Parsons, F. Smith, C. Sita, V. Linkov, Performance of electric forklift with low-temperature polymer exchange membrane fuel cell power module and metal hydride hydrogen storage extension tank, J. Power Sources 316 (2016) 239–250.
[558] M. Lototskyy, I. Tolj, Y. Klochko, M.W. Davids, D. Swanepoel, V. Linkov, Metal hydride hydrogen storage tank for fuel cell utility vehicles, Int. J. Hydrogen Energy (2019), https://doi.org/10.1016/j.ijhydene.2019.04.124. In press.
[559] M. Lototskyy, I. Tolj, M.W. Davids, P. Bujlo, F. Smith, B.G. Pollet, "Distributed hybrid" MH-CGH2 system for hydrogen storage and its supply to LT PEMFC power modules, J. Alloy. Comp. 645 (S1) (2015) S329–S333.
[560] Metal Hydride Hydrogen Storage Arrangement for Use in a Fuel Cell Utility Vehicle and Method of Manufacturing the Same, UK Patent Application 1806840 (3) (n.d.) 2018.
[561] E.D. Frank, A. Elgowainy, Y.S. Khalid, J.K. Peng, K. Reddi, Refueling-station costs for metal hydride storage tanks on board hydrogen fuel cell vehicles, Int. J. Hydrogen Energy 44 (57) (2019) 29849–29861.
[562] L. Pickering, M.V. Lototskyy, M.W. Davids, C. Sita, V. Linkov, Induction melted AB_2-Type metal hydrides for hydrogen storage and compression applications, Materials Today: Proceedings 5 (4) (2018) 10470–10478. Elsevier.
[563] S. Fashu, M. Lototskyy, M.W. Davids, L. Pickering, V. Linkov, S. Tai, et al., A review on crucibles for induction melting of titanium alloys, Mater. Des. 186 (2020) 108295.
[564] R.B. Falcão, E.D.C.C. Dammann, C.J. Rocha, M. Durazzo, R.U. Ichikawa, L.G. Martinez, et al., An alternative route to produce easily activated nanocrystalline TiFe powder, Int. J. Hydrogen Energy 43 (2018) 16107–16116.
[565] I. Saita, M. Sato, H. Uesugi, T. Akiyama, Hydriding combustion synthesis of TiFe, J. Alloy. Comp. 446–447 (2007) 195–199.
[566] S. Tan, K. Aydinol, T. Öztürk, S. Karakaya, Direct synthesis of Mg-Ni compounds from their oxides, J. Alloy. Comp. 504 (2010) 134–140.
[567] G. Sdanghi, G. Maranzana, A. Celzard, V. Fierro, Review of the current technologies and performances of hydrogen compression for stationary and automotive applications, Renew. Sustain. Energy Rev. 102 (2019) 150–170.
[568] Joseph Pratt, D. Terlip, C. Ainscough, J. Kurt, A. Elgowainy, H2FIRST Reference Station Design Task Project. Vol. NREL/TP-54, NREL Technical Report, 2015.
[569] K. Reddi, A. Elgowainy, E. Sutherland, Hydrogen refueling station compression and storage optimization with tube-trailer deliveries, Int. J. Hydrogen Energy 39 (2014) 19169–19181.
[570] V.A. Yartys, M. Lototskyy, V. Linkov, D. Grant, A. Stuart, J. Eriksen, et al., Metal hydride hydrogen compression: recent advances and future prospects, Appl. Phys. A 122 (2016) 415.
[571] J.J. Reilly, A. Holtz, R.H. Wiswall, A new laboratory gas circulation pump for intermediate pressures, Rev. Sci. Instrum. 42 (10) (1971) 1485–1486.
[572] S.S. Mohammadshahi, T.A. Webb, E.M.A. Gray, C.J. Webb, Experimental and theoretical study of compositional inhomogeneities in $LaNi_5D_x$ owing to temperature gradients and pressure hysteresis, investigated using spatially resolved in-situ neutron diffraction, Int. J. Hydrogen Energy 42 (10) (2017) 6793–6800.
[573] V.N. Verbetsky, S.A. Lushnikov, E.A. Movlaev, Interaction of vanadium alloys with hydrogen at high pressures, Inorg. Mater. 51 (8) (2015) 779–782.
[574] E.A.R. Galvis, F. Leardini, J.R. Ares, F. Cuevas, J.F. Fernandez, Simulation and design of a three-stage metal hydride hydrogen compressor based on experimental thermodynamic data, Int. J. Hydrogen Energy 43 (13) (2018) 6666–6676.
[575] K. Goshome, N. Endo, M. Tetsuhiko, Evaluation of a BCC alloy as metal hydride compressor via 100 MPa-class high-pressure hydrogen apparatus, Int. J. Hydrogen Energy 44 (21) (2019) 10800–10807.
[576] J. Li, X. Jiang, G. Li, X. Li, Development of $Ti_{1.02}Cr_{2-x-y}Fe_xMn_y$ ($0.6 \leq x \leq 0.75$, $y=0.25$, 0.3) alloys for high hydrogen pressure metal hydride system, Int. J. Hydrogen Energy 44 (29) (2019) 15087–15099, https://doi.org/10.1016/j.ijhydene.2019.03.241.
[577] S. Nayebossadri, D. Book, Development of a high-pressure Ti-Mn based hydrogen storage alloy for hydrogen compression, Renew. Energy 143 (2019) 1010–1021, https://doi.org/10.1016/j.renene.2019.05.052.
[578] T. Johnson, R. Bowman, B. Smith, L. Anovitz, C. Jensen, Metal hydride compression, in: US DOE Hydrogen Fuel Cell Annual Merit Review, 2017. https://www.hydrogen.energy.gov/pdfs/review19/in00.
[579] C. Corgnale, M. Sulic, High pressure thermal hydrogen compression employing $Ti_{1.1}CrMn$ metal hydride material, J. Phys. Energy 2 (2020), 014003.
[580] M. Lototskyy, M.W. Davids, D. Swanepoel, G. Louw, Y. Klochko, F. Smith, et al., Hydrogen refuelling station with integrated metal hydride compressor: layout features and experience of three-year operation, Int. J. Hydrogen Energy (2020), https://doi.org/10.1016/j.ijhydene.2019.05.133. In press.
[581] B.P. Tarasov, M.S. Bocharnikov, Y.B. Yanenko, P.V. Fursikov, M.V. Lototskyy, Cycling stability of RNi_5 (R=La, La+Ce) hydrides during the operation of metal hydride hydrogen compressor, Int. J. Hydrogen Energy 43 (9) (2018) 4415–4427.
[582] Eriksen, J. Denys, HYMEHC - the thermal hydrogen compressor by HYSTORSYS, in: 20th World Hydrogen Energy Conference, WHEC, 2014, pp. 603–606.
[583] E.I. Gkanas, D.M. Grant, M. Khzouz, A.D. Stuart, K. Manickam, G.S. Walker, Efficient hydrogen storage in up-scale metal hydride tanks as possible metal hydride compression agents equipped with aluminium extended surfaces, Int. J. Hydrogen Energy 41 (25) (2016) 10795–10810.
[584] G. Karagiorgis, C.N. Christodoulou, H. von Storch, G. Tzamalis, K. Deligiannis, D. Hadjipetrou, et al., Design, development, construction and operation of a novel metal hydride compressor, Int. J. Hydrogen Energy 42 (17) (2017) 12364–12374.
[585] N. Jasminská, T. Brestovič, Ľ. Bednárová, M. Lázár, R. Dobáková, Design of a hydrogen compressor powered by accumulated heat and generated in metal hydrides, Int. J. Eng. Res. Sci. 3 (9) (2017) 35–38.
[586] T. Brestovič, N. Jasminská, M. Lázár, R. Dobáková, Measurement of operating parameters of a hydrogen compressor using metal hydride materials, in: MATEC Web Conf., EDP Sciences, 2018, 06002.
[587] L. Bednárová, T. Brestovič, Design of a metalhydride compressor for a hydrogen technology lab, in: AIP Conference Proceedings 2118, 30004, AIP Publishing, 2019.
[588] M. Lototskyy, Y. Klochko, M.W. Davids, L. Pickering, D. Swanepoel, G. Louw, et al., Industrial-scale metal hydride hydrogen compressors developed at the South African Institute for Advanced Materials Chemistry, Mater. Today: Processing 54 (Part 2) (2018) 10514–10523, https://doi.org/10.1016/j.matpr.2017.12.383.
[589] S. Greenway, M. Sulic, A. Wilber, T. Motyka, B. Hardy, A. D'Entremont, et al., Hybrid Electrochemical Hydrogen/Metal Hydride Compression, in: Presentation to the US DOE Hydrogen Fuel Cell Annual Merit Review, US DOE, 2018. https://www.hydrogen.energy.gov/pdfs/review18/pd137_greenway_2018_o.pdf.
[590] E.A.R. Galvis, F. Leardini, J. Bodega, J.R. Ares, J.F. Fernandez, Realistic simulation in a single stage hydrogen compressor based on AB_2 alloys, Int. J. Hydrogen Energy 41 (23) (2016) 9780–9788.
[591] K.B. Minko, M.S. Bocharnikov, Y.B. Yanenko, M.V. Lototskyy, A. Kolesnikov, B.P. Tarasov, Numerical and experimental study of heat-and-mass transfer processes in two-stage metal hydride hydrogen compressor, Int. J. Hydrogen Energy 43 (48) (2018) 21874–21885.
[592] S.S. Bhogilla, H. Niyas, Design of a hydrogen compressor for hydrogen fueling stations, Int. J. Hydrogen Energy 44 (55) (2019) 29329–29337, https://doi.org/10.1016/j.ijhydene.2019.02.171.
[593] C. Corgnale, M. Sulic, Techno-economic analysis of high-pressure metal hydride compression systems, Metals 8 (6) (2018) 469.
[594] E. Stamatakis, E. Zoulias, G. Tzamalis, Z. Massina, V. Analytis, C. Christodoulou, et al., Metal hydride hydrogen compressors: current developments and early markets, Renew. Energy 127 (2018) 850–862.
[595] R.C. Bowman Jr., Metal hydride compressors with gas-gap heat switches: concept, development, testing, and space flight operation for the Planck sorption cryocoolers, Inorganics 7 (2019) 139.
[596] IEA, The Future of Hydrogen - seizing today's opportunities: report prepared by the IEA for the G20, Japan, in: IEA Report to G20 Conference, IEA, 2019. https://www.g20karuizawa.go.jp/assets/pdf/The future of Hydrogen.pdf.
[597] C. Acar, I. Dincer, Review and evaluation of hydrogen production options for better environment, J. Clean. Prod. 218 (2019) 835–849.
[598] R.W. Schefer, W.G. Houf, C. San Marchi, W.P. Chernicoff, L. Englom, Characterization of leaks from compressed hydrogen dispensing systems and related components, Int. J. Hydrogen Energy 31 (9) (2006) 1247–1260.
[599] US Department of Energy, Target Explanation Document: Onboard Hydrogen Storage for Light-Duty Fuel Cell Vehicles, US Drive, 2017 (May):1–29. http://energy.gov/sites/prod/files/2015/05/f22/fcto_targets_onboard_hydro_storage_explanation.pdf.
[600] Hydrogen CArrier for Renewable Energy Storage (HyCARE), Available from: https://hycare-project.eu/project/.
[601] MariGreen, Perspectives for the Use of Hydrogen as Fuel in Inland Shipping - A Feasibility Study, Interreg, 2018, https://www.dst-org.de/wp-content/uploads/2018/11/Hydrogen-Feasibility-Study-MariGreen.pdf.
[602] H. Fahlquist, D. Noréus, S. Callear, W.I.F. David, $Ga[GaH_3]_4^{5-}$ with a neopentane structure in $Rb_8Ga_5H_{15}$ and $[GaH_2]_n^{n-}$ with a polyethylene structure in $Rb_n(GaH_2)_n$, represent a new class of compounds with direct Ga-Ga bonds mimicking common hydrocarbons, J. Am. Chem. Soc. 37 (2011) 14574–14577.
[603] H. Fahlquist, D. Noréus, A hydrogenous Zintl phase containing propane-like polyanions $[Ga_3H_8]^{3-}$ and interstitial hydrogen, Inorg. Chem. 52 (12) (2013) 7125–7129.